Molecule Based Magnetic Materials: Homo/Heterometallic Clusters to Extended Porous Frameworks

A Thesis Submitted for the Degree of

Master of Science

as a part of the

Integrated Ph.D. Programme

(Materials Science)

By

Anindita Chakraborty

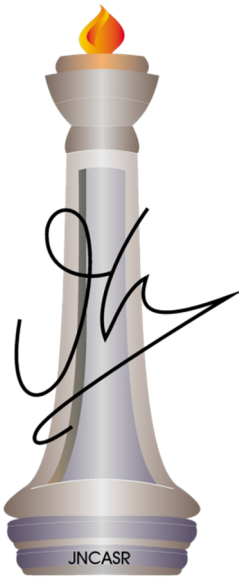

Chemistry and Physics of Materials Unit (CPMU)

Jawaharlal Nehru Centre for Advanced Scientific Research

(A Deemed University)

Bangalore – 560064

Dedicated
to My Parents

DECLARATION

I hereby declare that the matter embodied in the thesis entitled "***Molecule Based Magnetic Materials: Homo/Heterometallic Clusters to Extended Porous Frameworks***" is the result of investigations carried out by me at the Chemistry and Physics of Materials Unit, Jawaharlal Nehru Centre for Advanced Scientific Research, India under the supervision of Dr. Tapas Kumar Maji and that it has not been submitted elsewhere for the award of any degree or diploma.

In keeping with the general practice in reporting the scientific observations, due acknowledgement has been made whenever the work described is based on the findings of other investigators. Any omission that might have occurred due to oversight or error in judgement is regretted.

Anindita Chakraborty

CERTIFICATE

I hereby certify that the work described in this thesis entitled "***Molecule Based Magnetic Materials: Homo/Heterometallic Clusters to Extended Porous Frameworks***" has been carried out by Anindita Chakraborty under my supervision at the Chemistry and Physics of Materials Unit, Jawaharlal Nehru Centre for Advanced Scientific Research, India and that it has not been submitted elsewhere for the award of any degree or diploma.

Dr. Tapas Kumar Maji

CPMU, JNCASR

(Research Supervisor)

ACKNOWLEDGEMENT

It is my great pleasure to express my sincere gratitude to my research supervisor, Dr. Tapas Kumar Maji, who truly did usher the feel of research to me. I am thankful to him for all his support, criticism, guidance and invaluable suggestions, which I have been experienced all through the course of these investigations. I have had enough freedom to work on my own area of interest, and I am grateful to him for that. I am thankful to him for giving me an opportunity to work under his guidance.

Prof. C. N. R. Rao has always been a true source of inspiration, with all his extraordinary enthusiasm and energy. It is really a great opportunity to be in the same institute, to listen to his wonderful motivating speeches and to watch him every day.

I would like to sincerely thank Prof. Swapan. K. Pati and Mr. Arun Kumar Manna of TSU, JNCASR, and Prof. Joan Ribas of University of Barcelona, Spain, for fruitful collaborations.

I thank the past and present chairmen of CPMU for allowing me to use the facilities of the centre.

I am thankful to the faculty members of JNCASR and Indian Institute of Science (IISc) for the wonderful courses that have been really enjoyable with the pleasure to learn new things. In particular, I would like to thank Prof. S. Balasubramanian, Prof. S. K. Pati, Prof. G. U. Kulkarni, Prof. C. Narayana, Prof. H. Ila, Prof. K. S. Narayana, Dr. N. S. Vidhyadhiraja, Dr. R. Ganapathy, Prof. S. Narasimhan, Prof. A. Sundaresan, Prof. U. V, Waghmare, Prof. S. M. Shivaprasad, Dr. Ranjan Dutta, Dr. T. K. Maji, of JNCASR and Prof. Aloknath Chakraborty and Prof. T. N. Guru Row of IISc for their courses.

I am thankful to the technical staffs namely Mr. Anil, Mr. Vasu, Mr. Mahesh, Mr. Murthi and Mr. Srinivas of JNCASR for their prompt and willing assistance, during various experiments.

I would like to thank Prof. A. Sundaresan, Dr. Pranab Mandal, Mr. Nitesh Kumar, Mr. Bharath and Mr. Rana Saha, for the magnetic measurements. It has also been a great experience to have fruitful discussions with them.

I thank JNCASR Library, Complab, Hostel, Health Centre, Academics and Administration staff for providing and maintaining all the wonderful facilities.

I am grateful to my labmates Prakash, Sudip, Jayaram, Arpan, Ritesh, Suresh and Nivedita for providing a nice and healthy environment in the lab. It has been a great pleasure to learn many things, by interacting with them. Also I acknowledge all the visiting scientists and students (POCE and SRF) for their contributions. In particular, I would specially thank Krishna, Ashta and Soumya.

With great joy I thank all the Integrated Ph. D. students of CPMU and NCU. It has been really nice and a lot of fun to be part of the Integrated Ph. D. family. My sincere thanks to all my seniors, for sharing their knowledge with me and being very friendly. I sincerely acknowledge my batchmates, Ajmala, Darshana, Dibyajyoti and Prashant for the wonderful times we have had in the past 3 years. I am thankful to all my juniors too, all of whom have been really nice.

I have been fortunate to have a number of really nice friends in my life. In particular, I sincerely acknowledge Saheli, Bhaswati, Ananya, Ajmala, Darshana, Nivedita, Gayatri, Dhanya, Bhawani, Nitesh, Urmi, Piyush, Josena, Amrit and Pawan.

My family has been the greatest strength for me. Words are indeed insufficient to thank my parents and my brother, who always have been very supportive. Whenever things in my life did not go the right way, I always have been fortunate enough to have my parents, to be with me with all their care and love. It is all their supports which have always pushed me forward.

Last but not the least, I thank God almighty for providing me a truly blessed life.

PREFACE

This thesis consists of five chapters and articulates the design and fascinating properties of some molecule based magnetic materials.

Chapter 1 gives a brief overview of the molecule based magnetic materials and discusses about the origin of the magnetism in these compounds, their properties, importance and applications.

Chapter 2 deals with rational design, characterization and magnetic behaviour of two 1D magnetic systems of Cu(II) based on trinuclear and tetranuclear building blocks. To construct these novel magnetic systems, simple self-assembly process has been exploited using different blocking ligands. The observed magnetic behaviour have been correlated with the structures of the compounds and first principle DFT calculations.

Chapter 3 describes a heterometallic Cu(II)–Ni(II) decameric cluster, synthesized by self–assembly of metal ions and multinucleating ligand di(2–pyridyl)ketone (dpk). This high-nuclearity heterometallic cluster consists of two symmetry related distorted cubane–like pentanulcear cores. The origin of the different magnetic behaviour exhibited by this cluster has been explained in relation to the structure and also by DFT calculations.

Chapter 4 articulates synthesis, characterization and magneto-structural correlation of three different Cu(II)-azido compounds, ranging from a discrete dinuclear complex to an extended 2D network. This chapter shows that a nice control of the dimensionalities of Cu-azido systems can be achieved by tuning the blocking amine concentration. Different kind of binding modes of azido ligands results into different magnetic properties in these three novel compounds. To get further insight into the observed magnetic behaviour, intensive DFT calculations are presented.

Chapter 5 presents two isomorphous bimetallic Co(II)/Ni(II)-Ag(I) 3D porous frameworks fabricated based on a mixed-ligand system, where 2D M(II)-$Ag(CN)_2$ sheets are pillared by piperazine linker. Presence of both long-range ordering and adsorption properties in a single framework was observed for these compounds. The compounds were found to exhibit spin canting behaviour which arises because of the presence of

anisotropic Co(II) and Ni(II) ions in the 3D structure. The polar pore surfaces of these compounds render CO_2 selectivity, which is also elaborated in this chapter.

TABLE OF CONTENTS

DECLARATION iii
CERTIFICATE v
ACKNOWLEDGEMENT vii
PREFACE ix
TABLE OF CONTENTS xi

Chapter 1: Introduction 1

1.1 Molecular Magnetism 3
1.2 Magnetization and Different magnetic materials 4
1.3 Magnetism in Coordination Compounds 7
1.3.1 Superexchange Mechanism 7
1.3.2 Magnetic Molecular Clusters 9
1.3.2 Higher Dimensional Networks: Magnetism and Multifunctionality 13
1.4 Outlook 19
1.5 REFERENCES 20

Chapter 2: Assembly of Trinuclear and Tetranuclear Building Units of Cu(II) Towards Two 1D Magnetic Systems: Synthesis and Magneto-structural Correlations 25

Abstract 27
2.1 INTRODUCTION 28
2.2 EXPERIMENTAL SECTION 30
2.2.1 Materials 30
2.2.2 Synthesis 30
2.2.3 Single-crystal X-ray Diffraction 32
2.2.4 Physical Measurements 32
2.3 RESULTS AND DISCUSSION 33
2.3.1 Crystal Structure Description 33
2.3.1.1 Structural description of $[Cu_3(\mu_3\text{–}OH)(ppk)_3(\mu\text{–}N(CN)_2)(OAc)]_n$ (1) 33
2.3.1.2 Structural description of $\{[Cu_4(pdmH)_2(pdm)_2(\mu_2\text{–}OH)(H_2O)_2]\cdot(ClO_4)\}_n$ (2) 36
2.3.2 Magnetic properties 40
2.4 CONCLUSION 47
2.5 REFERENCES 47

Chapter 3: A Novel Heterometallic Cu(II)-Ni(II) Decameric Cluster: Synthesis, Structure and Magnetic Properties 53

Abstract 55

3.1 INTRODUCTION 56

3.2 EXPERIMENTAL SECTION 57

3.2.1 Materials 57

3.2.2 Synthesis 57

3.2.3 Single-crystal X-ray Diffraction 59

3.2.4 Physical Measurements 59

3.3 RESULTS AND DISCUSSION 59

3.3.1 Crystal Structure Description 59

3.3.2 Magnetic properties 62

3.4 CONCLUSION 66

3.5 REFERENCES 67

Chapter 4: Dimensionality Control in Cu-Azido System Based on Blocking Amine Stoichiometry: Synthesis and Magneto-structural Correlation 69

Abstract 71

4.1 INTRODUCTION 72

4.2 EXPERIMENTAL SECTION 74

4.2.1 Materials 74

4.2.2 Synthesis 74

4.2.3 Single-crystal X-ray Diffraction 77

4.2.4 Physical Measurements 77

4.2.5 Computational details: 77

4.3 RESULTS AND DISCUSSION 78

4.3.1 Crystal Structure Description 78

4.3.1.1 Structural description of $[Cu(\mu_{1,1}\text{-}N_3)(N_3)(Me_2en)]_2$ (1) 78

4.3.1.2 Structural description of $[Cu_2(\mu_{1,3}\text{-}N_3)(\mu_{1,1}\text{-}N_3)(N_3)_2(Me_2en)_2]_n$ (2) 79

4.3.1.3 Structural description of $[Cu_3(\mu_{1,1,1}\text{-}N_3)_2(\mu_{1,1,3}\text{-}N_3)(\mu_{1,1}\text{-}N_3)_2(\mu_{1,3}\text{-}N_3)(Me_2en)]_n$ (3) 80

4.3.2 Magnetic properties 84

4.3.2.1 Magnetic properties of Complex 1 84

4.3.2.2 Magnetic properties of Compound 2 87

4.3.2.2 Magnetic properties of Compound 3 90

4.4 CONCLUSION 93

4.5 REFERENCES 94

Chapter 5: 3D Porous Bimetallic Co(II)-Ag(I) and Ni(II)-Ag(I) Frameworks: Coexistence of Canted Antiferromagnetism and CO_2 Selectivity 97

Abstract 99

5.1 INTRODUCTION 100

5.2 EXPERIMENTAL SECTION 102

5.2.1 Materials 102

5.2.2 Synthesis 102

5.2.3 Single-crystal X-ray Diffraction 103

5.2.4 Physical Measurements 103

5.2.5 Adsorption Measurements 104

5.3 RESULTS AND DISCUSSION 104

5.3.1 Crystal Structure Description 104

5.3.2 Framework Stability: TGA, IR and PXRD Analysis 108

5.3.3 Magnetic properties 110

5.3.4 Adsorption study 117

5.4 CONCLUSION 119

5.5 REFERENCES 120

List of Publications 123

Chapter 1

Introduction

1.1 Molecular Magnetism

Molecular magnetism deals with the magnetic properties of materials consisting discrete molecules or assemblies of molecules. Generally, the molecular magnets consist of solid lattice made of molecular building blocks[1] (Figure 1). These compounds have drawn significant research interests to materials scientists because of their structural novelty as well as promising applications in high density data storage, quantum calculation, signal processing, thermal displays, optical devices, and pressure sensors.[2] Over the last few decades, both the description and application of molecule based magnetic materials have been immensely investigated by physicists and chemists.[3]

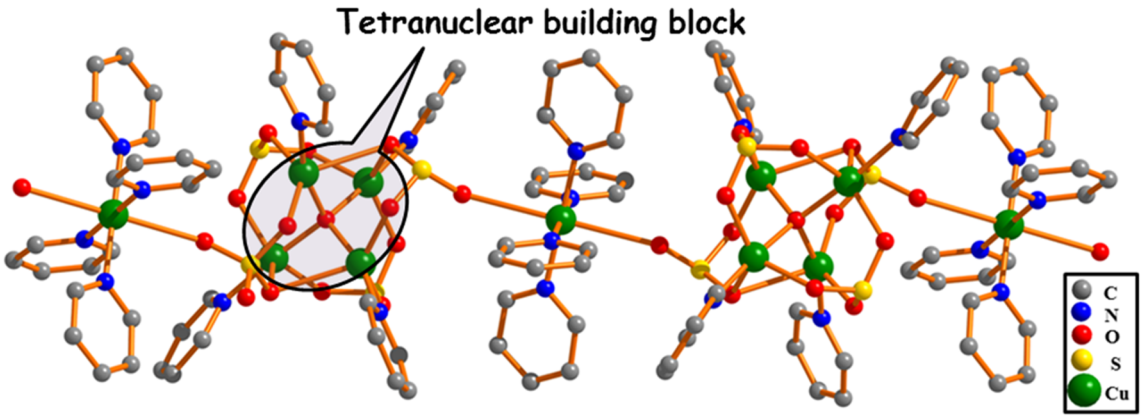

Figure 1. A molecular magnet composed of tetranuclear building block. Figure generated from reference 1c.

Recently, molecular magnets based on metal-organic coordination compounds have gained enormous interest. These compounds straddle the two different classes; conventional inorganic compounds and organic magnetic materials.[4] The advantage of the hybrid materials is their easy synthesis. These compounds are fabricated in mild conditions, mostly in room temperature and atmospheric pressure, in contrast to the high temperature synthetic conditions required for the conventional inorganic compounds. Moreover, the extraordinary flexibility of molecular chemistry allows modulation of novel structures with tunable properties. Rational synthetic strategies have been adopted by the molecular chemists to develop such magnetic materials and thus physicists are provided with model systems to investigate the fundamental magnetic behaviour. Further incorporation of other functionalities like porosity, electrical

conductivity, superconductivity and ferroelectricity into these molecular magnets are in the current focus of materials research community.[3]

1.2 Magnetization and Different magnetic materials

In order to appreciate different magnetic behaviour in coordination compound, first we need to know the basics of magnetism and different types of magnetic materials. Some of the fundamental properties along with different class of magnetic materials are discussed below.

The response of a material to an applied magnetic field, H, is called its *magnetic induction*, B. The relation of B and H is given by the equation $B = H + 4\pi M$, where M is the *magnetization* of the medium and it is defined as the magnetic moment per unit volume, $M = m/V$ emu/cm^3. The variation of the magnetic properties of a material with the applied field defines its magnetic behaviour and is given by the susceptibility (χ). χ is an experimental quantity and indicates how responsive a material is to an applied

Magnetic materials of different kinds and can be classified as diamagnetic, paramagnetic, ferromagnetic and antiferromagnetic, depending on their nature. In case of **diamagnetic** materials, the net magnetic moment is zero, which arises from the closed shell electronic configuration. When an external magnetic field is applied, a net orbital moment is created in opposite direction to the applied magnetic field (Figure 2a). Diamagnetism is an inherent property of all materials because they contain electrons in the closed shell and this property remains unaltered with the variation of temperature (Figure 2b).

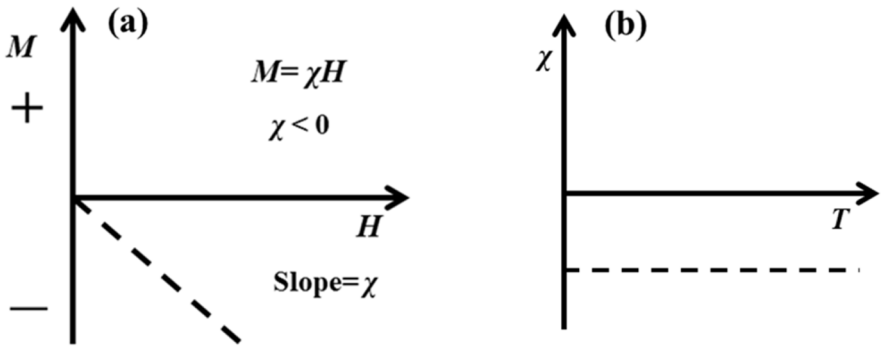

Figure 2. (a) Variation of magnetization versus applied field (dashed line) for a diamagnetic material. (b) Variation of susceptibility with temperature for diamagnetic materials.

For **paramagnetic** materials, individual moments are independent to each other and they are randomly oriented to give net zero magnetization in the absence of applied magnetic field. Paramagnetic materials have a positive magnetic susceptibility and hence in presence of an applied field, they are attracted to magnetic field (Figure 3a).

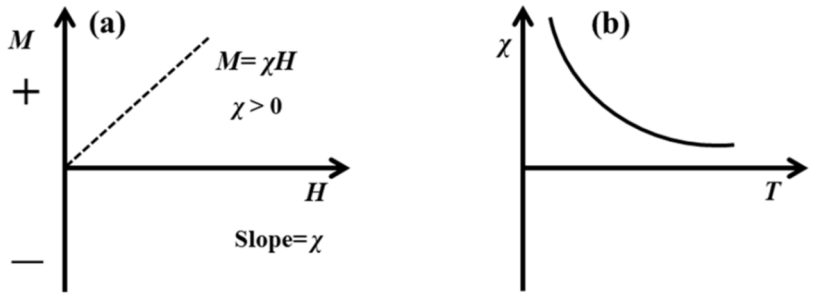

Figure 3. (a) Variation of magnetization versus applied field (dashed line) for a paramagnetic material. (b) Variation of susceptibility with temperature for paramagnetic materials.

The inverse variation of susceptibility with temperature for paramagnetic materials was suggested by Pierre Curie and is given by the equation $\chi = C/T$; where C is the Curie constant. This relation was later modified by Weiss to give a more general equation:

$\chi = C/(T-\theta)$; θ is called Weiss constant.

Weiss postulated existence of an internal interaction between the localized moment and he termed this interaction as a "molecular field." A positive value of θ indicates that the molecular field is acting in the same direction as the applied field; this tend to the elementary magnetic moments align parallel to each another and to the applied field. Negative value for θ suggests the existence of a negative Weiss molecular field, which causes the moments to anti-align. In **ferromagnetic** materials, individual moments are coupled to each other by means of exchange forces, which ensue spontaneous magnetization even in the absence of applied magnetic field. When a ferromagnetic material is in its demagnetized state, the magnetization vectors in different domains have different orientations and the total magnetization averages to zero. During the process of magnetization, a single domain is formed when magnetization flips in the applied magnetic direction and the saturation magnetization (M_s) is reached. The variation of magnetization versus magnetic field for a ferromagnetic material exhibits a hysteresis loop (Figure 4). At high enough temperature thermal energy can extinguish the exchange interaction of a ferromagnetic material resulting paramagnetism. The particular

temperature at which a ferromagnetic material becomes paramagnetic is called Curie temperature (T_C). Below T_C, the material is magnetically ordered and above T_C it obeys Curie-Weiss law with a positive value of Weiss constant. For **antiferromagnetic** materials, the interaction between the magnetic moments tends to align adjacent moments antiparallel to each other. Antiferromagnetism can be pictured as two interpenetrating and identical sublattices of magnetic ions, where the net moment of individual sublattices are same in magnitude but opposite in direction. Antiferromagnetic material remains in the ordered magnetic state below its Neel's temperature (T_N). Above T_N, it exhibits paramagnetic behaviour, as a consequence of the thermal effect (Figure 5). The paramagnetic state can be fitted to Curie-Weiss law with negative value of Weiss constant.

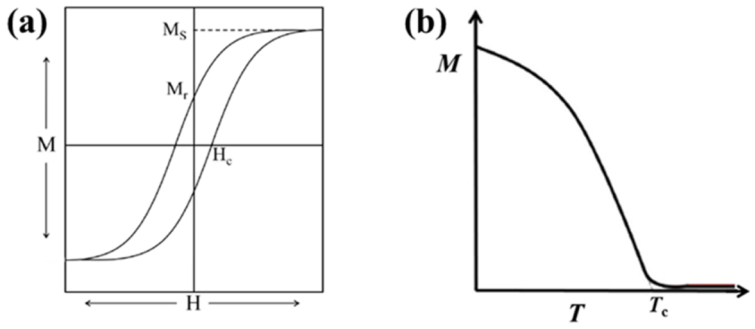

Figure 4. (a) Hysteresis loop of a typical ferromagnetic material, where H_c = Coercive field, M_r = Remnant magnetization and (b) M versus T plot for a ferromagnetic material.

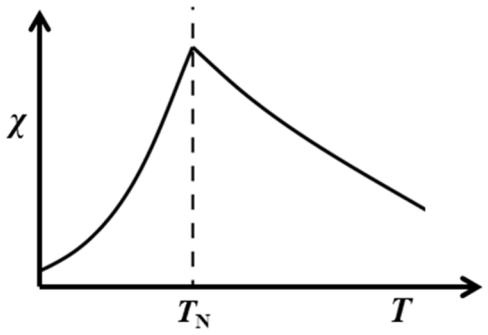

Figure 5. Variation of susceptibility for an antiferromagnetic material.

Sometimes, the antiferromagnetic spins are not perfectly aligned in an antiparallel fashion, but are canted by a few degrees. This **spin-canting** gives rise to a weak net

moment. In spin-canted system, magnetic anisotropy and antisymmetric exchange result into canting of the spins because the coupling energy is minimized when the two spins are perpendicular to each other. In **ferrimagnetism**, spins are also aligned antiparallel, but the magnitudes of the moments in each direction are unequal. Ferrimagnets can be viewed as a material containing two interpenetrating lattice of magnetic ions where the magnetic moments of the atoms on different sublattices are opposed, as in the case of antiferromagnets, but for ferrimagnetic materials the opposing moments are unequal and a spontaneous magnetization remains. Spin alignments for different types of magnetic materials are presented in Figure 6.

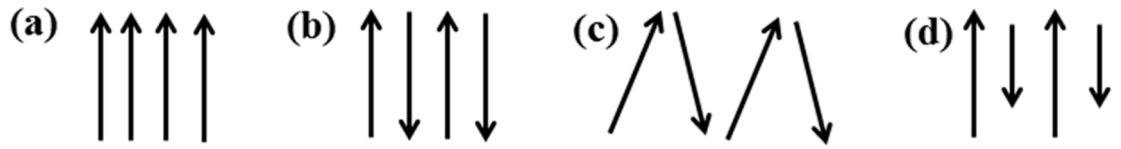

Figure 6. Arrangement of spin moments in (a) ferromagnetic, (b) antiferromagnetic, (c) canted antiferromagnet and (d) ferromagnetic material.

1.3 Magnetism in Coordination Compounds

1.3.1 Superexchange Mechanism

As we have mentioned earlier, magnetism has played a central role in the solid state chemistry of metal-organic compounds. These compounds possess inorganic-organic structure containing metal ions/clusters linked by ligands (inorganic or organic) and can be of different dimensionality, ranging from zero dimensional clusters to higher dimensional networks, such as 1D chains, 2D sheets and 3D frameworks. Prussian blue, $Fe^{III}_4[Fe^{II}(CN)_6]_3 \cdot nH_2O$ would be the history's first coordination compound, which has a 3D face centred cubic framework based on hexacyanoferrate and was accidentally synthesised by Heinrich Diesbach in Berlin in 1974 and later ferromagnetic ordering at 5.6 K was also observed for the same.[5] Thereafter, intensive studies on novel metal-organic compounds have been continued to explore their importance as molecule based magnetic material. Before discussing the different magnetic behaviour of these compounds, we should understand first how the magnetic interaction is established in these compounds. The magnetic coupling of metal centres is mainly mediated by the ligand orbital via superexchange mechanism. This superexchange mechanism is summarized on the basis of the Goodenough–Kanamori rules[6], which was a breakthrough

discovery during the 1950s. This rule includes consideration of the bond angle and the symmetry of the metal and ligand orbitals concerned. There are two mechanisms for superexchange interactions: the kinetic exchange mechanism (J_{KE}) and the potential exchange mechanism (J_{PE}).[7] Kinetic exchange is mediated by a direct pathway of the overlapping orbitals, which connects the two interacting magnetic orbitals. It is antiferromagnetic in nature as a consequence of the Pauli principle, leading to an antiparallel spin ordering via a common covalent bond. On the other hand, potential exchange is effective between orthogonal magnetic orbitals with comparable orbital energy. The mechanism producing ferromagnetic interaction is indeed the exchange energy that gives rise to Hund's rules leading to a parallel spin alignment, i.e. ferromagnetic interaction. In this case, the exchange energy is minimized if all the electrons have the same spin alignment.

To understand the superexchange mechanism, let us take the example of Prussian blue analogues. In this case, the metal *d*-orbitals split into t_{2g} and e_g set by the CN ligands. Therefore, based on magnetic orbital symmetry, we can understand whether the orbital superexchange among each of the orbitals on metal ions is J_{KE} or J_{PE}. When the magnetic orbital symmetries of the metals are the same, the superexchange interaction is J_{KE}. Conversely, when the magnetic orbital symmetries of the metals are different, the superexchange interaction is J_{PE}. The total superexchange interaction is given by the sum of all of the orbital exchange contributions between the transition metal ions (Figure 7).

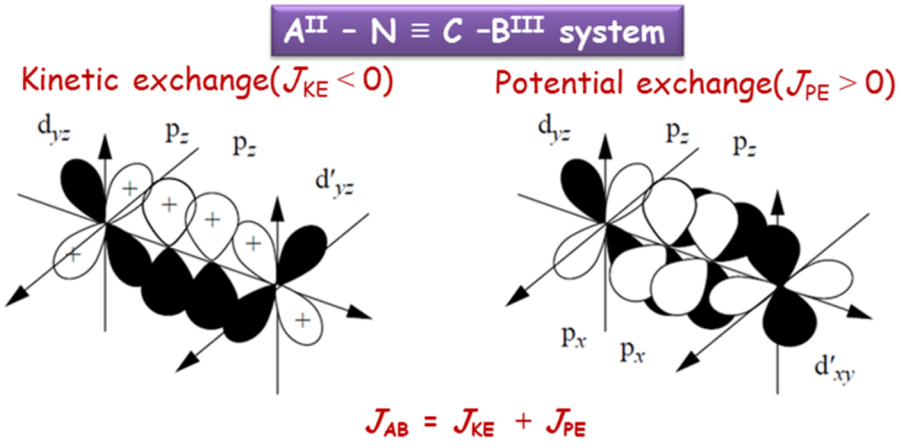

Figure 7. The two basic mechanisms for the isotropic exchange in the magnetic coupling between the A^{II} and B^{III} ions in the CN-bridged complex. Kinetic exchange (J_{KE}) pathways ($d_{yz}\| \pi_z \| d_{yz'}$) dominate in the left one, while on the right is one of significant potential exchange (J_{PE}) pathways ($d_{yz}\| \pi_z \perp \pi_x \| d_{xy'}$). The superexchange coupling between A^{II} and B^{III} (J_{AB}) involves a superposition of J_{PE} and J_{KE}.

For example, let us consider the case of the hexacyanochromate cyanide $A^{II}_{y}[Cr^{III}(CN)_6]$, with Cr^{III} being $(t_{2g})^3$ and S_{Cr}= 3/2 . There is no overlap between Cr^{III} and A^{II} magnetic orbitals, if all of the magnetic orbitals of A^{II} have e_g symmetry. In this situation, the potential exchange mechanism becomes dominant, leading to a ferromagnetic interaction between Cr^{III} and A^{II}. In case of $Cs^{I}Ni^{II}[Cr^{III}(CN)_6]$, a high-spin state exists for $Ni^{II}((t_{2g})^6(e_g)^2$, S_{Ni} = 1), and ferromagnetic interaction operates between Cr^{III} and Ni^{II}.[14b] In contrast, when all of the A^{II} magnetic orbitals have t_{2g} symmetry, the overlap between the t_{2g} (A) and t_{2g} (Cr) orbitals gives rise to kinetic exchange, leading to an antiferromagnetic interaction. In $Cs^{I}Mn^{II}[Cr^{III}(CN)_6]$, with a high-spin state for $Mn^{II}((t_{2g})^3(e_g)^2$, S_{Mn}= 5/2), the interaction between Cr^{III} and Mn^{II} is antiferromagnetic, and the compound is a ferrimagnet.

The succeeding discussion will try to give an overview of the magnetic clusters and higher dimensional networks, some of which can also serve as multifunctional materials and model compounds in biological systems.

1.3.2 Magnetic Molecular Clusters

Homo or hetero-metallic clusters are zero dimensional compounds and can be constructed by various types of organic ligands. In biological systems, these clusters are quite important because of their involvement in several catalytic processes in living organisms.[8] For example, multicopper oxidases (*e.g.*, ascorbate oxidase and laccase) contain a triangular unit of copper atoms. In regard to molecular magnetism, cluster based compounds have drawn immense interests as they can serve as model compounds to understand low-dimensional magnetism and frustrated magnetic systems[9]. Different kind of exchange interactions can be established in these clusters, depending on the structural parameters, such as metal-ligand bridging mode, bond angle and bond distances etc. Hydroxido, alkoxido or phenoxido bridged Cu(II) clusters[10] have been investigated widely and the bond angles are significant factor to determine the nature of exchange interaction in these compounds. Orthogonality of the magnetic orbitals can results into ferromagnetic behaviour and experimentally, for Cu–O–Cu < 97.5°, the ground state is a triplet state.[10] When X is made less electronegative, the orthogonality is realized for larger value of Cu–X–Cu angle.

Pseudohalides have also been proved to be very proficient ligands to design novel structures that exhibit interesting magnetic properties and the azide based clusters deserve

special attention with the opportunity of exploring novel structures that exhibit interesting magnetic properties.[11] Different kind of exchange interaction can be achieved depending on the diverse binding modes of azide. The most commonly observed bridging modes are the end-to-end (EE) and end-on (EO). The EE mode mainly exhibit antiferromagnetic interaction with a few exceptions while the EO mode can mediate both ferro and antiferromagnetic interactions depending on the metal–N–metal bond angle.[12] Calculations based on density functional theory (DFT) predicted that EO mode can exhibit antiferromagnetic behaviour if the metal–N_{EO}–metal angle is above the critical angle 104°.[12] Spin polarization through the π_g orbital of azide group is believed to another important factor to control the nature of exchange interaction in Cu-azide systems.[13,14] Figure 8 illustrates this mechanism. For the EO binding mode, the electron on the bridging nitrogen (with the α spin, as shown in Figure 8a) is partially delocalized toward the d_{xy} orbitals of metals resulting each unpaired electron localized in its magnetic orbital to have a probability of β spin higher than 0.5. This favours the ferromagnetic interaction. In case of EE mode, if an α spin is delocalised toward $(d_{xy})_A$, a β electron would be symmetrically delocalized toward $(d_{xy})_B$ (Figure 8b). Thus, the unpaired electron around A will have a probability of β spin higher than 0.5 and the unpaired electron around B will have a probability of α spin higher than 0.5, resulting the antiferromagnetic interaction.

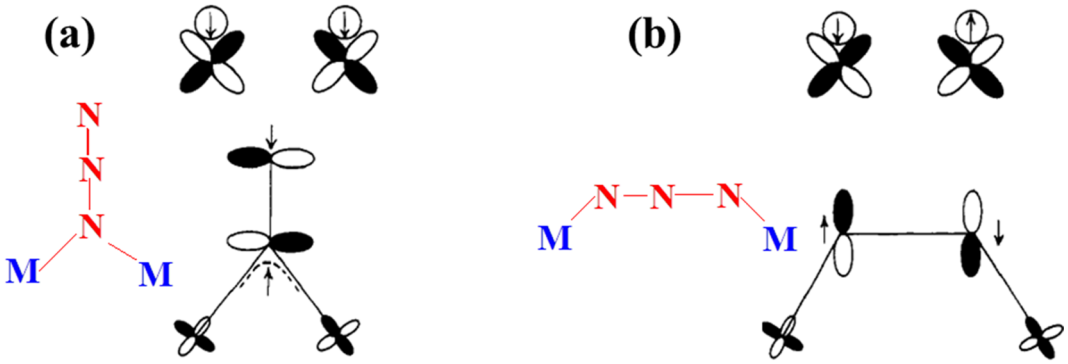

Figure 8. Spin polarization through the π_g orbital of azide in (a) EO and (b) EE mode.[14]

A large number of metal-azide cluster of different nuclearity have been reported by various research groups and their magnetic behaviour depends on the above discussed factors. However, there are cases where exceptional behaviour have been exhibited by many compounds and the general rules are not always satisfied. A dimer $[Cu_2L_2(N_3)_2]$ (L

= 1-(*N*-salicylideneamino)-2-aminoethane), shows antiferromagnetic interaction which has a Cu-N_{EO}-Cu angle of 89.1°[11l], where antiferromagnetism generally arise only when the Cu-N_{EO}-Cu angle is greater than 104°. In this compound, Cu centres are connected through an end-on bridge where the N_{EO} occupies the basal plane of one Cu centre but occupies apical position of the other Cu. Moreover, the Cu–N_{EO} distance is quite higher than the critical Cu–N distance for the interaction being ferromagnetic. These factors cumulatively result in the observed weak antiferromagnetic behaviour. Karmakar *et al.* have reported another interesting Ni-azido complex $[Ni_4(\mu_2\text{-}N_3)_4(\mu_3\text{-}N_3)_2(N_3)_2(enbzpy)_2]\cdot 2H_2O$ (enbzpy = [*N*,*N*-bis(pyridin-2-yl)benzylidene]ethane-1,2-diamine), which contains a tetranuclear double-open dicubane structure (Figure 9a).[11m] In this compound, doubly and triply bridged EO azide groups result in a global ferromagnetic behaviour (Figure 9b).

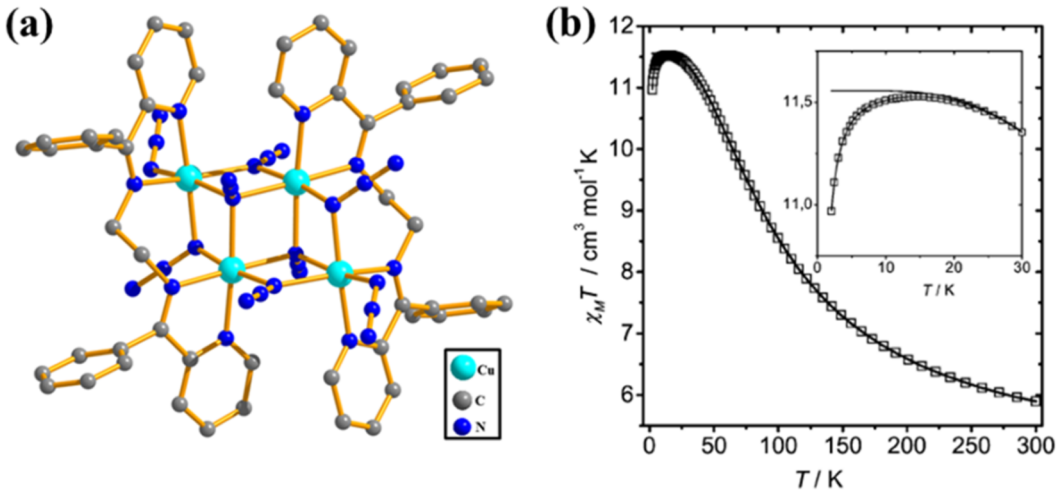

Figure 9. (a)Tetranuclear dicubane Ni-azide complex and (b) the plot of $\chi_M T$ *vs.* *T* for this compound. The line represents the best fit and the points the experimental data. The theoretical behaviour of a fully isotropic ferromagnetic Ni_4 cluster is included as a dotted line in the inset. From reference 11m. Reproduced by permission of The Royal Society of Chemistry.

Antiferromagnetic compounds with a frustrated lattice have been of a long term interest to understand **spin frustration** mechanism. Trinuclear or tetranuclear cluster based hybrid compound can exhibit geometric frustration. For a triangular antiferromagnetic lattice, it is evident that only two of the three spin constrains can be satisfied simultaneously, leading to spin frustration (Figure 10a). In Figure 10b, the tetrahedron comprised of four edge-sharing equilateral triangles is also a geometrically frustrated system, as only two of the four equivalent nearest neighbour interactions can be satisfied simultaneously.

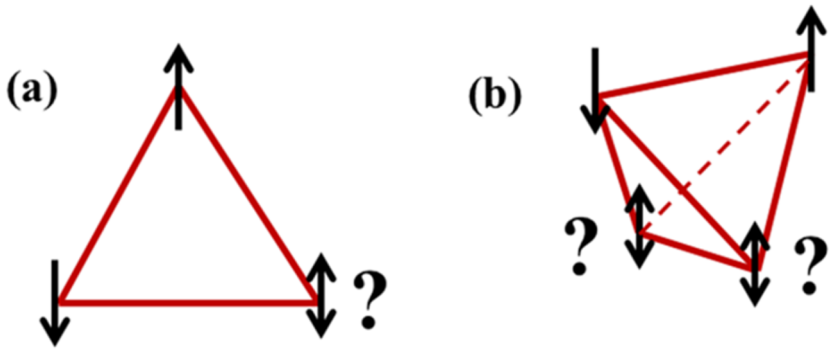

Figure 10. Spin frustration in (a) equilateral triangle and (b) tetrahedron.

A number of compounds have been reported with a trinuclear and tetranuclear core. Special attentions have been devoted to construct S=½ triangular lattice with the pursuit of magnetic frustration.[14c] Ghosh *et al.* have reported two trinuclear complexes $[(CuL_3)_3\text{-}(\mu_3\text{-}OH)](ClO_4)_2{\cdot}H_2O$ and $[(CuL_4)_3(\mu_3\text{-}OH)](ClO_4)_2{\cdot}H_2O$ where HL_3 = 7-(ethylamino)-4-methyl-5-azahept-3-en-2-one, and HL_4 = 4-methyl-7-(methylamino)-5-azahept-3-en-2-one, which were derived from tridentate Schiff bases (HL_3 and HL_4). At low temperature, these compounds exist in spin frustrated doublet state, as evidenced from the EPR spectra at 4 K.

Study on the magnetic clusters have been boosted after the discovery of **single molecule magnets** (SMMs).[15] These are isolated or discrete molecules which have a large ground state spin and a high negative magnetic anisotropy. These features give rise to a high barrier for switching from total spin up to total spin down at low temperatures (specifically below the 'blocking temperature', T_B, below which relaxation is slow). These compounds are promising for high density information storage and quantum computation,[16] as the magnetic information is being stored at a molecular level and potentially the density of information being stored could be increased by several order of magnitude. Molecular clusters exhibiting SMM behaviour have attracted considerable research interest not only due to their promising applications, but also because of the unique opportunity to understand the classical/quantum interplay. The first compound to exhibit SMM is the "Mn_{12}" cluster, which was discovered by Gatteschi and co-workers (S =10 ground state; T_B = 10 K).[15a] A series of compounds containing Mn_{12} clusters with the general formula $[Mn_{12}O_{12}(RCOO)_{16}(H_2O)_x]Y$, where Y= solvent molecules, and R= alkyl or phenyl groups have also been synthesized. In an attempt to increase the ground state spin, and thus to improve the properties of the SMM, bigger clusters of transition metal ions have been developed. Christou *et al*. have reporetd a Mn_{25} cluster with the formula

$[Mn_{25}O_{18}(OH)_2(N_3)_{12}(pdm)_6(pdmH)_6](Cl)_2.12MeCN$ which exhibits SMM behaviour.[15h] The same group successfully fabricated a Mn_{84} cluster using top-down approach.[15i] Lanthanide based SMMs also have gained significant interests due to their large magnetic anisotropies. However, achieving high-spin ground states is difficult with purely lanthanide based systems, as they tend to form ionic bonds that limit magnetic exchange coupling. In contrast, transition-metal SMMs usually possess high-spin ground states, but insufficient magnetic anisotropies. To overcome this problem, a possible way out is the design of heterometallic clusters. This approach began with the report of a Mn_8Ce cluster.[15j] The complex and different possible exchange interactions between the different metal centers have made the magneto-structural study of heterometallic clusters really attractive.[17] Though a good number of reports have appeared in recent past concerning the study of heterometallic clusters, there are much to explore in this field in order to truly appreciate the underlying complex magnetic interaction.

1.3.2 Higher Dimensional Networks: Magnetism and Multifunctionality

Higher dimensional compounds such as 1D chains, 2D networks and 3D frameworks are of particular interest because of their novel topology, interesting magnetic behaviours and enhancement of bulk magnetic properties. One interesting class of 1D compounds are Single Chain Magnets (SCMs). In these compounds, significant magnetic anisotropy is present and the 1D chains are well separated from each other, which result in the slow relaxation of magnetization. With the quest of theoretical understanding of the SCM behaviour, the study of SCMs have attained significant importance.[18]

There have been continuous efforts to design higher dimensional compounds, specially 3D frameworks. This is because of the fact that bulk magnetism is intrinsically a three-dimensional (3D) property and thus to achieve spontaneous magnetization beyond a certain temperature (T_c), it is necessary to develop a 3D lattice of interacting magnetic centres. However, construction of such systems is not always straightforward. Different strategies have been perceived by the synthetic chemists to solve this problem. Higher dimensional Cu-azide systems have been widely investigated[11] and still remains as a fascinating research topic with the opportunity of exploring interesting magnetic properties. Further extension of metal-azide assemblies have been carried out by using neutral organic linkers with a few recent examples where ionic organic linkers have also been used.[19] Alternatively, the use of more azide anion by addition of a countercation,

such as $N(CH_3)_4^+$ has also been established.[20] Introduction of an auxiliary blocking ligand can be another fruitful approach, as the relative molar quantities of blocking ligand and azide have strong influence on the bridging mode of the azido ligand and the dimensionality of polynuclear metal-azido systems.[20c]

Several oxygen-bridged magnetic frameworks have been constructed based on oxides, hydroxides, phosphates, phosphites, sulfates, and carboxylates ligand to invoke magnetic interaction.[21] In such systems, organic molecules are either small or extended polytopic ligands, but the magnetic properties are governed by the M–O–C–O–M or M–O–M structural motifs, which lead to strong interactions compared to the magnetic pathways defined by bridged metal ions through multitopic ligands. Different magnetic behaviour have been observed by different compounds and those which exhibit ferromagnetic properties have attained considerable interest. A chiral 3D nickel glutarate, $[Ni_{20}(H_2O)_8(C_5H_6O_4)20\cdot 40H_2O]$ shows pure co-operative ferromagnetic behaviour (Tc ≈ 4 K), without any spin frustration.[22a] The low Tc value is due to the weakening of the ferromagnetic interaction for a Ni–O–Ni bridge angle significantly larger than 90°. A 3D framework $Co_5(OH)_6(SO_4)_2(H_2O)_4$ which consists of M^{II}-OH layers of edge-sharing octahedra, which are pillared by $O_3SO\text{-}Co(H_2O)_4\text{-}OSO_3$, shows ferromagnetic behaviour with a Curie temperature of 14 K.[22b] A strong magnetic exchange is provided via Co-O-Co pathways on a triangular lattice and weak Co-O-S-O-Co interlayer exchange through the pillar. Neutron diffraction data suggests long-range ordering of only the moments within the layer, while the one between the layers is random.

Ferrimagnetic and canted behaviour have also been observed in a large number hybrid compounds. Kurmoo *et al*. reported a cobalt 1,4-cyclohexane dicarboxylate, $[Co_5(OH)_8(CHDC)\cdot 4H_2O]$, (chdc = *trans*-1,4-cyclohexanedicarboxylate)[23], that contains metal–hydroxide octahedral–tetrahedral layers pillared by chdc. 1-D channels situated between the chdc pillars are occupied by noncoordinated water molecules.

Single crystalline nature of the material retains during dehydration from $[Co_5(OH)_8(CHDC)\cdot 4H_2O]$ to $Co_5(OH)_8(CHDC)$ via an intermediate $[Co_5(OH)_8(CHDC)\cdot 2H_2O]$ upon heating or evacuation. The magnetic susceptibility data of both the hydrated and dehydrated compound indicates ferrimagnetic behaviour with a T_c of 60 K (Figure 11a). The value of the saturation magnetization at 2 K is explained by

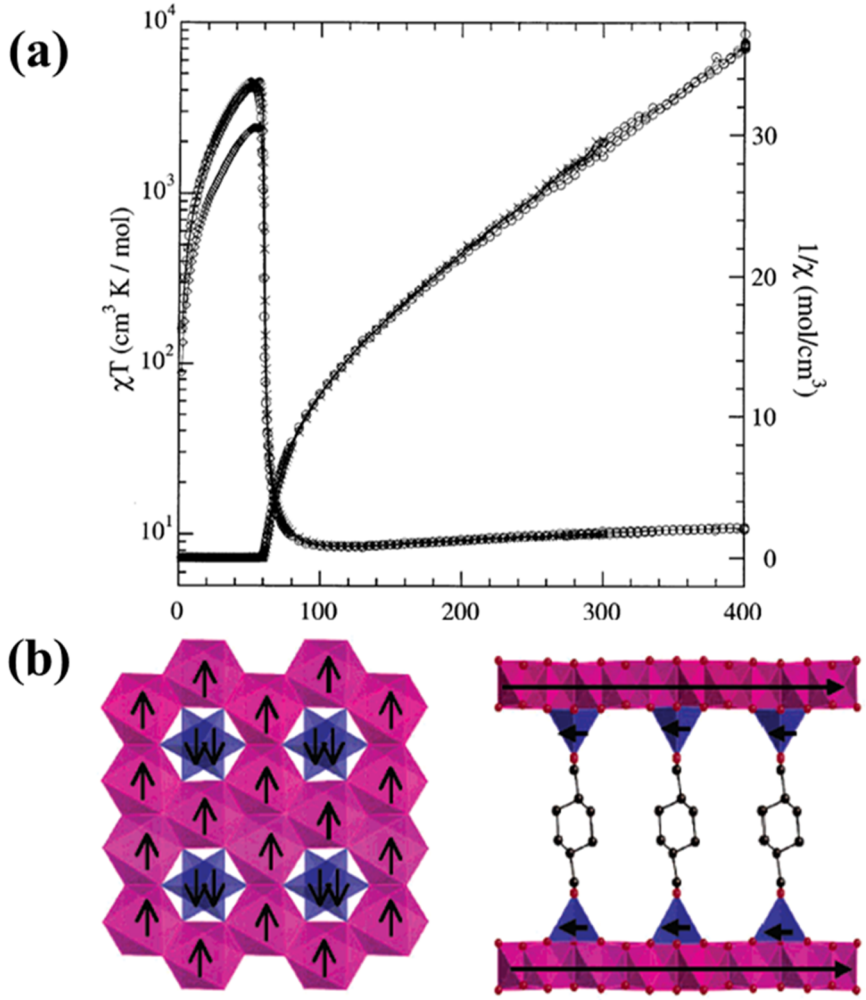

Figure 11. (a) temperature dependence of the inverse magnetic susceptibility and of the product of susceptibility and temperature: virgin (O), dehydrated (X) and rehydrated (♦) and (b) Diagrammatic representation of the proposed magnetic ordering at the tetrahedral and octahedral cobalt(II) sites in $[Co_5(OH)_8(CHDC)\cdot 4H_2O]$ Reprinted with permission from reference 23.

a model of two sublattices, one containing three octahedral cobalt atoms and another comprising two tetrahedral cobalt atoms (Figure 11b).

Spin canting in hybrid material can arise from magnetic anisotropy and antisymmetric Dzyaloshinsky–Moriya (DM) interaction.[24] The DM term arises from the spin-orbit coupling resulting the antisymmetric interaction and the Hamiltonain is $H = D_{ij}\cdot[S_i \times S_j]$, while the Hamiltonian used to describe a symmetric exchange between normal antiferromagnetically coupled spins S_i and S_j is given as $H = -2J\sum S_i \cdot S_j$. This anisotropy and the antisymmetric interaction are indeed intrinsic effects due to the particular crystal symmetry. Judicious choice of appropriate system satisfying these factors thus can lead to spin canting behaviour. In this regard, two isomorphous compounds, $[M_2(L)_2(H_2O)_2]_n$ (M= Co, Ni; L = 2,1,3-thiadiazole- 4,5-dicarboxylate) were reported by Batten *et. al*.[25]

The Co^{II} compound shows spin-canted antiferromagnetism while simple antiferromagnetic coupling is observed for the Ni^{II} analogue. Below 6 K, the $\chi_M T$ *vs.* T plot of Co^{II} compound exhibits a rapid increase (Figure 12a), which is due to the long range ordering. The plot of reduced magnetization *vs*. temperature, the field dependence of $\chi_M T$ and the ac susceptibility data also confirm the spin canted behaviour (Figure 12).

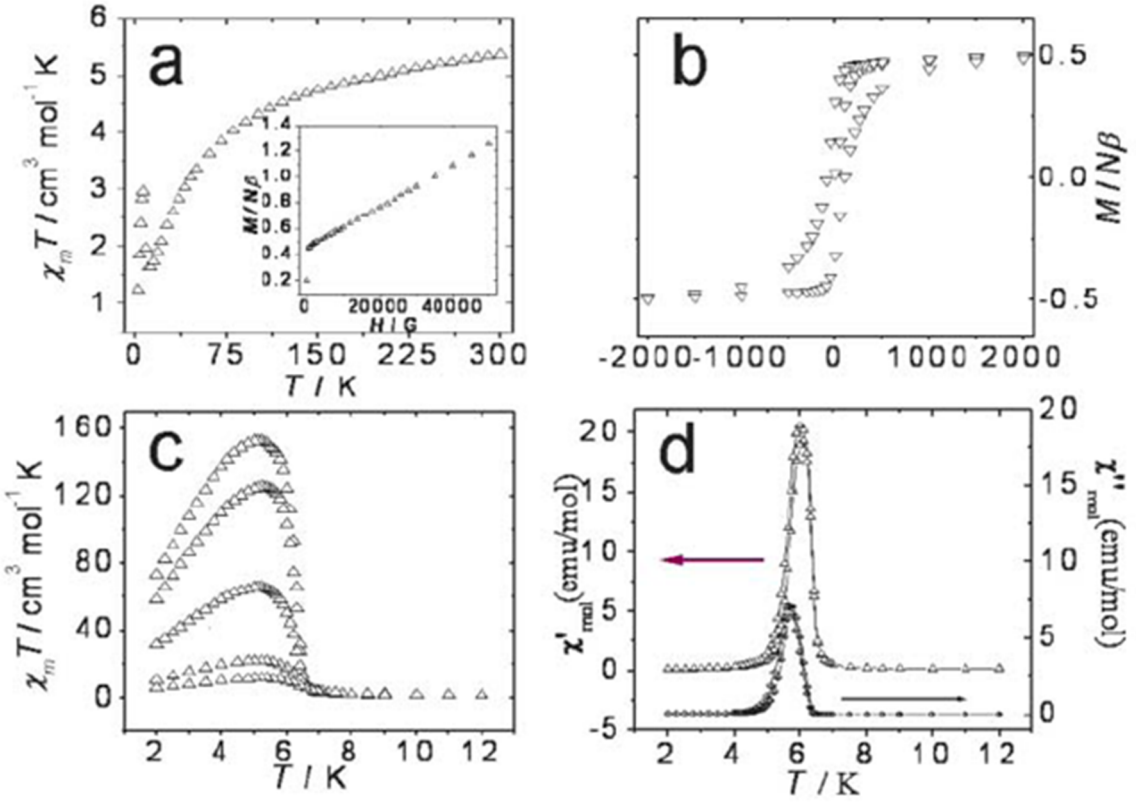

Figure 12. Magnetic behaviour of the Co^{II} compound. (a) $\chi_M T$ *vs.* T plot (insert: plot of the reduced magnetization at 2 K). (b) Hysteresis loop. (c) $\chi_M T$ *vs.* T plots at different fields (from 1000 to 50 G) in the low temperature region. (d) Plot of the ac susceptibility. From reference 25. Reproduced by permission of The Royal Society of Chemistry.

The antiferromagnetic nature of the Ni^{II} compound is reflected in its $\chi_M T$ *vs.* T plot (Figure 13). Despite the structural similarity, the different behaviour of these compounds originates from the difference in anisotropy of the two metal ions. Antisymmetric exchange interaction being of the same order for these isomorphous compounds, the much higher single ion anisotropy of Co^{II} than the Ni^{II} ions results in spin canting in the Co^{II} compound.

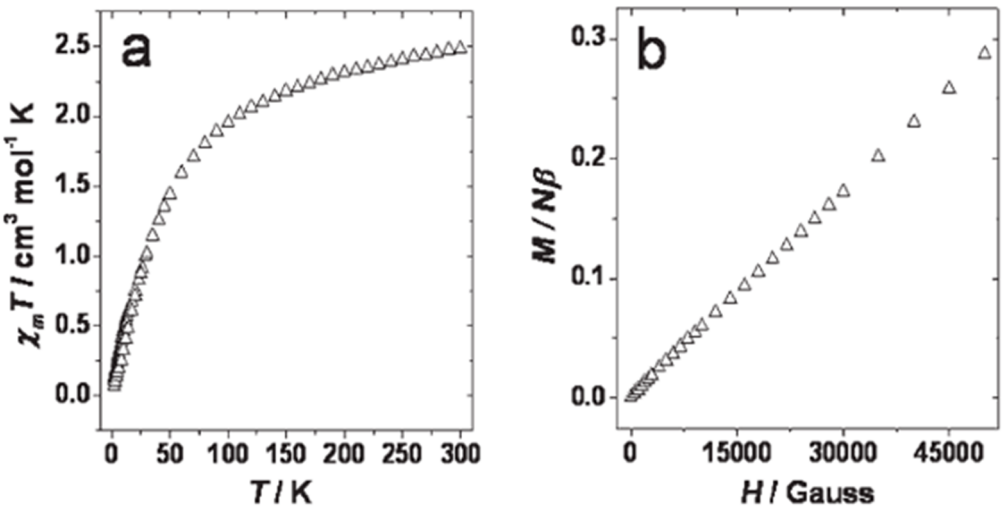

Figure 13. (a) Plot of $\chi_M T$ *vs.* T and (b) the reduced magnetizationat 2 K for the Ni^{II} compound. From reference 25. Reproduced by permission of The Royal Society of Chemistry.

Incorporation of other functionalities such as ferroelasticity,[26] non-linear optical effects,[27] chemical storage[28] into such magnetic materials have always been an attractive goal. Development of such new material requires the combination of properties within the same material. Among these multifunctional materials, designs of porous magnet have attracted special attention.[29] It is a real challenge to construct a material where two opposing properties, porosity and long range magnetic ordering are present because of the fact that magnetic exchange generally requires short bridges between the spin carriers, whereas porosity usually rely on the use of long connecting ligands. Introduction of organic linkers can be an efficient and rational approach to introduce porosity (Figure 14).

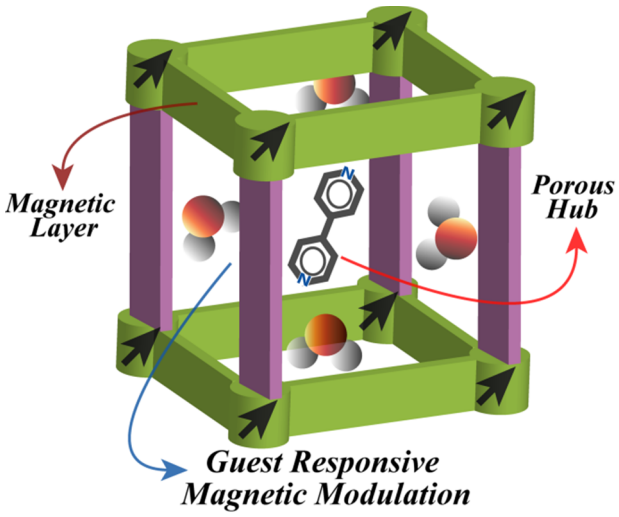

Figure 14. Bimodal functionality (porosity and magnetism) in a framework material. From reference 30. Reproduced by permission of The Royal Society of Chemistry.

An interesting example is a 3D porous framework $\{[Mn_3(bipy)_3(H_2O)_4][Cr(CN)_6]_2 \cdot 2(bipy) \cdot 4(H_2O)\}_n$ (bipy= 4.4′-bipyridyl)[30] which shows ferrimagnetic behaviour. In this compound, cyanometallate anion $[Cr(CN)_6]_3^-$ is used as magnetic hub while use of long linker 4,4′-bipyridyl helps to invoke porosity. Porous magnets can exhibit striking features like unique change in the magnetic properties with response to the adsorption/desorption of guest molecules. Kurmoo *et al.* have reported a reversible crystal-to-crystal transformation accompanied by change from ferromagnetic to antiferromagnetic ground states at 8 K, upon dehydration-rehydration in a nanoporous MOF $[Co^{II}_3(OH)_2(C_4O_4)_2] \cdot 3H_2O$.[31] The later compound sustains its void volume without structural destruction and exhibit transformations between different magnetic ground states following water adsorption–desorption.

The incorporation of electronic switches, in the form of spin crossover (SCO) centres, into microporous solids can exhibit interesting guest dependent behaviour. In the SCO compounds, depending on the relative magnitude of the orbital splitting energy (Δ) and the electron pairing energy (P), the compound can exist in the high-spin state ($\Delta < P$) or in the low-spin state ($\Delta > P$). The electronic configuration of the metal centre can be changed (high spin↔low spin), as a result of the perturbation caused by the change in

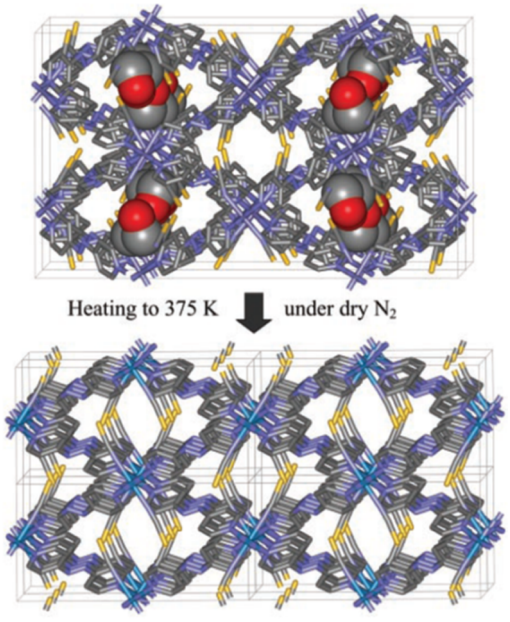

Figure 15. X-ray crystal structures of 1·(EtOH) at 150 K and **1** at 375 K, viewed approximately down the 1-D channels (*c* axis). Framework atoms are represented as sticks and atoms of the ethanol guests as spheres. Removal of ethanol by heating gives single crystals of **1**, which has empty, equivalent 1-D channels and a concomitant quartering of the unit cell. Hydrogen atoms are omitted for clarity. Reproduced by permission from reference 33.

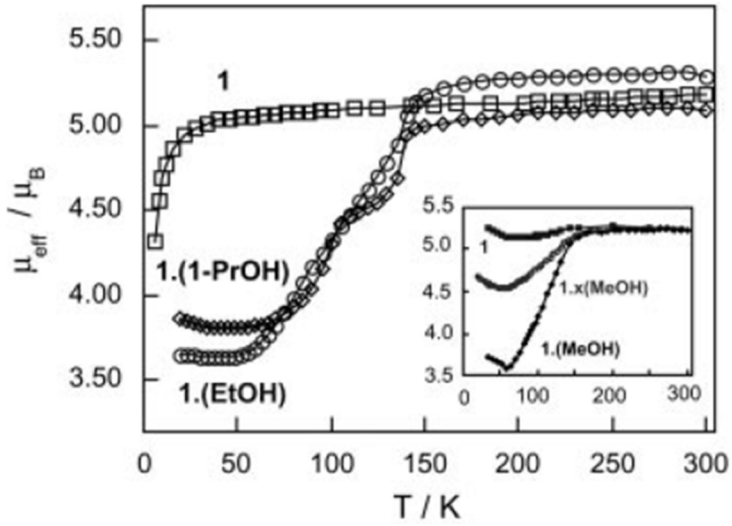

Figure 16. The temperature-dependent magnetic moment of 1·x(guest), recorded on a single sample at different stages of guest desorption and resorption, showing 50% spin crossover behaviour between 50 and150 K for the fully loaded phases and an absence of spin crossover for the fully desorbed phase **1**. The ethanol and methanol- loaded phases undergo a single step spin crossover, whereas the 1-propanol adduct shows a two-step crossover with a plateau at 120 K. Reproduced by permission from reference 33.

temperature, pressure, light irradiation or magnetic field.[32] A fine control between Δ and *P* required for spin crossover is exhibited by the compound $Fe_2(azpy)_4(NCS)_4$·(EtOH) (1·EtOH; azpy is *trans*-4,4'–azopyridine and EtOH is ethanol), which was reported by Halder *et al* (Figure 15).[33] This compound consists of two interpenetrated lattices made of two-dimensional rhombic grids. When the guest EtOH molecules are present in the lattice, approximately half of the iron atoms in the lattice undergo a spin crossover beyond 150 K, but no spin crossover is observed when the guest molecules are removed, even though the guest molecules are not bound to any of the iron(II) atoms (Figure 16).

The loss of guest molecules results a considerable rearrangement of the lattice, with the crystals expanding in volume by 6%, while the volume of the pores relative to the total volume of the crystal drops from 12% to 2%. The sample retains its single-crystalline behaviour throughout the transition. Crystallinity is retained even when the guest molecules are reabsorbed and the original structure is regenerated. It is suggested that hydrogen bonds between the alcohol guests and other ligands on the iron atoms are responsible for the change in SCO behaviour.

1.4 Outlook

Major advances have been made in the field of molecular magnetism and multifunctional coordination compounds over the last two decades and a large number of

reports have appeared on both the description and applications of such materials. Improvement of their properties such as increasing the T_c and finding potential gas adsorbents under ambient condition are the present challenges to the material scientists. However, proper understandings of the elemental magnetic exchange behaviour and chemical nature of these compounds still require further investigations. Scientists will continue to use their perception, backed to the fundamental theories to predict and furnish new materials with versatile properties.

This thesis has tried to describe some of the fascinating behaviours exhibited by such molecular materials, along with the fundamental understandings. In particular, the succeeding discussions of this thesis will focus on the magneto-structural correlation of homo/hetero-metallic clusters and extended networks consisting of polynuclear building blocks, long-range ordering in three-dimensional frameworks and further incorporation of other functionalities (like porosity) into such magnetic materials.

1.5 REFERENCES

[1] (*a*) M. Kurmoo, *Chem. Soc. Rev.,* 2009, **38**, 1353; (*b*) D. Maspoch, D. Ruiz-Molina and J. Veciana, *Chem. Soc. Rev*., 2007, **36**, 770; (*c*) D. Maspoch, D. Ruiz-Molina and J. Veciana*, J. Mater. Chem.*, 2004, **14**, 2713; (*d*) G. Li, Y. Xing, S. Song, N. Xu, X. Liu and Z. Su, *J. Solid State Chem*., 2008, **181**, 2406.

[2] J. S. Miller, *Adv. Mater*., 1990, **2**, 98.

[3] E. Coronado, P. Delhaes, D. Gatteschi and J. S. Miller, Dordrecht, *Molecular magnetism: From the molecular assemblies to the Devices*, NATO ASI series no. E321, Dordrecht, 1996.

[4] J. S. Miller and A. J. Epstein, *Angew. Chem. Int. Ed.*, 1994, **33***,* 385.

[5] W. E. Buschmann, J. Ensling, P. Gulich, J. S. Miller, *Chem. Eur. J.*, 1999, **5**, 3019.

[6] (*a*) J. B. Goodenough, *Phys. Rev.*, 1959, **100**, 564; (*b*) J. B. Goodenough, *J. Phys. Chem. Solids*, 1958, **6**, 287; (*c*) J. Kanamori, *J. Phys. Chem. Solids*, 1959, **10**, 87.

[7] (*a*) A.P. Ginsberg, *Inorg. Chim. Acta. Rev.*, 1971, **5**, 45; (*b*) S. Ohkoshi and K. Kasimoto, *J. Photochem. Photobiol. C*, 2001, 71.

[8] (*a*) E. I. Solomon, U. M. Sundaram and T. E. Machonkin, *Chem. Rev*., 1996, **96**, 2563; (*b*) R. H. Holm, P. Kennepohl and E. I. Solomon, *Chem. Rev*., 1996, **96**, 2239; (*c*) W. Kaim and J. Rall, *Angew. Chem. Int. Ed*., 1996, **35**, 43.

[9] John E. Greedan, *J. Mater. Chem.*, 2001, **11**, 37.

[10] (*a*) M. P. Suh, M.Y. Han, J. H. Lee, K. S. Min and C. Hyeon, *J. Am. Chem. Soc*., 1998, **120**, 3819; (*b*) E. Ruiz, P. Alemany, S. Alvarez and J. Cano, *J. Am. Chem. Soc*., 1997, **119**, 1297.

[11] (*a*) Y. Song, S. Ohkoshi, Y. Arimoto, H. Seino, Y. Mizobe and K. Hashimoto, *Inorg. Chem.*, 2003, **42**, 1848; (*b*) M. A. M. Abu-Youssef, A. Escuer, M. A. S. Goher, F. Mautner, G. J. Reib and R. Vicente, *Angew. Chem. Int. Ed.*, 2000, **39**, 1624; (*c*) X. T. Liu, X. Wang, W. -X. Zhang, P. Cui and S. Gao, S. *Ad*v. *Mater.* 2006, **18**, 2852; (*d*) T. F. Liu, D. Fu, S. Gao, Y. Z. Zhang, H. L. Sun, G. Su and Y. -J. Liu, *J. Am. Chem. Soc.* 2003, **125**, 13976; (*e*) C. S. Hong, J. -E. Koo, S. -K. Son, Y. S. Lee, Y.-S. Kimand and Y. Do, *Chem. Eur. J.* 2001, **7**, 4243; (*f*) H. H. Ko, J. H. Lim, H. C. Kim and C. S. Hong, *Inorg. Chem.* 2006, **45**, 8847; (*g*) A. Escuer, M. A. S. Goher, F. A. Mautner and R. Vicente, *Inorg. Chem.* 2000, **39**, 2107; (*h*) A. Escuer, R. Vicente, M. S. El, M. A. Fallah, S. Goher and F. A. Mautner, *Inorg. Chem.* 1998, **37**, 4466; (*i*) A. Das, G. M. Rosair, M. S. Fallah, J. Ribas and S. Mitra, *Inorg. Chem.* 2006, **45**, 3301; (*j*) P. S. Mukherjee, T. K. Maji, G. Mostafa, T. Mallah and N. R. Chaudhuri, *Inorg. Chem.* 2000, **39**, 5147; (*k*) Z. Shen, J.-L. Zuo, S. Gao, Y. Song, C.-M. Che, H. -K. Fu and X.-Z. You, *Angew. Chem. Int. Ed.*, 2000, **39**, 3633; (*l*) S. Koner, S. Saha, T. Mallah and K. -I. Okamoto, *Inorg. Chem.*, 2004, **43**, 840; (*m*) T. K. Karmakar, S. K. Chandra, J. Ribas, G. Mostafa, T. H. Lu and B. K. Ghosh, *Chem. Commun.*, 2002, 2364.

[12] E. Ruiz, J. Cano, S. Alvarez and P. Alemany, *J. Am. Chem. Soc*. 1998, **120**, 11122.

[13] P. de Loth, P. Cassoux, J. P. Daudey and J. P. Malrieu, *J. Am. Chem. Soc.* 1981, **103**, 4007.

[14] (*a*) O. Kahn, S. Sikorav, J. Gouteron, S. Jeannin and Y. Jeannin, *Inorg. Chem.*, 1983, **22**, 2877; (*b*) K. M. Thomas, *Dalton Trans.*, 2009, 1487; (*c*) P. Kanoo, C. Madhu, G. Mostafa, T. K. Maji, A. Sundaresan, S. K. Pati and C. N. R. Rao, *dalton Trans.*, 2009, 5062; (*d*) M. Ray, S. Chattopadhyay, M. G. B. Drew, A. Figuerola, J. Ribas, C. Diaz and A. Ghosh, *Eur. J. Inorg. Chem*., 2005, 4562.

[15] (*a*) A. Caneschi, D.Gatteschi, R. Sessoli, A. L. Barra, L. C. Brunel and M. Guillot, *J. Am. Chem. Soc.*, 1991, **113**, 5873; (*b*) R. Sessoli, H. L. Tsai, A. R. Schake, S. Wang, J. B. Vincent, K. Folting, D. Gatteschi, G. Christou and D. N. Hendrickson, *J. Am. Chem. Soc*., 1993, **115**, 1804; (*c*) R. Sessoli, D. Gatteschi, A. Caneschi and M. A. Novak, *Nature*, 1993, **365**, 141; (*d*) J. H. Eppley, H. L. Tsai, N. de Vries, K. Folting, G. Christou and D. N. Hendrickson, *J. Am. Chem. Soc*., 1995, **117**, 301; (*e*)

L. Thomas, F. Lionti, R. Ballou, D. Gatteschi, R. Sessoli and B. Barbara, *Nature,* 1996, **383**, 145; (*f*) D. Gatteschi and R. Sessoili, *Angew. Chem. Int. Ed*., 2003, **42**, 268; (*g*) W. Wernsdorfer and R. Sessoli, *Science*, 1999, **383**, 145. (*h*) M. Murugesu, M. Habrych, W. Wernsdorfer, K. A. Abboud and George Christou, *J. Am. Chem. Soc*., 2004, **126**, 4767; (*i*) A. J. Tasiopoulos, A. Vinslava, W. Wernsdorfer, K. A. Abboud and G. Christou, *Angew. Chem. Int. Ed*., 2004, **43**, 2117; (*j*) A. Mishra, A. J. Tasiopoulos, W. Wernsdorfer, E. E. Moushi, B. Moulton, M. J. Zaworotko, K. A. Abboud and G. Christou *Inorg. Chem*., 2008*,* **47***,* 4832.

[16] (*a*) H. Miyasaka and M. Yamashita, *Dalton Trans*., 2007, 399; (*b*) G. Christou, D. Gatteschi, D. N. Hendrickson and R. Sessoli, *MRS Bull*., 2000, **25**, 66; (*c*) D. Gatteschi and R. Sessoli, *J. Magn. Magn. Mater*., 2004, **272**, 1030.

[17] (*a*) H. Oshio, M. Nihei, A. Yoshida, H. Nojiri, M. Nakano, A. Yamaguchi, Y. Karaki and H. Ishimoto, *Chem. Eur. J*., 2005, **11**, 843; (*b*) V. Chandrasekhar, B. Pandian, R. Azhakar, J. Vittal and R. Clerac, *Inorg. Chem*., 2007, **46**, 5140; (*c*) L. Zou, L. Zhao, Y. Guo, G. Yu, Y. Gu, J. Tang and Y. Li, *Chem. Commun*., 2011, **47**, 8659.

[18] (*a*) H. Miyasaka, K. Nakata, L. Lecren, C. Coulon, Y. Nakazawa, T. Fujisaki, K. Sugiura, M. Yamashita and R. Clerac, *J. Am. Chem. Soc*., 2006, **128**, 3770; (*b*) L. Bogani, A. Vindigni, R. Sessoli and D. Gatteschi, *J. Mater. Chem.*, 2008, **18**, 4750; (*c*) D. Gatteschi, L. Bogani, A. Cornia, M. Mannini, L. Sorace and R. Sessoli, *Solid State Sci.*, 2008, **10**, 1701.

[19] (*a*) F.-C. Liu, Y.-F. Zeng, J. R. Li, X.-H. Bu, H. J. Zhang and J. Ribas, *Inorg. Chem.* 2005, **44**, 7298; (b) F. C. Liu, Y. –F. Zeng, J. Jiao, J. R. Li, X.-H. Bu, J. Ribas and S. R. Batten, *Inorg. Chem*., 2006, **45**, 6129.

[20] (*a*) M. A. S. Goher, J. Cano, Y. Journaux, M. A.M. Abu-Youssef, F. A. Mautner, A. Escuer and R. Vicente, *Chem. Eur. J*., 2000, **6**, 778; (*b*) S. Mukherjee, B. Gole, Y. Song and P. S. Mukherjee, *Inorg. Chem*., 2011, **50,** 3621.

[21] H. Kumagai, M. A.-Tanaka, K. Inoue and M. Kurmoo, *J. Mater. Chem*., 2001, **11**, 2146.

[22] (*a*) N. Guillou, C. Livage, M. Drillon and G. F´erey, *Angew.Chem. Int. Ed,* 2003, **42**, 5314; (*b*) M. B. Salah, S. Vilminot, G. André, M. Richard-Plouet, T. Mhiri, S. Takagi, and M. Kurmoo, *J. Am. Chem. Soc.*, 2006, **128**, 7972.

[23] M. Kurmoo, H. Kumagai, S.M. Hughes and C. J. Kepert, *Inorg. Chem.,* 2003, **42**, 6709.

[24] (*a*) I. Dzyaloshinsky, *J. Phys. Chem. Solids*, 1958, **4**, 241; (*b*) T. Moriya, *Phys. Rev.*, 1960, **120**, 91; (*c*) T. Moriya, *Phys. Rev.*, 1960, **117**, 635.

[25] J. Li, Q. Yu, Y. Tao, X.Bu, J. Ribas and S. R. Batten, *Chem. Commun.*, 2007, 2290.

[26] M. E. Brown and M. D. Hollingsworth, *Nature,* 1995, **376**, 323.

[27] V. Ramamurthy and D. F. Eaton, *Chem. Mater*., 1994, **6**, 1128.

[28] F. Toda, S. Hyoda, K. Okada and K. Hirotsu, *J. Chem. Soc., Chem. Commun*., 1995, 1531.

[29] (*a*) R. J. Kuppler, D. J. Timmons, Q.-R. Fang, J.-R. Li, T. A. Makal, M. D. Young, D. Yuan, D. Zhao, W. Zhuang and H.-C. Zhou, *Coord. Chem. Rev.*, 2009, **253**, 3042; (*b*) P. Dechambenoit and Jeffrey R. Long, *Chem. Soc. Rev.*, 2011, **40**, 3249.

[30] A. Hazra, P. Kanoo and T. K. Maji, *Chem. Commun.*, 2011, **47**, 538.

[31] M. Kurmoo, H. Kumagai, K. W. Chapman and C. J. Kepert, *Chem. Commun*., 2005, 3012.

[32] J. Aldana, Y. A. Wang, X. G. Peng, *J. Am. Chem. Soc.*, 2011, **123**, 8844.

[33] G. J. Halder, C. J. Kepert, B. Moubaraki, K. S. Murray, J. D. Cashion, *Science*, 2002, **298**, 1762.

Chapter 2

Assembly of Trinuclear and Tetranuclear Building Units of Cu(II) Towards Two 1D Magnetic Systems: Synthesis and Magneto-structural Correlations

Abstract

This chapter describes synthesis, structural characterization and magneto-structural correlation of two 1D coordination polymer chains of Cu(II) (S = ½) based on trinuclear and tetranuclear Cu(II) building blocks. The compounds $[Cu_3(\mu_3\text{–}OH)(ppk)_3(\mu\text{–}N(CN)_2)(OAc)]_n$ (**1**) and $\{[Cu_4(pdmH)_2(pdm)_2(\mu_2\text{–}OH)(H_2O)]\cdot ClO_4\}_n$ (**2**) have been synthesized based on two different blocking ligands phenyl-2-pyridylketoxime (ppk) and pyridine–2,6-dimethanol ($pdmH_2$). In compound **1,** hydroxido-bridged trinuclear core, $\{Cu_3(\mu_3\text{-}OH)(ppk)_3(OAc)\}$, acts as secondary building unit and $N(CN)_2^-$ anions connect these cores resulting in an one dimensional (1D) coordination polymer. The 1D coordination chains further interact via $\pi\text{–}\pi$ interactions giving rise to a 3D supramolecular framework. In compound **2**, tetrameric $[Cu_4(pdmH)_2(pdm)_2(H_2O)]^{2+}$ cores are connected through hydroxido groups forming a zigzag 1D coordination chain where non-coordinated ClO_4^- anions are intercalated between the chains. Investigation of the magnetic properties of **1** reveals that in the trinuclear $Cu_3(\mu_3\text{–}OH)$ cores Cu(II) ions are antiferromagnetically coupled with $J = -459.7$ cm^{-1} and $g = 2.11$ while the cores are further weakly coupled antiferromagnetically ($zj' = -5.25$ cm^{-1}) through the $N(CN)_2^-$ bridging ligand. In compound **2**, Cu(II) centres are coupled antiferromagnetically in the tetranuclear core with $J = -27.1$ cm^{-1} and $g = 2.17$; the $\{Cu(II)\}_4$ cores are further coupled antiferromagnetically with $zj' = -9.65$ cm^{-1}. The experimental magnetic behaviour of **1** and **2** are correlated by first principle DFT calculations which provide a qualitative understanding of the origin of antiferromagnetic interactions in both cases.

2.1 INTRODUCTION

Polynuclear coordination clusters have recently come under intensive research interest with its contribution to the understanding and application of fundamental magnetic properties.[1] This field has become much more fascinating after the emergence of single molecule magnets (SMMs) and single chain magnets (SCMs)[1-2] with several possible potential applications including high density information storage and quantum computation.[3] Polynuclear Cu(II) complexes have been well studied and still are in the current focus due to the involvement of these compounds in several catalytic processes in living organisms,[4] for example multicopper oxidases (*e.g.*, ascorbate oxidase and laccase) contain a triangular unit of copper atoms.[4c] Moreover, this type of polynuclear complexes often provide the possibility to study the superexchange phenomenon which essentially leads to the insights into magneto-structural correlations. The magnetic studies based on trinuclear and tetranuclear Cu(II) complexes have been extensively studied because these can be regarded as geometrical frustrated systems leading to the unusual electronic properties.[5] Furthermore, several reports have appeared in the recent past on the linking of small magnetic clusters through the self-assembly process towards the formation of multidimensional networks.[6-8] Oxido, hydroxido, azido, halogenoto groups can act as excellent multidentate bridging entities in the formation of dinuclear, trinuclear, tetranuclear, hexanuclear[9-11] clusters supported by different organic blocking ligands. These cores can further be extended to higher dimensional networks by other organic or inorganic bridging linkers.[8] However, the syntheses of such extended systems are not straightforward because of the difficulty in control over the self-assembly process. For rational synthesis and towards the understanding of the type and magnitude of exchange interactions in such systems, several important parameters like geometry of metal ions, stereochemistry of the blocking ligands, identity of the bridging chemical entities, distance between the metal ions, angles at the bridging atoms etc. are important. In this context, there are several reports on the synthesis, characterization and magnetic properties of trinuclear $Cu_3(\mu_3–X)$ compounds (X = O, OH, Cl, Br, I) and tetranuclear oxido bridged copper complexes, but the magneto-structural correlation of 1D coordination polymers wherein the repeating trinuclear[8c] or tetranuclear[10i-10k] units are linked by organic or inorganic bridging ligand are yet to be properly explored. Here, we have envisioned the use of two blocking ligands; phenyl–2–pyridylketoxime (ppk) and pyridine–2,6–dimethanol ($pdmH_2$) (Scheme 1), which are able to chelate and oxido or

hydroxido group can bridge a number of metal centres and thus can allow the formation of polynuclear cluster. The ligands ppk and $pdmH_2$ have already established themselves as versatile cluster forming agents in different metal systems (Mn(II), Cr(III), Ni(II), Co(II) etc.) with different nuclearities.[12] The alkoxido groups of the $pdmH_2$ ligand formed by deprotonation and the anion of ppk are excellent bridging units that can facilitate the formation of high-nuclearity clusters. The presence of a tridentate chelate *O,N,O′* unit within $pdmH^-/pdm^{2-}$ is expected to give high stability in the products. However, there are few reports on the use of these ligands in Cu(II) polynuclear cluster chemistry.[13]

This chapter deals with the synthesis, structural characterization and detailed magnetic study of two novel 1D coordination polymer chains, $[Cu_3(\mu_3\text{–}OH)(ppk)_3(\mu\text{–}N(CN)_2)(OAc)]_n$ (**1**) and $\{[Cu_4(pdmH)_2(pdm)_2(\mu_2\text{–}OH)(H_2O)]\cdot ClO_4\}_n$ (**2**) based on trinuclear and tetranuclear Cu(II) building blocks. The structure determination of compound **1** reveals that cyclic trinuclear $[Cu_3(\mu_3\text{–}OH)(ppk)_3(OAc)]$ cores are connected by $N(CN)_2^-$ linker forming a 1D coordination chain and each chain undergoes π-π interactions forming a 3D supramolecular framework. In compound **2** tetranuclear cores are connected by the hydroxido (OH^-) groups resulting in a 1D chain and the ClO_4^- anions are intercalated between the chains. Temperature dependent magnetic measurements suggest in both the trinuclear $[Cu_3(\mu_3\text{–}OH)(ppk)_3(OAc)]^+$ and tetranuclear $[Cu_4(pdmH)_2(pdm)_2(H_2O)]^{2+}$ cores Cu(II) centres are antiferromagnetically coupled by the hydroxido or oxido bridges, respectively. The experimental observations are supported by the density functional theory (DFT) based calculations. The trinuclear and tetranuclear cores are further weakly antiferromagnetically coupled by the $N(CN)_2^-$ and OH^- bridges in **1** and **2**, respectively.

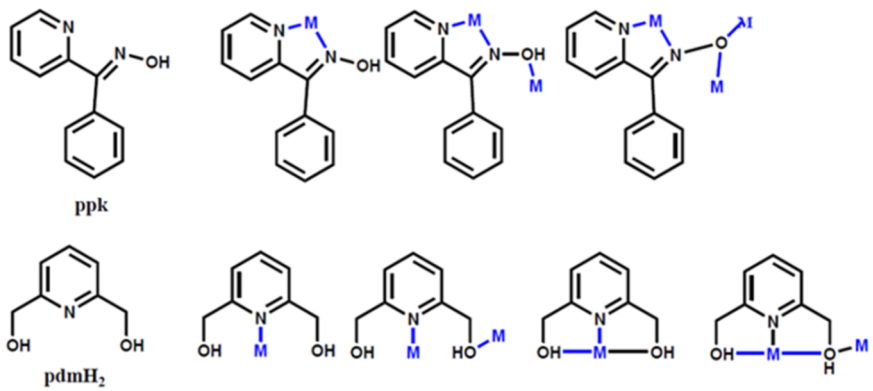

Scheme 1. Structure and different observed binding modes for phenyl-2-pyridylketoxime (ppk) and pyridine-2,6-dimethanol ($pdmH_2$) with different metal ions.

2.2 EXPERIMENTAL SECTION

2.2.1 Materials

All the reagents and solvents employed are commercially available and used as supplied without further purification. $Cu(OAc)_2 \cdot H_2O$, $Cu(ClO_4)_2 \cdot 6H_2O$, sodium dicyanamide ($NaN(CN)_2$), phenyl–2–pyridylketoxime and pyridine–2,6–dimethanol were obtained from the Aldrich chemical Co.

2.2.2 Synthesis

$[Cu_3(\mu_3\text{–}OH)(ppk)_3(\mu\text{–}N(CN)_2)(OAc)]_n$ (1) $Cu(OAc)_2 \cdot H_2O$ (0.5 mmol, 0.099 g) was dissolved in 40 mL CH_3CN and then methanolic solution (20 mL) of phenyl–2–pyridylketoxime (0.6 mmol, 0.1 g) was dropwise added to the above solution with constant stirring. The resulting green coloured solution was stirred for ten minutes. Then aqueous solution (20 mL) of $NaN(CN)_2$ (0.33 mmol, 0.029 g) was dropwise added to the above reaction mixture and the whole solution turned to green which was stirred for overnight. Then the reaction mixture was filtered and kept for slow evaporation at room temperature. Green coloured single-crystals suitable for X-ray analysis were isolated after one week and washed with H_2O and CH_3CN. Yield, 75%, relative to Cu. Selected IR data (KBr, cm^{-1}); 3424 br, 3151 w, 3070 w, 2279 s, 2223 s, 1658 m, 1604 m, 1556 m, 1416 m, 1392 s, 1091 sh, 890 sh (Figure 1). Anal. calcd. for $C_{40}H_{31}Cu_3N_9O_6$: C, 51.97; H, 3.38; N,13.64. Found: C, 51.67; H, 3.31; N, 13.96. The very well correspondence of the simulated and bulk phase PXRD patterns indicates high purity of the sample (Figure 2).

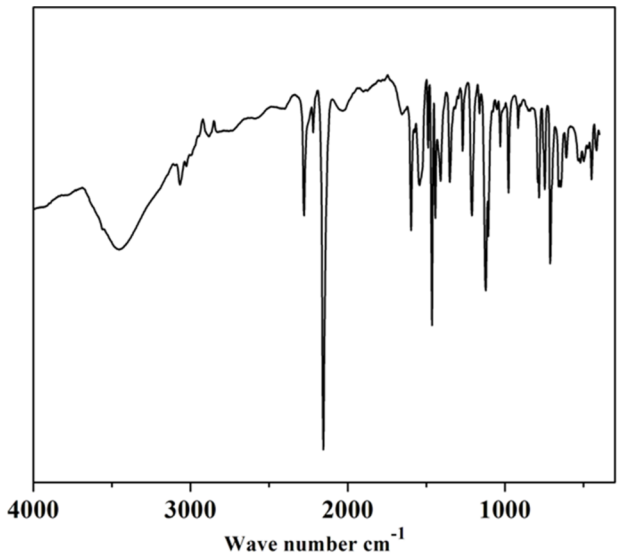

Figure 1. FT-IR spectrum for **1**.

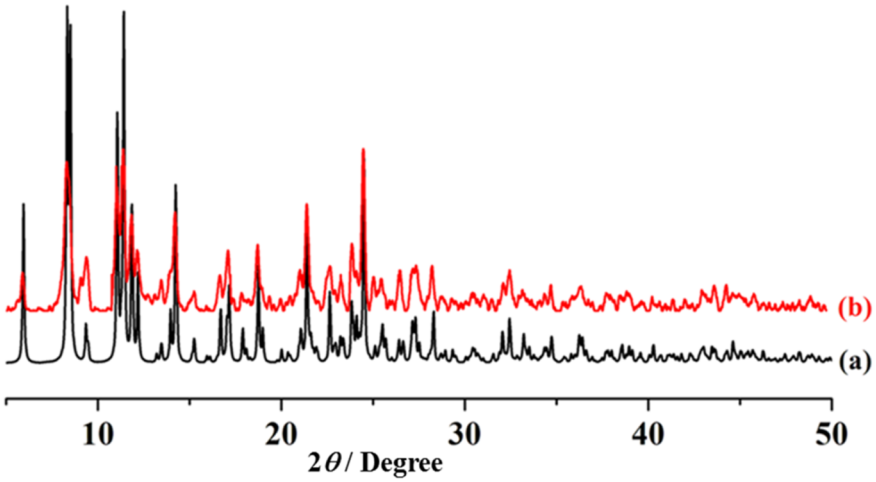

Figure 2. PXRD patterns of compound **1**: (a) simulated; (b) bulk as-synthesized. Similarity in simulated and as-synthesized pattern indicates high purity of the compound.

$\{[Cu_4(pdmH)_2(pdm)_2(\mu_2\text{–}OH)(H_2O)_2]\cdot(ClO_4)\}_n$ (2). $Cu(ClO_4)_2\cdot 6H_2O$ (1 mmol, 0.370 g) was dissolved in 10 mL water and 10 mL methanolic solution of pyridine–2,6–dimethanol (1mmol, 0.139 g) was dropwise added to the above metal solution. Then the resulting green solution was stirred for four hours and filtered. The filtrate was kept for slow evaporation at room temperature and after one week blue crystals were isolated. The crystals were washed with water and methanol. Yield, 69%, relative to Cu. Selected IR data (KBr, cm^{-1}) 3097 w, 2829 w,1606 m, 1471 m, 1268 m, 1093 s, 781 m, 625 m (Figure 3). Anal. calcd. for $C_{28}H_{35}Cu_4N_4O_{15}Cl$: C, 35.13; H, 3.68; N,5.85. Found: C, 35.09; H, 3.62; N, 5.88%. The phase purity was checked by comparing the PXRD pattern of the bulk powder sample with the simulated data from single-crystal (Figure 4).

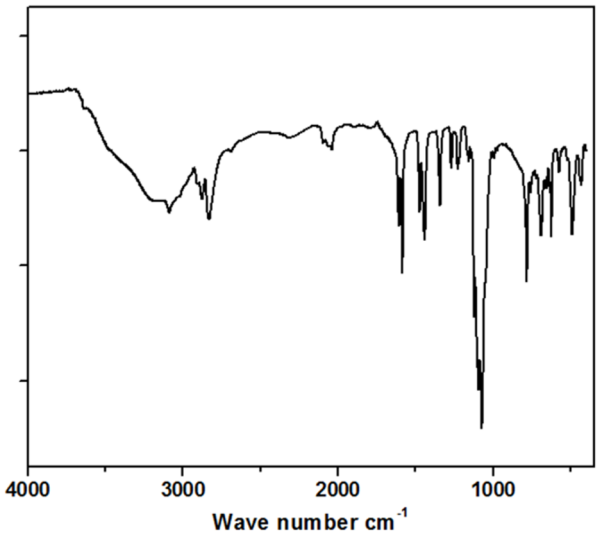

Figure 3. FT-IR spectrum for **2**.

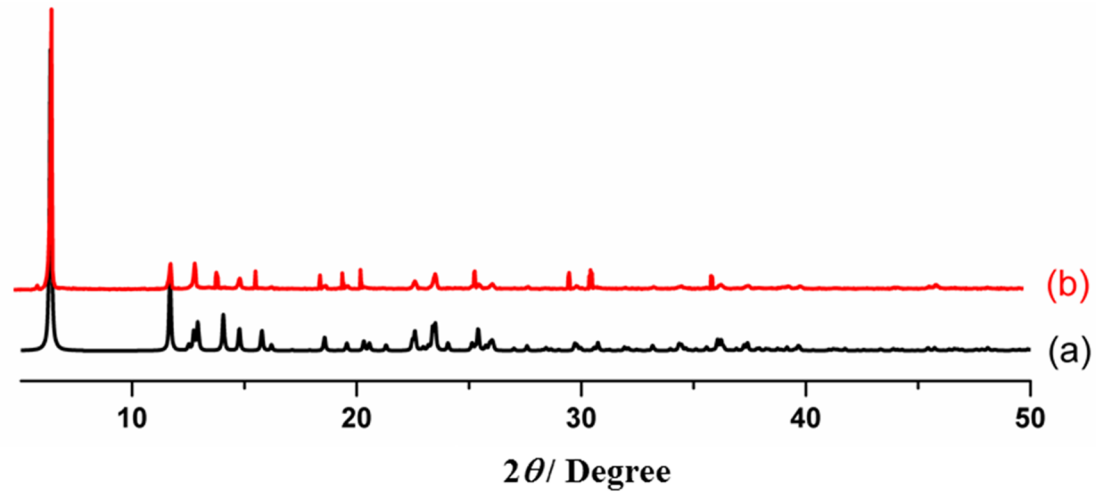

Figure 4. PXRD patterns of compound **2**: (a) simulated; (b) bulk as-synthesized. The phase purity of the compound is confirmed by the similarity between simulated and as-synthesized patterns.

2.2.3 Single-crystal X-ray Diffraction

X-ray single-crystal structural data of **1** and **2** were collected on a Bruker Smart–CCD diffractometer equipped with a normal focus, 2.4 kW sealed tube X-ray source with graphite monochromated Mo–Kα radiation (λ = 0.71073 Å) operating at 50 kV and 30 mA. The SAINT program[14a] was used for integration of diffraction profiles and absorption correction was made with SADABS[14b] program. Both the structures were solved by SIR 92[14c] and refined by full matrix least square method using SHELXL 97.[14d] All the non hydrogen atoms were refined anisotropically and all the hydrogen atoms were fixed by HFIX and placed in ideal positions. All calculations were carried out using SHELXL 97, PLATON[14e] and WinGX system, Ver 1.70.01.[14f] All crystallographic and structure refinement data of **1** and **2** are summarized in Table 1. Selected bond lengths and angles are displayed in Tables 2–4.

2.2.4 Physical Measurements

Elemental analyses were carried out on a Perkin Elmer 2400 CHN analyser. IR spectra were recorded in KBr pellets on a Bruker IFS 66v/S spectrophotometer in the region of 4000 – 400 cm^{-1}. The magnetic measurements (300 –2.5 K) for polycrystalline powder sample of **1** and **2** were carried out using Vibrating Sample Magnetometer (VSM) in physical property measurement system (PPMS, Quantum Design, USA). Susceptibility data were collected using an external magnetic field of 500 Oe and obtained data were corrected with respect to the diamagnetic contribution of the constituent atoms (on the basis of Pascal constants).[15]

2.3 RESULTS AND DISCUSSION

2.3.1 Crystal Structure Description

2.3.1.1 Structural description of $[Cu_3(\mu_3\text{–}OH)(ppk)_3(\mu\text{–}N(CN)_2)(OAc)]_n$ (1)

Compound **1** crystallizes in the monoclinic $P2_1/n$ space group. The structure determination of **1** shows that cyclic trinuclear Cu(II) units (Figure 5) of formula $[Cu_3(\mu_3\text{–}OH)(ppk)_3(OAc)]^+$ are bridged by $N(CN)_2^-$ (dicyanamide) anions resulting in an one dimensional coordination chain (Figure 6). In the asymmetric unit each trinuclear core contains a triangular Cu_3 skeleton where each Cu(II) centre is present in a distorted square pyramidal (4+1) geometry (Figure 5).

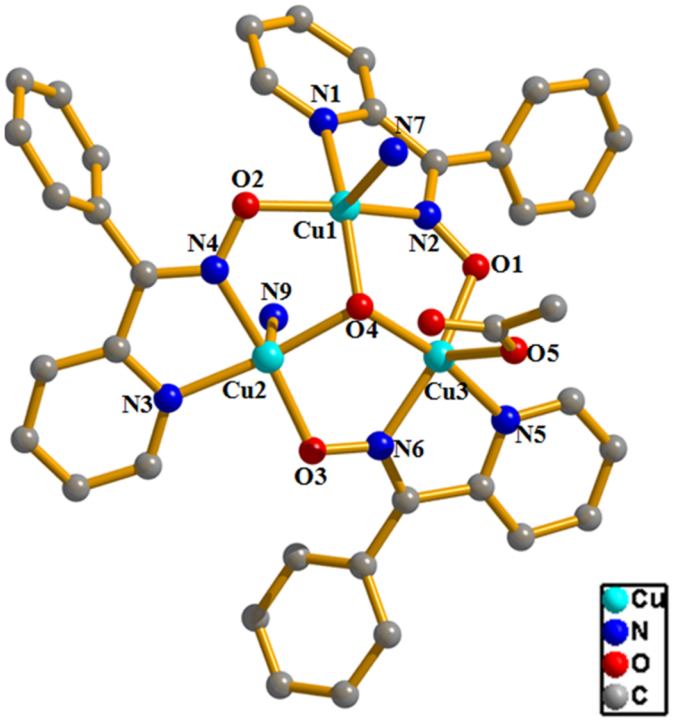

Figure 5. View of the trinuclear building unit $[Cu_3(\mu_3\text{–}OH)(ppk)_3(OAc)]$ of **1** showing the square pyramidal coordination environment of each Cu(II) ion.

Cu1 is chelated to one ppk ligand (N1, N2) and connected to another ppk ligand by O2 oxygen atom and forms the equatorial plane involving the bridging μ_3–O4 atom. The axial position is occupied by the N7 nitrogen atom from the bridging $N(CN)_2^-$ ligand. For Cu2, the basal plane is occupied by two chelated nitrogen atoms (N3, N4) from one ppk ligand, O3 from another ppk ligand and μ_3–O4 and the axial position is ligated through N9 from the bridging $N(CN)_2^-$ ligand.

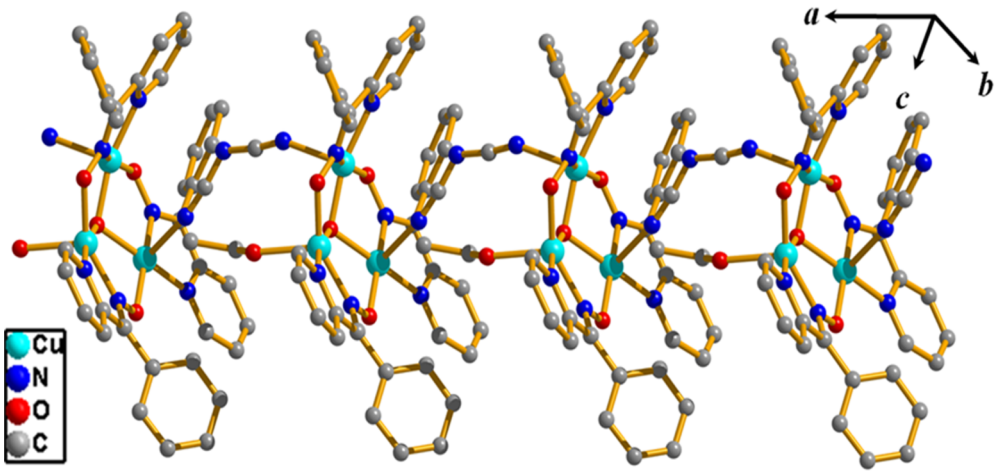

Figure 6. View of the 1D coordination chain of **1** showing trinuclear $\{Cu_3(\mu_3\text{–OH})\}$ core connected by the $N(CN)_2^-$ anions.

The oxygen atom (O5) from the pendent acetate group is attached in the axial position around Cu3 and the equatorial positions are occupied by the chelated nitrogen atoms (N5, N6) from one ppk ligand, O1 from the another ppk liagnd and μ_3–O4.The Cu–O and Cu–N bond lengths are in the range of 1.928(4)–2.146(4) Å and 1.955(4)–2.261(6) Å respectively (Table 2). The degree of distortion from the ideal square pyramidal geometry is reflected in the angles of the basal plane of the Cu atoms (Table 3). The addison parameter (τ)[16] have been calculated and the values are 0.06, 0.05 and 0.33 for Cu1, Cu2 and Cu3, respectively. In the trinuclear $[Cu_3(\mu_3\text{–OH})(ppk)_3(OAc)]^+$ core the copper atoms are held together by two kind of bridging; (i) the μ_3–OH oxygen atom (O4) bridging three Cu(II) centres (Cu1–O4, 1.949(4); Cu2–O4, 1.961(3) and Cu3–O4, 1.962(4) Å) and (ii) the N–O group from the ppk ligand bridging two Cu(II) centres. In the tricnuclear core, Cu–O4–Cu bond angles are in the range 105.98(17)°–114.99(17)° and the Cu1–Cu2, Cu1–Cu3 and Cu2–Cu3 distances are 3.122(1), 3.298(1) and 3.225(1) Å, respectively. The average Cu–N–O–Cu torsion angle is 19.8°. The μ_3–OH oxygen atom (O4) is located above the mean plane defined by the three copper atoms by 0.616 Å. The dihedral angles between the adjacent basal planes are 50.23° (Cu(1) plane-Cu(2) plane), 33.69° (Cu(1) plane–Cu(3) plane), and 32.46° (Cu(2) plane–Cu(3) plane). The Cu1 atom of one trinuclear core is connected to the Cu2 atom of another trinuclear core through the N7, N9 atoms of the $N(CN)_2^-$ ligand resulting in a 1D coordination polymer (Figure 6). The distance between Cu1 and Cu2 via $N(CN)_2^-$ bridging is about 8.210 Å. Each 1D coordination chain undergoes π–π interactions through the phenyl and pyridyl rings of the ppk ligands (cg–cg distances are 3.836(4) Å and 4.529(4) Å, respectively)

forming a 2D supramolecular network in the crystallographic *ac* plane (Figure 7a). The 2D networks are further assembled by π–π interactions mediated through phenyl–phenyl and pyridyl–pyridyl rings of ppk ligands with cg–cg distances 4.040(4) Å and 3.976(3) Å, respectively, resulting in a 3D supramolecular framework (Figure 7b).

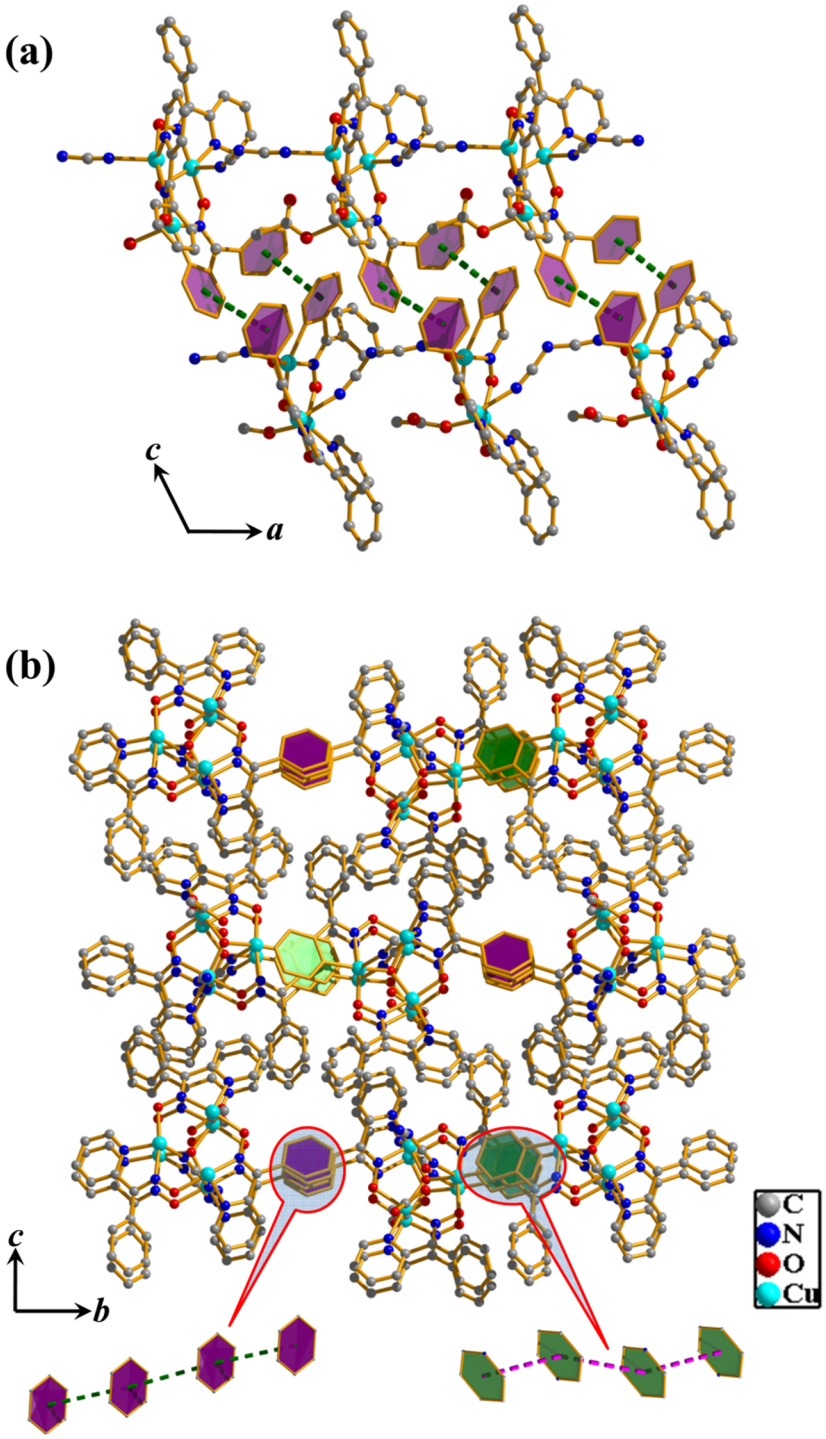

Figure 7. (a) View of the 2D supramolecular sheet formed by π–π interactions between the 1D coordination chains lying in the crystallographic *ac* plane and (b) View of the 3D supramolecular framework formed by the π–π interactions between the 2D supramolecular sheets of compound **1**.

2.3.1.2 Structural description of $\{[Cu_4(pdmH)_2(pdm)_2(\mu_2\text{–}OH)(H_2O)_2]\cdot(ClO_4)\}_n$ (2)

Compound **2** crystallizes in the orthorhombic $Pbn2_1$ space group with formula $\{[Cu_4(pdmH)_2(pdm)_2(\mu_2\text{–}OH)(H_2O)_2]\cdot(ClO_4)\}_n$. Single-crystal X–ray diffraction study reveals that asymmetric unit of **2** contains four Cu(II) centres, four pyridine–2,6–dimethanol ligands [two act as monoanionic ligand (pdmH) and two act as dianionic ligand (pdm)], two coordinated H_2O molecules, one μ_2–OH group and a non-coordinated ClO_4^- anion (Figure 8).

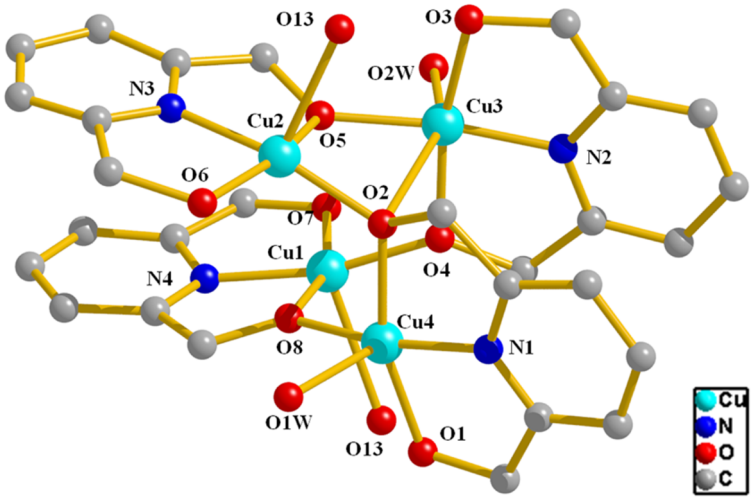

Figure 8. View of the tetranuclear building unit $[Cu_4(pdmH)_2(pdm)_2(H_2O)]^{2+}$ of **2** showing the different coordination environment around Cu(II) ion.

In the tetranuclear $[Cu_4(pdmH)_2(pdm)_2(H_2O)_2]^{2+}$ core, Cu1 locates itself in a distorted square pyramidal (4+1) geometry and the equatorial coordinations are furnished by one tridentate chelated pdmH ligand (O7, O8, N4 atoms) and one bridging pdm ligand (O4 atom). The apical position is occupied by O13 atom coming from bridging μ_2–OH group. Similarly Cu2 adopts distorted square pyramidal geometry with coordinations coming from N3, O5, O6 atoms from one tridentate chelated pdm ligand, O2 atom from a pdmH ligand and O13 atom from the μ_2-OH group. Cu3 is present in a distorted octahedral (4+2) coordination environment where the equatorial positions are occupied by one tridentate chelated pdm ligand (O3, O4 and N2 atoms) and the O5 oxygen atom from another pdm ligand. The axial positions are occupied by O2 and O2w oxygen atoms. Cu4 adopts a distorted square pyramidal geometry where O1, N1, O2, O8 atoms define the square plane and O1w atom from a water molecule occupies the apical position. The equatorial Cu–O and Cu–N bond distances for all the Cu(II) centres are in the range of

1.885(6) – 2.007(6) Å and 1.881(6) – 1.943(8) Å, respectively. However, the apical bonds are elongated (2.425(5) – 2.791(5) Å) due to Jahn–Teller distortion. In all cases the degree of distortion is reflected in the bond lengths and bond angles around the Cu(II) centres (Table 4 and Table 5). The τ values are for Cu1, Cu2 and Cu4 are 0.05, 0.08 and 0.12 respectively. In the tetranuclear core Cu(II) ions are held together by different alkoxido oxygen atoms where μ_2–O4, μ_2–O8 and μ_2–O5 atoms bridge Cu1, Cu3; Cu1, Cu4 and Cu2 and Cu3 atoms respectively, while Cu2, Cu3 and Cu4 atoms are connected by μ_3–O2 atom.

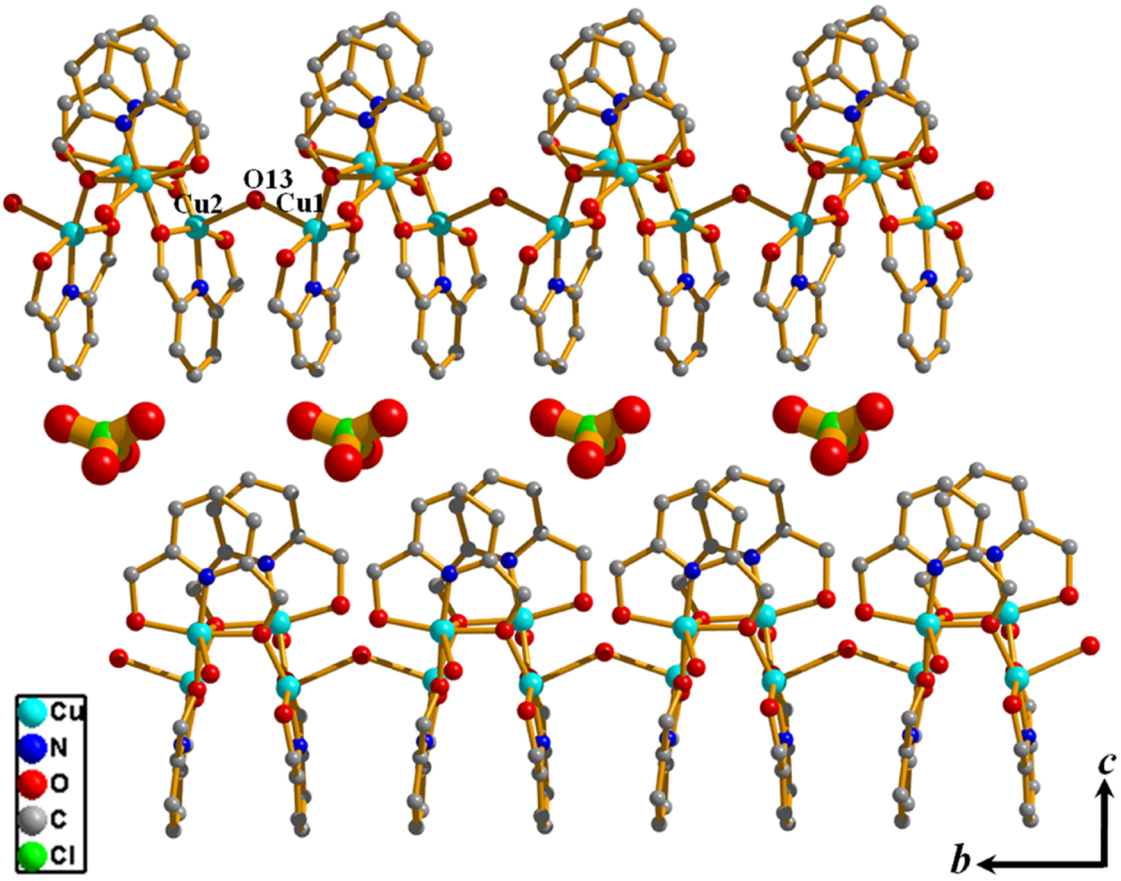

Figure 9. View of the 1D chain formed by the linking of $[Cu_4(pdmH)_2(pdm)_2(H_2O)]^{2+}$ cores by μ-OH where ClO_4^- anions are intercalated between the chains.

The Cu1 of one tetranuclear core is connected to the Cu2 atom of another tetranuclear core by μ_2–OH (O13) linkage to form a 1D coordination chain and the ClO_4^- anions are intercalated between the 1D chains (Figure 9). The distance between Cu1 and Cu2 via μ_2–OH bridging is 4.569 Å.

Table 1. Crystal data and structure refinement parameters for **1** and **2**.

parameters	**1**	**2**
empirical formula	$C_{40}H_{31}Cu_3N_9O_6$	$C_{28}H_{35}Cu_4N_4O_{15}Cl$
formula weight	924.36	957.21
crystal system	monoclinic	orthorhombic
space group	$P2_1/n$	$Pbn2_1$
a, Å	8.4798(3)	7.9039(2)
b, Å	20.8033(7)	15.7253(4)
c, Å	21.2503(8)	27.7552(8)
α, deg	90	90
β, deg	92.601(2)	90
γ, deg	90	90
V, Å^3	3744.9(2)	3449.73(16)
Z	4	4
T, K	298	298
μ, mm^{-1}	1.751	2.587
D_{calcd}, g/cm^3	1.640	1.843
F (000)	1876	1936
reflections [$I>2\sigma(I)$]	4036	5295
unique reflections	8515	6150
measured reflections	24643	35361
R_{int}	0.106	0.054
GOF on F^2	0.97	1.08
$R_1[I>2\sigma(I)]^a$	0.0648	0.0635
R_w[all data]^b	0.1464	0.1762
$\Delta\rho$ max/min [e Å^{-3}]	0.93, -0.87	2.71, -1.10

$^a R = \sum||F_o|-|F_c||/\sum|F_o|$; $^b R_w = [\sum\{w(F_o^2-F_c^2)^2\}/\sum\{w(F_o^2)^2\}]^{1/2}$

Table 2. Selected Bond Distances (Å) for **1**.

Cu1-O2	1.985(4)	Cu1-O4	1.949 (4)
Cu1-N1	1.997(4)	Cu1-N2	1.994(4)
Cu1-N7	2.213(6)	Cu2-O3	1.928(4)
Cu2-O4	1.961(3)	Cu2-N3	1.998(4)
Cu2-N4	1.955(4)	Cu2-N9_a	2.261(6)
Cu3-O1	1.979(4)	Cu3-O4	1.962(4)
Cu3-O5	2.146(4)	Cu3-N5	2.001(4)
Cu3-N6	1.989(4)		

Symmetry code: a = −1+x, y, z

Table 3. Selected bond angles (°) for **1**.

O1-Cu1-O2	158.29(14)	N3-Cu2-N9_a	100.8(2)
O1-Cu1-O4	68.70(13)	N4-Cu2-N9_a	89.1(2)
O1-Cu1-N1	102.30(15)	O1-Cu3-O3	144.98(15)
O1-Cu3-O4	93.86(16)	O1-Cu1-N7	98.89(16)
O1-Cu3-O5	94.01(17)	O2-Cu1-O4	91.94(15)
O1-Cu3-N5	92.77(17)	O2 -Cu1-N1	92.82(17)
O1-Cu3-N6	149.00(19)	O2-Cu1-N2	163.41(18)

Table 3 continued…			
O3-Cu3-O4	67.57(13)	O2 –Cu1-N7	93.50(18)
O3-Cu3-O5	116.55(14)	O4-Cu1-N1	160.04(16)
O3-Cu3-N5	101.99(15)	O4-Cu1-N2	89.65(16)
O4-Cu1-N7	98.58(19)	O4-Cu3-O5	96.21(15)
N1-Cu1-N2	80.43(17)	O4 -Cu3-N5	168.67(17)
N1-Cu1-N7	100.5(2)	O4-Cu3-N6	89.69(16)
N2-Cu1-N7	102.60(17)	O5-Cu3-N5	92.49(18)
O2-Cu2-O3	162.42(14)	O5-Cu3-N6	116.23(18)
O2-Cu2-O4	68.30(13)	N5-Cu3-N6	79.93(18)
O2-Cu2-N3	103.43(14)	Cu1-O1-Cu3	81.63(13)
O2-Cu2-N9_a	82.81(18)	Cu3-O1-N2	112.9(3)
O3-Cu2-O4	94.32(16)	Cu1-O2-Cu2	77.25(12)
O3-Cu2-N3	93.21(17)	Cu1-O2-N4	111.4(3)
O3-Cu2-N4	170.05(17)	O3-Cu2-N9_a	99.8(2)
Cu2-O3-Cu3	79.79(12)	O4-Cu2-N3	167.31(16)
Cu2-O3-N6	111.9(3)	O4-Cu2-N4	90.41(16)
O4-Cu2-N9_a	87.96(19)	Cu1-O4-Cu2	105.98(17)
N3-Cu2-N4	80.66(19)	Cu1-O4-Cu3	114.99(17)
Cu2-O4-Cu3	110.60(17)		

Symmetry code: a = −1+x, y, z

Table 4. Selected bond distances (Å) for **2**.

Cu1-O4	1.922(5)	Cu1-O7	1.956(6)
Cu1-O8	1.989(5)	Cu1-N4	1.917(8)
Cu1-O13_b	2.506(5)	Cu2-O2	1.916(5)
Cu2-O5	1.961(5)	Cu2-O6	1.987(7)
Cu2-O13	2.425(5)	Cu2-N3	1.943(8)
Cu3-O2	2.791(5)	Cu3-O2W	2.768(5)
Cu3-O3	2.007(6)	Cu3-O4	1.954(5)
Cu3-O5	1.895(6)	Cu3-N2	1.881(6)
Cu4-O1	2.004(6)	Cu4-O1W	2.418(5)
Cu4-O2	1.984(5)	Cu4-O8	1.885(6)
Cu4-N1	1.908(6)		

Symmetry code: b = 1+x, y, z

Table 5. Selected bond angles (°) for **2**.

Cu1-O8-Cu4	113.1(3)	Cu1_a-O13-Cu2	135.8(4)
Cu2-O2-Cu4	115.9(3)	Cu1-O4-Cu3	114.6(3)
Cu3-O2-Cu4	101.59(19)	O2-Cu3-O5	70.63(19)
Cu2-O5-Cu3	109.9(3)	O4-Cu1-O8	93.1(2)
O4-Cu1-O7	100.4(2)	O2W-Cu3-O4	81.31(18)
O2W-Cu3-O3	107.09(18)	O2W-Cu3-O5	88.6(2)
O4-Cu1-O13_b	91.6(2)	O5-Cu1-O8	77.6(2)
O5-Cu1-O7	94.8(2)	O3-Cu3-O5	96.6(2)
O3-Cu3-O4	166.9(2)	O7-Cu1-O8	160.8(2)
O4-Cu3-O5	93.6(2)	O7-Cu1-O13_b	104.7(2)
O1-Cu4-O1W	102.9(2)	O8-Cu1-O13_b	88.5(2)
O1-Cu4-O2	161.2(2)	O1-Cu4-O4	91.2(2)

Table 5 continued…			
O2-Cu2-O5	92.7(2)	O1-Cu4-O8	97.1(3)
O2-Cu2-O6	100.8(3)	O2-Cu2-O13	92.9(2)
O1W-Cu4-O2	91.88(19)	O1W-Cu4-O4	159.1(2)
O5-Cu2-O6	160.8(3)	O1W-Cu4-O8	93.5(2)
O5-Cu2-O13	91.6(2)	O2-Cu4-O4	78.17(17)
O6-Cu2-O13	101.1(3)	O2-Cu4-O8	93.5(2)
O4-Cu4-O8	69.10(18)	O2-Cu3-O2W	151.93(19)
O2-Cu3-O3	94.21(17)	O2-Cu3-O4	81.42(17)

Symmetry codes: b= 1+x, y, z

2.3.2 Magnetic properties

The temperature dependence of the χ_M and $\chi_M T$ product (χ_M being the magnetic susceptibility per Cu_3 entity) for **1** are shown in Figure 10. At room temperature the $\chi_M T$ value is much lower (0.47 cm^3 mol^{-1} K) with respect to the value expected for three uncoupled S = ½ spins (ca. 1.12 cm^3 mol^{-1} K) and it decreases steadily with decreasing temperature and becomes 0.34 cm^3 mol^{-1} K at temperature 2.5 K. This behaviour indicates that a strong antiferromagnetic coupling operates between the Cu(II) ions. In order to investigate the magnetic coupling in this compound, an isotropic Heisenberg–Dirac–van Vleck (HDVV) Hamiltonian formalism (eq 1) was used.

$$\hat{H}_{HDVV} = -J_{12}\hat{S}_1\,\hat{S}_2 - J_{13}\hat{S}_1\,\hat{S}_3 - J_{23}\hat{S}_2\,\hat{S}_3 \quad \text{.....(1)}$$

Since the three copper atoms of the $Cu_3(\mu_3\text{–OH})$ unit resemble a quasi-equilateral triangle (see Table 3 and 4), the three exchanges (Cu1–Cu2, Cu2–Cu3 and Cu3–Cu1) can be considered equivalent and so $J_{12} = J_{13} = J_{23} = J$. From this Hamiltonian, a solution of the magnetic susceptibility may be derived as follows:

$$(\chi_M)_{tri} = (N\beta^2 g^2/4kT)[1 + 5\exp(3J/2kT)]/[1 + \exp(3J/2kT)] \text{..... (2)}$$

Where N, g, β, k and T have their usual meanings.

Moreover in compound **1**, trinuclear $Cu_3(\mu_3\text{–OH})$ cores are further connected by the $N(CN)_2^-$ anions, therefore, the exchange interaction between the trinuclear units cannot be entirely ignored. The interaction between trinuclear cores was introduced and the overall equation is

$$\chi_M = (\chi_M)_{tri}/[1-(2zj'/N\beta^2 g^2)(\chi_M)_{tri}] \text{.....(3)}$$

where zj' is the inter-trinuclear coupling.

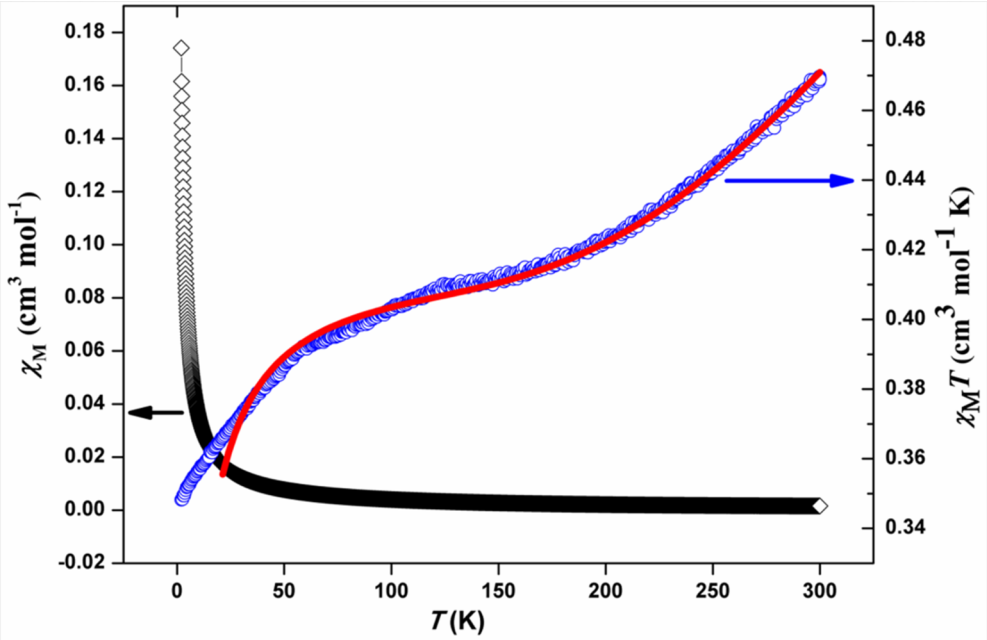

Figure 10. The plots of χ_M *vs.* *T* and $\chi_M T$ *vs.* *T* for **1**. The solid red line indicates the best fit obtained.

Using the equation 3, the experimental data were fitted satisfactorily in the temperature range 300–20 K and the best fit parameter are $J = -459.7$ cm^{-1}, g = 2.11, $zj' = -5.25$ cm^{-1} and $R = 3.4\times10^{-6}$ $\{R = \sum[(\chi_M)^{obs} - (\chi_M)^{calc}]^2/[(\chi_M)^{obs}]^2\}$ (Figure 10). It is worth mentioning that we have not considered antisymmetric exchange in our analysis which is expected to be present in such systems and could also influence low temperature data. The observed deviation of the fitted curve from the experimental curve in the low temperature region is probably due to the antisymmetric exchange interaction.[17,18] The values of the coupling constant *J* and *zj'* indicate the existence of a strong antiferromagnetic coupling within the trinuclear core and a weak antiferromagnetic coupling between the trinuclear core through the $N(CN)_2^-$ bridges. The *M vs H* curve at 5 K reaches a maximum value of 0.4 Nβ, being markedly below from the expected 3 Nβ (Figure 11), corroborating strong antiferromagnetic interactions operating within the $\{Cu(II)\}_3$ triangle.

For a detailed understanding of the exact magnetic exchange pathways towards antiferromagnetic interactions, we have performed extensive computational study based on density functional theory (DFT) within the broken symmetry (BS) formalism[19a] using GAUSSIAN 03 package.[19b] For the DFT calculations, we have looked at trinuclear $Cu_3(\mu_3$–OH) core and the connecting organic linker ppk to find the sign and magnitude of the magnetic coupling. We have considered B3LYP exchange and correlation functional

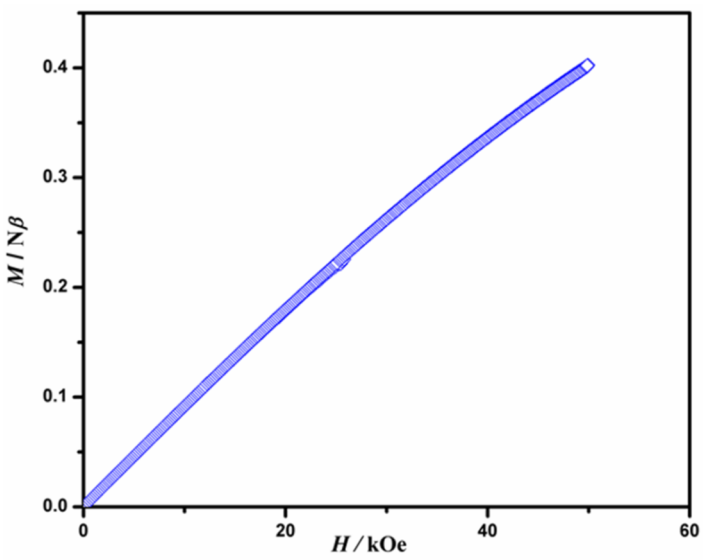

Figure 11. The *M vs. H* curve for **1** at 5 K.

LANL2DZ basis set for the whole trinuclear core. Our calculations show that, for the trinuclear core, the doublet state is stable than the quartet state by 0.2028 eV. This result also suggest that Cu(II) centres in trinuclear core are strongly antiferromagnetically coupled. The predominant antiferromagnetic interactions can be further confirmed by spin density plot, showing delocalization of opposite spins through O atom of μ_3–OH group (Figure 12).

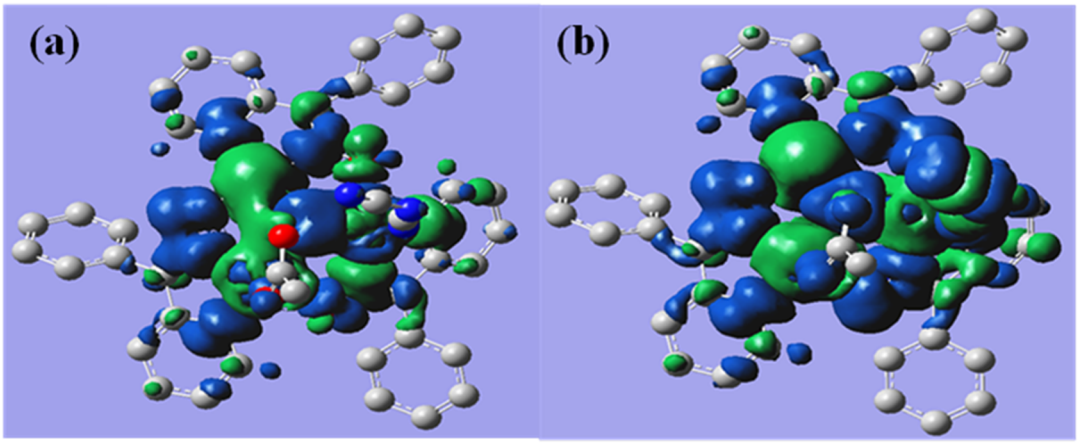

Figure 12. The spin density plot for **1:** (a) doublet and (b) quartet spin state.

The magnetic exchange in cyclic trinuclear complexes with $Cu_3(\mu_3$–OH) core can be correlated by considering a simple three electron spin system. The magnetic interaction in $Cu_3(\mu_3$–OH) core involve Cu–(μ–OH)–Cu superexchange pathways and can exist in either a spin frustrated doublet or in a spin polarized quartet state. Magneto-structural correlations for trimers with the $Cu_3O(H)$ core have already been described in relation to

the two potential bridges: the tridentate central oxygen and the bidentate N, N or N, O peripheral ligand (Table 6).

Table 6. Comparison of structural parameters concerning the μ_3–OH in Cu_3O trinuclear clusters.

Compounds	**O(H)….Cu_3 plane/Å**	**Cu-O(H) /Å (av)**	**Cu-Cu'/Å (av)**	**-*J*/cm^{-1}**	**References**
A	0.352	1.868	3.177	1000	21
B	0.695	1.964	3.194	122	21
C	0.816	1.973	3.111	109	25
D	0.92	2.003	3.101	400	17
E	0.66	1.942	3.166	220	18
F	-	1.891	3.275	500	8f
G	-	1.992	3.251	140	22
H	0.576	2.013	3.341	191.2	23
I	0.478	1.99	3.351	200	24
J	0.473	1.991	3.355	197.7	5c
K	0.564	2.000	3.341	190.9	5c
L	0.433	2.007	3.371	198.2	5c
1	**0.616**	**1.957**	**3.215**	**459.7**	**This work**

A=$[Cu_3(O)L'_3(ClO_4)]_2$, HL'= 1,2-diphenyl–2–(methylimino)ethanone–1–oxime; B=$[Cu_3(OH)L''_3(ClO_4)]^+$, HL''= 3–(phenylimino)butanone-2-oxime;C=$[Cu_3(amox)_3(\mu_3\text{–}OH)(\mu_3\text{–}Cl)]ClO_4$, amoxH= 4–amino–4–methylpentan–2–one oxime; D=$[Cu_3(PhPyCNO)_3(OMe)(Cl)(ClO_4)]$, PhPyCNO= phenyl–2-pyridyl ketooxime; E=$[Cu_3(PhPyCNO)_3(\mu_3\text{-}OH)(2,4,5\text{–}T)_2]$, 2,4,5–T= 2,4,5–trichlorophenoxyacetate; pz=pyrazole; F=$[PPN]_2[Cu_3(\mu_3\text{–}O)(\mu\text{–}pz)_3Cl_3]$,G=$Cu_3(\mu\text{–}OH)(\mu\text{–}Cl)(pz)_3(py)_2Cl_2$; H=$[Cu_3(\mu_3\text{–}OH)(hppt)_3(NO_3)_2](H_2O)_4$; hppt =3–(2–hydroxyphenyl)–4–phenyl–1,2,4–triazole; I=$[Cu_3(\mu_3\text{-}OH)(pz)_3(NO_3)(Hpz)_2](NO_3).H_2O$,J=$[Cu_3(OH)(aat)_3(CF_3SO_3)(H_2O)_2](CF_3SO_3)$, K=$[Cu_3(OH)(aat)_3(NO_3)(H_2O)_2](NO_3).(H_2O)_2$; L=$[Cu_3(OH)(aat)_3(ClO_4)(H_2O)_2](ClO_4)$.

Cu-OH-Cu angle is a major factor controlling the spin coupling between the metal centres in hydroxide, alkoxide or phenoxide bridged compounds.[20] For the larger Cu–OH–Cu angles, like greater than ≥97.5°, the antiferromagnetic interactions predominates. In fact, in our system all the Cu–OH–Cu angles are in the range of 105.98(17)–114.99(17)° which fall in the range of similar parameters of trinuclear core showing antiferromagnetic interactions. The magnitude of the magnetic interaction depends on the coplanarity of the coordination planes around each copper atom and the distance of μ_3–O(H) from the mean Cu_3 plane.[21] The more flattened is the $Cu_3O(H)$ core, the stronger will be the magnetic interaction.[8f] Moreover, lower interplanar angle between the equatorial planes of copper(II) gives rise to higher *J* value as it results in larger overlap of

the $d_{x^2-y^2}$ magnetic orbital.[11d] For trinuclear $Cu_3O(H)$ systems, the highest J value of -1000 cm^{-1} was reported for an oximate compound, $[Cu_3(O)L'_3(ClO_4)]_2$ (**A**), HL'= 1,2–diphenyl–2–(methylimino)ethanone–1–oxime[21] which has an average interplanar angle of 20.5° and a distance of 0.352 Å of μ_3–OH from the mean Cu_3 plane. Recently, Afrati *et al*[17,18] have reported a trinuclear Cu_3-OH core similar to **1**, using phenyl–2–pyridylketoxime ligand with $J \geq -400$ cm^{-1} obtained experimentally as well as theoretically. The average Cu···Cu distance (3.22 Å) and the deviation of μ_3–OH (0.59 Å) from the mean Cu_3 plane in $[Cu_3(PhPyCNO)_3(OH)(CH_3OH)_2(ClO_4)_2]$ (PhPyCNO = phenyl–2–pyridylketoxime)[18] is similar to compound **1,** which are 3.21 Å and 0.616 Å, respectively. Furthermore, in **1** the average inter planar angle between the equatorial planes of Cu(II) is 38.79°. Therefore, the J value obtained in **1** (-457.9 cm^{-1}) is reasonable which also corresponds well with the J value for above compound (-456.5 cm^{-1}) which was obtained theoretically. A comparison of important structural parameters and the corresponding J values of copper compounds containing a $Cu_3O(H)$ core is given in Table 6**.**

The obtained magnetic data for **2** is plotted as $\chi_M T$ and χ_M *vs.* T as shown in Figure 13. The $\chi_M T$ value at 300 K is 1.56 cm^3 mol^{-1} K. This value is slightly higher than the spin only value expected for a cluster comprising four Cu(II) non-interacting ions (1.50 cm^3 mol^{-1} K with g = 2). The $\chi_M T$ product continuously decreases with decreasing temperature and becomes 0.112 cm^3 mol^{-1} K at temperature 2.7 K. This indicates antiferromagnetic interactions operating in **2**. The M *vs* H curve at 5 K reaches a maximum value of 0.21 Nβ, which is well below from the expected 4 Nβ (Figure 14), also suggesting the antiferromagnetic interactions operating within the tetranuclear Cu(II) core. In order to avoid over parameterization, we have simplified the tetranuclear cluster by considering only the significant interactions (i.e. Cu1–O4–Cu3, Cu3–O5–Cu2, Cu2–O2–Cu4, and Cu4–O8–Cu1) (Scheme 2). Since the apical Cu–O bond distances are quite

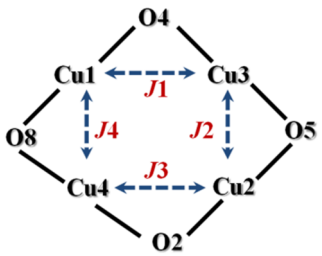

Scheme 2. Simplified coupling scheme between the Cu(II) centres for **2**.

large (see table 4), all other interactions except above four mentioned ones (the bridges involved in these four interactions are in the equatorial positions) can be approximated to be negligible.

Now the bond distances and bond angles involved in these four interactions are almost same (see Table 4 and 5) and the exchange interactions can be considered to be equivalent, and therefore *J1* = *J2* = *J3* = *J4*= *J*. Hence for the interactions in the tetranuclear core an isotropic Heisenberg Hamiltonian formalism (eq 4) is:

$$H = -J(\hat{S}_1 \hat{S}_3 + \hat{S}_2 \hat{S}_3 + \hat{S}_2 \hat{S}_4 + \hat{S}_4 \hat{S}_1) \quad \text{.....(4)}$$

Now the general relation between $\chi_M T$ and T is

$$\chi_M T = (N\beta^2 g^2/kT)[_{i=16}\Sigma(S_z)^2 e^{-Ei(J)/KT}]/[\Sigma e^{-Ei(J)/KT}] \quad \text{.....(5)}$$

For compound **2**, 16 spin states (six states with $S_z = 0$, eight with $S_z = 1$ and two states with $S_z = 2$) are possible. Now from equations 4 and 5, the equation of the temperature dependence of the magnetic susceptibility can be derived as:

$$(\chi_M)_{tetra} = (N\beta^2 g^2/kT)[4 + 2\exp(J/kT) + 10\exp(-J/kT)]/[7 + \exp(2J/kT) + 3\exp(J/kT) + 5\exp(-J/kT)] \quad \text{.....(6)}$$

As we have mentioned earlier that the tetranuclear cores are further connected by the hydroxido groups forming a 1D coordination chain, therefore an intertetramer *zj′* term was introduced which results to the final expression as:

$$\chi_M = (\chi_M)_{tetra}/[1-(2zj'/N\beta^2 g^2)(\chi_M)_{tetra}] \quad \text{.....(7)}$$

The best fit parameters obtained based on equation 7 are $J = -27.09$ cm^{-1}, $zj' = -9.65$ cm^{-1} with g= 2.17 and $R = 2.67\times10^{-3}$ where $R = \sum[(\chi_M)^{obs} - \chi_M)^{calc}]^2/[(\chi_M)^{obs}]^2\}$ (Fig. 7). We have mentioned previously that for oxido-bridged Cu(II) complexes the spin-coupling between the copper ions depend strongly on the geometry of the Cu(II) centre and the Cu–O–Cu bridging angles and distances. In the tetranuclear core of **2** all the Cu–O–Cu angles involved in the important magnetic exchange pathways are in the range of 109–115° which falls under the range of antiferromagnetic interaction. To gain insight into the magnetic exchange mechanism in **2** spin-unrestricted calculations were performed using the Gaussian 03 package at the B3LYP level employing the LanL2DZ basis set. We have considered a $\{[Cu_4(pdmH)_2(pdm)_2(\mu_2\text{–}OH)(H_2O)]\cdot ClO_4\}$ unit for

calculating ground state energy of the singlet, triplet and the quintet states. The triplet state was found to be the most stable one, followed by the quintet and singlet states, respectively. The triplet state is more stable than the quintet state by 0.1069 eV suggesting the dominant antiferromagnetic exchange coupling among the Cu(II) centres within the tetranuclear core. This fact is further proved by the spin density plots (Figure15).

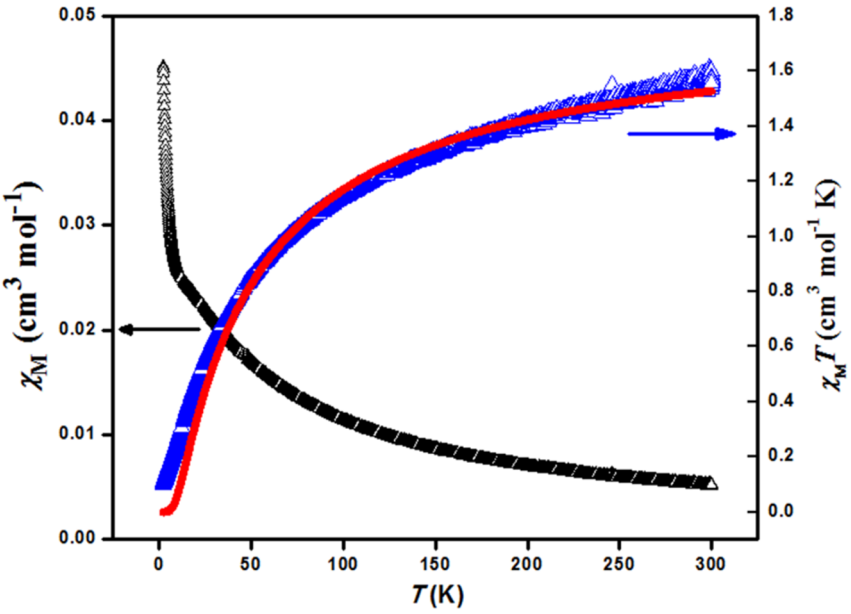

Figure 13. The plots of χ_M *vs. T* and $\chi_M T$ *vs. T* for **2**. The red line indicates the possible best fit obtained.

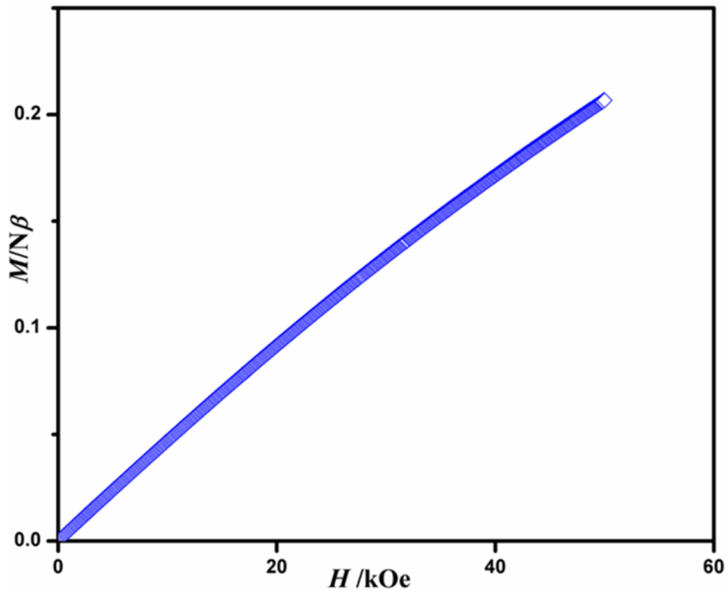

Figure 14. The M *vs. H* curve for **2** at 5 K.

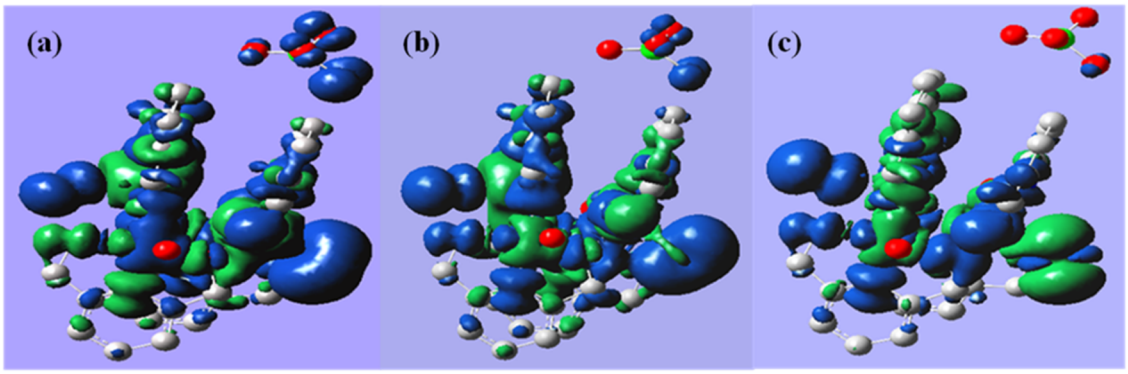

Figure 15. The spin density plot for **2:** (a) quintet, (b) triplet and (c) singlet spin state.

2.4 CONCLUSION

Exploiting the use of two different blocking ligands and using simple self-assembly approach, we were able to synthesize and structurally characterize two novel magnetic systems, to be precise 1D coordination chains of Cu(II) (S = ½). The chains are based on trinuclear and tetranuclear building blocks $Cu_3(\mu_3\text{–}OH)(ppk)_3(OAc)$ and $[Cu_4(pdmH)_2(pdm)_2(H_2O)_2]$; which are connected by $N(CN)_2^-$ and OH^- groups, respectively. Temperature dependent magnetic studies show that for both the compounds, antiferromagnetic interactions operate between the metal centres in the trinuclear and the tetranuclear cores. Weak antiferromagnetic interactions prevail between the cores in both the cases. Magneto-structural correlations suggest the observed dominant antiferromagnetic interactions associate with the bridging angles and distances between Cu(II) centres. The magnetic behaviour has also been qualitatively explained by DFT calculations. The study of such systems is of paramount importance as trinuclear and tetranuclear core exhibit spin frustrated behaviour and their proper understanding will shed some light into fundamental aspects of molecular magnetism.

2.5 REFERENCES

[1] (a) E. Coronado, P. Delhaes, D. Gatteschi and J. S. Miller, Dordrecht, *Molecular magnetism: From the molecular assemblies to the Devices*, NATO ASI series no. E321, Dordrecht, 1996; (*b*) R. Sessoli, H. L. Tsai, A. R. Schake, S. Wang, J. B. Vincent, K. Folting, D. Gatteschi, G. Christou and D. N. Hendrickson, *J. Am. Chem. Soc*., 1993, **115**, 1804; (*c*) R. Sessoli, D. Gatteschi, A. Caneschi and M. A. Novak, *Nature*, 1993, **365**, 141; (*d*) J. H. Eppley, H. L. Tsai, N. de Vries, K. Folting, G. Christou and D. N. Hendrickson, *J. Am. Chem. Soc*., 1995, **117**, 301; (*e*) L. Thomas, F. Lionti, R. Ballou, D. Gatteschi, R. Sessoli and B. Barbara, *Nature,*

1996, **383**, 145; (*f*) D. Gatteschi and R. Sessoili, *Angew. Chem. Int. Ed.*, 2003, **42**, 268; (*g*) W. Wernsdorfer and R. Sessoli, *Science*, 1999, **383**, 145; (*h*) A. J. Tasiopoulos, A. Vinslava, W. Wernsdorfer, K. A. Abboud and G. Christou, *Angew. Chem. Int. Ed.*, 2004, **43**, 2117.

[2] (*a*) H. Miyasaka, K. Nakata, L. Lecren, C. Coulon, Y. Nakazawa, T. Fujisaki, K. Sugiura, M. Yamashita and R. Clerac, *J. Am. Chem. Soc.*, 2006, **128**, 3770; (*b*) M. Murugesu, W. Wernsdorfer, K. A. Abboud, E. K. Brechin and G. Christou, *Dalton Trans.*, 2006, 2285.

[3] (*a*) H. Miyasaka and M. Yamashita, *Dalton Trans.*, 2007, 399; (*b*) G. Christou, D. Gatteschi, D. N. Hendrickson and R. Sessoli, *MRS Bull.*, 2000, **25**, 66; (*c*) D. Gatteschi and R. Sessoli, *J. Magn. Magn. Mater.*, 2004, **272**, 1030.

[4] (*a*) E. I. Solomon, U. M. Sundaram and T. E. Machonkin, *Chem. Rev.*, 1996, **96**, 2563; (*b*) R. H. Holm, P. Kennepohl and E. I. Solomon, *Chem. Rev.*, 1996, **96**, 2239; (c) W. Kaim and J. Rall, *Angew. Chem. Int. Ed.*, 1996, **35**, 43.

[5] (*a*) L. Gutierrez, G. Alzuet, J. A. Real, J. Cano, J. Borras and A. Castineiras, *Inorg. Chem.*, 2000, **39**, 3608; (*b*) Kahn, O. *Chem. Phys. Lett.*, 1997, **265**, 109; (*c*) S. Ferrer, J. G. Haasnoot, J. Reedijk, E. Muller, M.B. Cingi, M. Lanfranchi, A. M. M. Lanfredi and J. Ribas, *Inorg. Chem.*, 2000, **39**, 1859.

[6] (*a*) W. Wernsderfer, N. Aliaga-Alcalde, D. N. Hendricson and G. Christou, *Nature*, 2002, **416**, 406; (*b*) E. E. Moushi, T. C. Stamatatos, W. Wernsdorfer, V. Nastopoulos, G. Christou and A. J. Tasiopoulos, *Angew. Chem. Int. Ed.*, 2006, **45**, 7722.

[7] (*a*) J. Kim, M. L. Jin and Y. Do, *Eur. J. Inorg. Chem.*, 2003, **14**, 2563; (*b*) Y. Z. Zheng, M. L. Tong, W. Xue, W. Zhang, X. M. Chen, F. Grandjean and G.J. Long, *Angew. Chem. Int. Ed.*, 2007, **46**, 6076; (*c*) P. Albores and E. Rentschler, *Inorg. Chem.*, 2008, **47**, 7960.

[8] (*a*) W. Quellette, M. H. Yu, C. J. O'Connor, D. Hagrman and J. Zubieta, *Angew. Chem. Int. Ed.*, 2006, **45**, 3497; (*b*) B. Ding, L. Yi, P. Cheng, D.Z. Liao and S.P. Yan, *Inorg. Chem.*, 2006, **45**, 5799; (*c*) S. Ferrer, F. Lloret, I. Bertomeu, G. Alzuet, J. Borrás, S. García-Granda, M. Liu-González and J. G. Hassnoot, *Inorg. Chem.*, 2002, **41**, 5821; (*d*) M. Casarin, C. Corvaja, C. Di Nicola, D. Falcomer, L. Franco, M. Monari, L. Pandolfo, C. Pettinari, F. Piccinelli, and P. Tagliatesta, *Inorg. Chem.*, 2004, **43**, 5865; (*e*) M. Casarin, C. Corvaja, C. D. Nicola, D. Falcomer, L. Franco, M. Monari, L. Pandolfo, C. Pettinari and F. Piccinelli, *Inorg. Chem.*, 2005, **44**,

6265; (*f*) P.A. Angaridis, P. Baran, R. Boèa, F. Cervantes-Lee, W. Haase, G. Mezei, R. G. Raptis and R. Werner, *Inorg. Chem*., 2002, **41**, 2219.

[9] (*a*) C. D. Nicola, Y. Y. Karabach, A. M. Kirillov, M. Monari, L. Pandolfo, C. Pettinari, and A. J. L. Pombeiro, *Inorg. Chem*., 2007, **46**, 221; (*b*) S. J, Seo, D. Whang, H. Lee, S. I. Jun, J. Oh, Y. J. Jeon and K. Kim, *Nature*, 2000, **404**, 982; (*c*) G. Férey, C. Mellot-Draznieks, C. Serre, F. Millange, J. Dutour, S. Surble and I. Margiolaki, *Science*, 2005, **309**, 2040; (*d*) Q. Fang, G. Zhu, M. Xue, J. Sun, Y. Wei, S. Qiu and R. Xu, *Angew. Chem. Int. Ed*., 2005, **44**, 3845; (*e*) A. Biswas, M. G. B. Drew, J. Ribas, C. Diaz and A. Ghosh, *Eur. J. Inorg. Chem*., 2011, 2405; (*f*) K. Sakai, Y. Yamada, T. Tsubomura, M. Yabuki and M. Yamaguchi, *Inorg. Chem*., 1996, **35**, 542. (*g*) B. Sarkar, M. Sinha Ray, Y. Li, Y. Song, A. Figuerola, E. Ruiz, J. Cirera, J. Cano and A. Ghosh, *Chem. Eur. J*., 2007, **13**, 9297; (*h*) M. Ray, S. Chattopadhyay, M. G. B. Drew, A. Figuerola, J. Ribas, C. Diaz and A. Ghosh, *Eur. J. Inorg. Chem*., 2005, 4562.

[10] (*a*) S. R. Breeze, S. N. Wang and L.Q. Chen, *J. Chem. Soc. Dalton Trans*., 1996, 1341; (*b*) J. Reim, K. Griesar, W. Haase and B. Krebs*, J. Chem. Soc. Dalton Trans*., 1995, 2649; (*c*) J. T. Guy, J. C. Cooper, R. D. Gilardi, J. L. Flipen-Anderson and C. F. George, *Inorg. Chem*., 1988, **27**, 635; (*d*) S. Teipel, K. Griesar, W. Haase, and B. Krebs, *Inorg. Chem*., 1994, **33**, 456; (*e*) M. Bera, W. T. Wong, G. Aromi, J. Ribas and D. Ray, *Inorg. Chem*., 2004, **43**, 4787; (*f*) A. Fragoso, M. L. Kahn, A. Castineiras, J. P. Sutter, O. Kahn and R. Cao, *Chem. Commun*., 2000, **24**, 1547; (*g*) S. Mukherjee, T. Weyhermüller, E. Bothe, K. Wieghardt and P. Chaudhuri, *Eur. J. Inorg. Chem*., 2003, 863; (*h*) S. Mukherjee, B. Gole, Y. Song and P. S. Mukherjee, *Inorg. Chem*., 2011, **50,** 3621; (*i*) G. Li, Y. Xing, S. Song, N. Xu, X. Liu and Z. Su, *J. Solid State Chem*., 2008, **181**, 2406; (*j*) X. Zhang, Y. Wang and E. Gao, *Eur. J. Inorg. Chem*., 2010, 1249; (*k***)** J. Zhao, D. Shi, H. Cheng, L. Chen, P. Ma and J. Niu, *Inorg. Chem. Commun*., 2010, **13**, 822; (*l*) S. Sain, T. K. Maji, G. Mostafa, T. H. Lu and N. Ray Chaudhuri, *Polyhedron*, *2003*, **21**, 2293.

[11] (*a*) S. Mukherjee, B. Gole, R. Chakrabarty and P. S. Mukherjee, *Inorg. Chem*., 2009, **48**, 11325; (*b*) V. Chandrasekhar, T. Senapati and E. C. Sañudo, *Inorg. Chem*., 2008, **47**, 9553; (*c*) V. Chandrasekhar, R. Azahar, T. Senapati, P. Thialagar, S. Ghosh, S. Verma, R. Boomishankar, A. Steiner and P. Kögerler, *Dalton Trans*., 2008, 1150; (*d*) S. Karmakar, O. Das, S. Ghosh, E. Zangrando, M. Johann, E.

Rentschler, T. Weyhermüller, S. Khanra and T. K. Paine, *Dalton Trans*., 2010, **39**, 10920.

[12] (*a*) P. Chaudhuri, *Coord*. *Chem*. *Rev*., 2003, **243**, 143; (*b*) Th. C. Stamatatos, K. V. Pringouri, C. P. Raptopoulou, R. Vicente, V. Psycharis, A. Escuer and S. P. Perlepes, *Inorg*. *Chem*. *Commun*., 2006, 1178; (*c*) C. J. Milios, P. Kyritsis, C. P. Raptopoulou, A. Terzis, R. Vicente, A. Escuer and S. P. Perlepes, *Dalton Trans*., 2005, 501; (*d*) Th. C. Stamatatos, A. K. Boudalis, Y. Sanakis and C. P. Raptopoulou, *Inorg*. *Chem*., 2006, **45**, 7372; (*e*) Th. C. Stamatatos, S. Dionyssopoulou, G. Efthymiou, P. Kyritsis, C. P. Raptopoulou, A. Terzis, R. Vicente, A. Escuer and S. P. Perlepes, *Inorg*. *Chem*., 2005, **44**, 3374; (*f*) Th. C. Stamatatos, J. C. Vlahopoulou, Y. Sanakis, C. P. Raptopoulou, V. Psycharis, A. K. Boudalis and S. P. Perlepes, *Inorg*. *Chem. Commun*., 2006, **9**, 814; (*g*) Th. C. Stamatatos, E. Diamantopoulou, C. P. Raptopoulou, V. Psycharis, A. Escuer and S. P. Perlepes, *Inorg*. *Chem*., 2007, **46**, 2350; (*h*) F. Mori, T. Ishida and T. Nogami, *Polyhedron*, 2005, **24**, 2588; (*i*) M. Alexiou, C. Dendrinou-Samara, A. Karagianni, S. Biswas, C. M. Zaleski, J. Kampf, D. Yoder, J. E. Penner-Hahn, V. L. Pecoraro and D. P. Kessissoglou, *Inorg*. *Chem*., 2003, **42**, 2185; (*j*) T. Taguchi, Th. C. Stamatatos, K. A. Abboud, C. M. Jones, K. M. Poole, T. A. O'Brien and G. Christou, *Inorg*. *Chem*., 2008, **47**, 4095.

[13] (*a*) S. Winter, W. Seichter and E. Z. Weber, *Anorg*. *Allg*. *Chem*., 2004, **630**, 434; (*b*) Th. C. Stamatatos, G. C. Vlahopoulou, C. P. Raptopoulou, A. Terzis, A. Escuer and S. P. Perlepes, *Inorg*. *Chem*., 2009, **48**, 4610; (*c*) G. C. Vlahopoulou, D. I. Alexandropoulos, C. P. Raptopoulou, S. P. Perlepes, A. Escuer and Th. C. Stamatatos, *Polyhedron*, 2009, **28**, 3235; (*d*) G. Liu, W. Guo, S. Nishihara and X. Ren, *Inorg*. *Chim*. *Acta*, 2011, **368**, 165.

[14] (*a*) SMART (V 5.628), SAINT (V 6.45a), XPREP, SHELXTL; Bruker AXS Inc. Madison, Wisconsin, USA, 2004; (*b*) G. M. Sheldrick, Siemens Area Detector Absorption Correction Program, University of Göttingen, Göttingen, Germany, 1994; (*c*) A. Altomare, G. Cascarano, C. Giacovazzo, A. Gualaradi, *J*. *Appl*. *Cryst*., 1993, **26**, 343; (*d*) G. M. Sheldrick, SHELXL-97, Program for Crystal Structure Solution and Refinement; University of Göttingen, Göttingen, Germany, 1997; (*e*) A. L. Spek, *J*. *Appl*. *Cryst*., 2003, **36**, 7; (*f*) L. J. Farrugia, WinGX–A Windows Program for Crystal Structure Analysis, *J*. *Appl*. *Crystallogr*., 1999, **32**, 837.

[15] E. König, *Landolt-Börnstein, Neue Serie*; Springer: Berlin, 1966; Vol. II/2, 1.

[16] A. W. Addison, T. N. Rao, J. Reedijk, J. van Rijn and G. C. Verschoor, ***J. Chem**. Soc., Dalton Trans*., 1984, 1349.

[17] T. Afrati, C. Dendrinou-Samara, C. Raptopoulou, A. Terzis, V. Tangoulis and D. P. Kessissoglou, *Dalton Trans*., 2007, 5156.

[18] T. Afrati, C. Dendrinou-Samara, C. Raptopoulou, A. Terzis, V. Tangoulis, A. Tsipis and D. P. Kessissoglou, *Inorg*. *Chem*., 2008, **47**, 7545.

[19] (*a*) L. Noodleman, *J*. *Chem*. *Phys*., 1981, **74**, 5737; (*b*) M. J. Frisch et al. GAUSSIAN 03, Revision C.02, Gaussian Inc., Wallingford, CT, 2004.

[20] (*a*) M. P. Suh, M.Y. Han, J. H. Lee, K. S. Min and C. Hyeon, *J*. *Am*. *Chem*. *Soc*., 1998, **120**, 3819; (*b*) E. Ruiz, P. Alemany, S. Alvarez and J. Cano, *J*. *Am*. *Chem*. *Soc*., 1997, **119**, 1297.

[21] R. J. Butcher, C. J. O'Connor and E. Sinn, *Inorg*. *Chem*., 1981, **20**, 537.

[22] M. Angaroni, G. A. Ardizzoia, T. Beringhelli, G. L. Monica, D. Gatteschi, N. Masciocchi and M. Moret, *J*. *Chem*. *Soc*. *Dalton Trans*., 1990, 3305.

[23] W. Vreugdenhil, Ph.D. Thesis, Leiden University, The Netherlands, 1987.

[24] F. B. Hulsbergen, R. W. M. Hoedt, J. Verschoor, J. Reedijk and A. L. J. Spek, *J. Chem*. *Soc*., *Dalton Trans*., 1983, 539.

[25] Y. Jiang, H. Kou, R. Wang, A. Cui and J. Ribas, *Inorg*. *Chem*., 2005, **44**, 709.

Chapter 3

A Novel Heterometallic Cu(II)-Ni(II) Decameric Cluster: Synthesis, Structure and Magnetic Properties

Abstract

Synthesis, structural characterization and magnetic study of a heterometallic Cu(II)–Ni(II) decameric cluster are presented in this chapter. The compound {[$Ni_4Cu_6(\mu$–$OH_2)_2(dpkO_2)_8(OAc)_4(H_2O)_4]\cdot 2CH_3OH\cdot 17H_2O$} (**1**), [$dpkO_2 = (C_5NH_4)_2CO_2$] has been synthesized by self–assembly of metal ions and multinucleating ligand di(2–pyridyl)ketone (dpk), and is structurally characterized. The decanuclear cluster has been formed by the union of two symmetry related distorted cubane–like pentanulcear [$Ni_2Cu_3(\mu$–$OH_2)(dpkO_2)_4(OAc)_2(H_2O)$] cores, consisting of two Ni(II) and three Cu(II) centres. Magnetic study of **1** reveals that antiferromagnetic interactions operate through the Ni–O–Ni pathway while Cu–O–Cu pathways contribute to ferromagnetic interactions.

3.1 INTRODUCTION

The rich chemistry of high spin clusters or coordination polymers is an area of substantial research due to the large diversity in intriguing structures and potential applications in the field of molecular magnetism.[1] Recently, enormous interest has been directed towards the study of polynuclear heterometallic clusters[2] to explore their importance in bioinorganic chemistry[3] and also as new molecule based magnetic materials. In biological systems, polynuclear metal centres are present at the active sites of a number of metalloproteins or enzymes. Prominent examples are the iron storage proteins ferritin, the tetranuclear manganese cluster in photosystem II, the heteronuclear active sites in nitrogenase and several oxidases. In the context of molecular magnetism, polynuclear heterometallic clusters are promising candidates as single molecule magnet (SMM)[4-5], which have potential application in high density information storage and quantum computation.[6] The greater size of the local spins, larger anisotropy and higher spin–orbit coupling values in the high-nuclearity heterometallic cluster play important role to achieve SMM behaviour. Though there are some reports on small single molecule magnets (SMMs), consisting of heterometallic (3d and 4f) polynuclear clusters,[7] a larger database is required to get insight into their magneto structural correlations for understanding basic magnetic exchange phenomenon and technologically applicable properties. The design of cluster based on two transition metal ions, like Cu(II) and Ni(II), having different coordination geometry remains a challenge as precise control over the nuclearity of the cluster having large number of metal ions is very difficult. Thus to achieve desired structure by self–assembly, it is necessary to conceive a rational approach based on the ligand binding mode and the right coordination environment of metal ions.[8a] Polytopic ligands, like di(2–pyridyl)ketone, (dpk) with well-defined and appropriately separated coordination compartments, in principle have a better control over the outcome of a self-assembly process to produce a cluster with a predefined nuclearity. Moreover, dpk can be *in situ* translated into a new ligand in aqueous or alcoholic medium through nucleophilic attack to keto group in presence of metal ions.[8b] This *in situ* generation of new ligand renders further flexibility towards binding more number of metal centres. Here we envisioned that spontaneous self-assembly of dpk with two different transition metal ions, Cu(II) and Ni(II), would furnish subtle balance between coordination algorithm of the metals and the flexible binding mode of the ligands without any geometrical restrictions. In this chapter, we present synthesis, structure and magnetic

properties of a heterometallic decanuclear complex {$[Ni_4Cu_6(\mu\text{–}OH_2)_2(dpkO_2)_8(OAc)_4(H_2O)_4]\cdot 2CH_3OH\cdot 17H_2O$} (**1**) [$dpkO_2^{2-}$=$(C_5NH_4)_2CO_2$ (Scheme 1)] formed by the self-assembly of Cu(II) and Ni(II) and the multinucleating ligand dpk in water/MeOH medium. The pentanuclear core $[Ni_2Cu_3(\mu\text{–}OH_2)(dpkO_2)_4(OAc)_2(H_2O)]$ is connected by water bridge to form the decanuclear cluster and to the best our knowledge this is the first example of such heterometallic system. Temperature dependent magnetic study suggests that antiferromagnetic interactions operate through the Ni–O–Ni pathway whereas Cu–O–Cu pathways result ferromagnetic interaction.

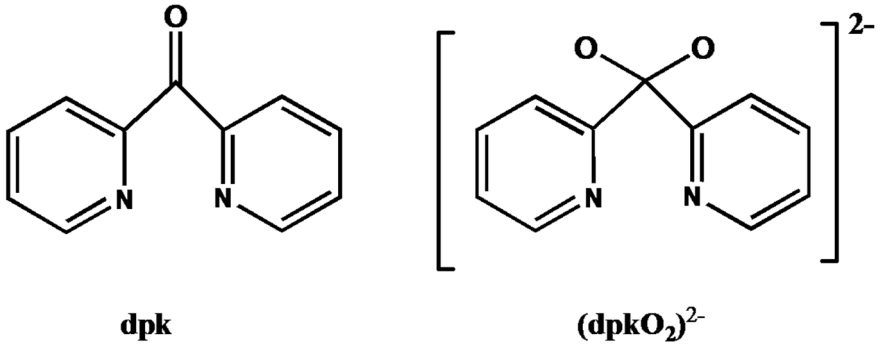

dpk **$(dpkO_2)^{2-}$**

Scheme 1. Structures of dpk and $(dpkO_2)^{2-}$.

3.2 EXPERIMENTAL SECTION

3.2.1 Materials

All the reagents and solvents used are commercially available and used as supplied without further purification. $Cu(OAc)_2\cdot H_2O$, $Ni(OAc)_2\cdot H_2O$ and di(2-pyridyl)ketone (dpk) were obtained from the Aldrich chemical Co.

3.2.2 Synthesis

$Cu(OAc)_2\cdot H_2O$ (1 mmol, 0.199 g) was dissolved in 10 mL H_2O and then CH_3OH solution (5 mL) of dpk (1 mmol, 0.184 g) was dropwise added to the above solution with constant stirring. The resulting solution was stirred for 15 minutes. Then aqueous solution (10 mL) of $Ni(OAc)_2\cdot H_2O$ (1 mmol, 0.249 g) was dropwise added to the above reaction mixture and the whole reaction mixture turned to green which was stirred for one hour. Then the reaction mixture was filtered and kept for slow evaporation at room temperature. Green colour single crystals suitable for X-ray analysis were isolated after two weeks and washed with H_2O and CH_3OH (Yield: 53% relative to Cu). Selected IR data (KBr, cm^{-1}); 3424 br, 1604s, 1583 s, 1375 s, 1046 m, 665 m (Figure 1). Compound purity was verified

by PXRD (Figure 2) and elemental analysis result. Anal. calcd. for **1** : C, 40.14; H, 4.47; N,7.64. Found: C, 40.07; H, 4.12; N, 7.94%.

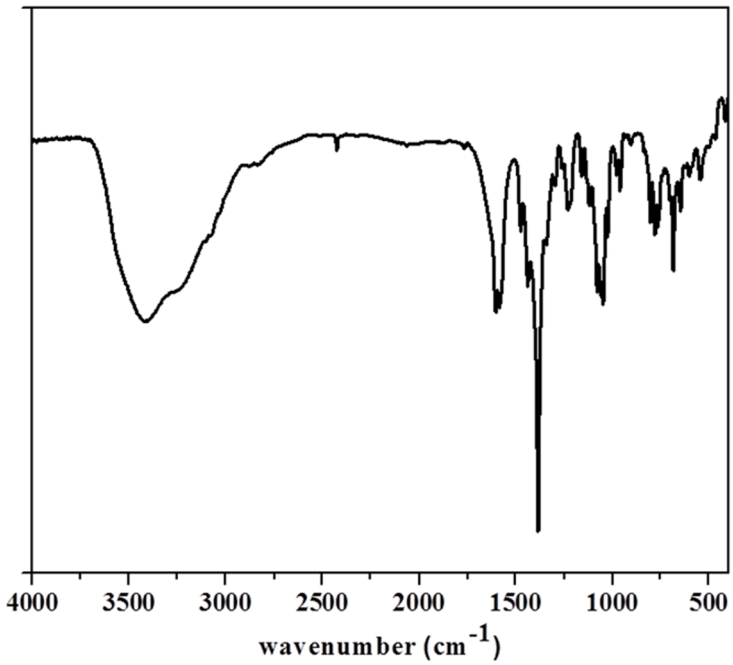

Figure 1. FT-IR spectrum for **1**.

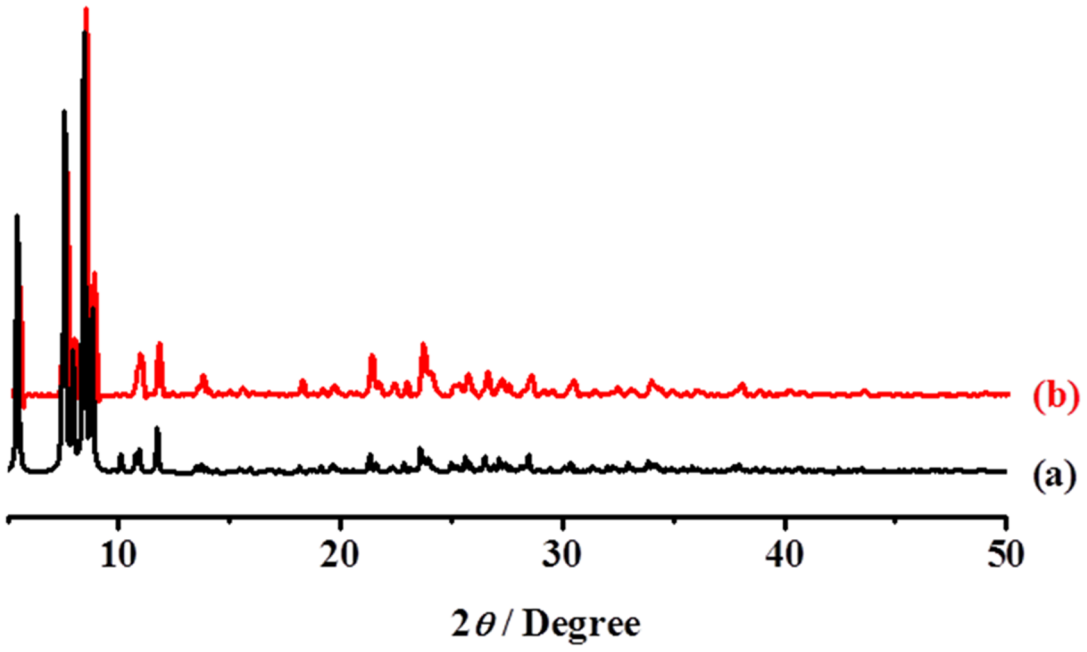

Figure 2. PXRD pattern of compound **1**: (a) simulated; (b) bulk as-synthesized. High purity of the compound is reflected by the similarity in simulated and as-synthesized pattern.

3.2.3 Single-crystal X-ray Diffraction

Crystallographic data were collected on a Bruker Smart-CCD diffractometer equipped with a normal focus, 2.4 kW sealed tube X-ray source with graphite monochromated Mo-Kα radiation (λ = 0.71073 Å) operating at 50 kV and 30 mA. The programme SAINT[9a] was used for integration of diffraction profiles and absorption correction was made with SADABS[9b] programme. The structure was solved by SIR 92[9c] and refined by full matrix least square method using SHELXL-97.[9d] All the non-hydrogen atoms (except the guest water molecules and O12W atom) were refined anisotropically and all the hydrogen atoms were fixed by HFIX and placed in ideal positions. All calculations were carried out using SHELXL 97, PLATON[9e] and WinGX system, Ver 1.70.01.[9f]

3.2.4 Physical Measurements

Elemental analyses were carried out on a Perkin Elmer 2400 CHN analyser. IR spectra were recorded in KBr pellets on a Bruker IFS 66v/S spectrophotometer in the region of 4000 – 400 cm^{-1}. Powder X-ray diffraction (PXRD) patterns were recorded on a Bruker D8 Discover instrument using Cu–Kα radiation. DC magnetic susceptibility data of powdered crystalline samples of **1** were collected on a Vibrating Sample Magnetometer, PPMS (Physical Property Measurement System, Quantum Design, USA) in the temperature range of 3 K to 300 K, with an applied field of 500 Oe. Field variation (−5 kOe to 5 kOe) magnetization measurement was carried out at 2 K. Inductively coupled plasma atomic emission spectroscopy (ICP-AES) study was carried out using a Perkin-Elmer Optima 2100 DV spectrometer.

3.3 RESULTS AND DISCUSSION

3.3.1 Crystal Structure Description

Single crystal X–ray diffraction study reveals that compound **1** crystallizes in monoclinic $P2_1/c$ space group and contains a decanuclear cluster comprised of two symmetry related pentanuclear cores with formula $Ni_2Cu_3(\mu\text{–}OH_2)(dpkO_2)_4(OAc)_2(H_2O)]$. Presence of both Cu(II) and Ni(II) is supported by the ICP and energy dispersive X–ray spectroscopy (EDX) data (Figure 3).

ICP data supports the relative molar ratio of Ni:Cu (2:3) in the complex **1**. The positions of the metal atoms were assigned on the basis of coordination geometry and str-

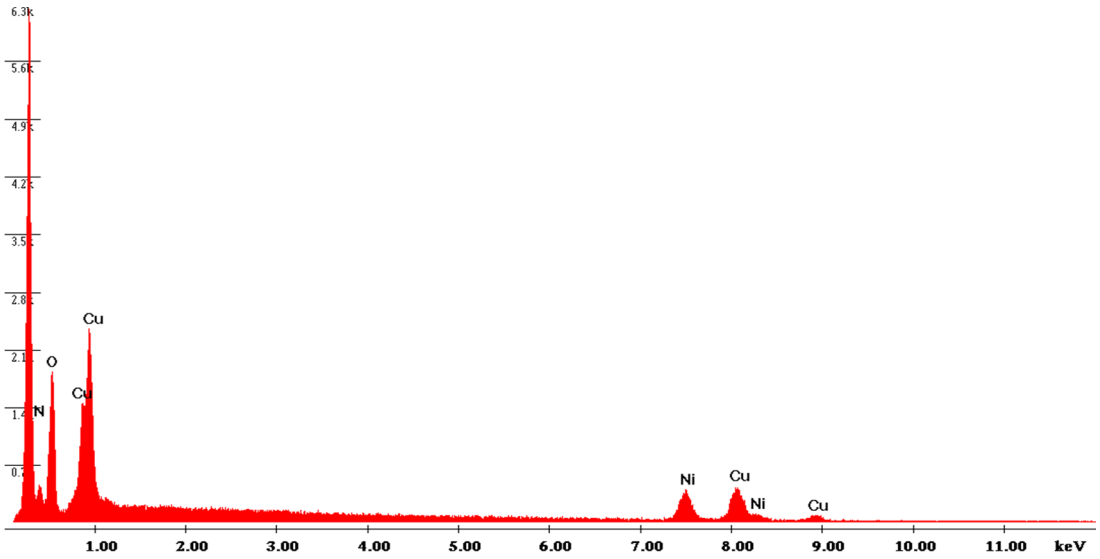

Figure 3. EDX analysis for **1** confirming the presence of both Cu(II) and Ni(II).

-ucture refinement parameters. The pentanuclear core (Figure 4) contains two crystallographically independent Ni(II) centres and three crystallographically independent Cu(II) centres having different coordination environments. The metal centres are bridged by three $dpkO_2$, doubly deprotonated anions of the gem-diol form $(C_5NH_4)_2C(OH)_2$, formed by the *in situ* reaction in presence of metal ions. Ni1 and Ni2 display octahedral coordination as preferred by virtue of the high octahedral site stabilzation energy (OSSE) of Ni(II). Ni1 adopts distorted octahedral geometry and chelated to two different $dpkO_2$ ligands; (O1, N1; O3, N3 atoms), the other two coordinations are furnished by O7 atom of another $dpkO_2$ ligand and O14 atom of a coordinated water molecule. Ni2 also locates itself in a distorted octahedral geometry. Three different $dpkO_2$ ligands (O3, N4; O5, N6; and O7, N8 atoms) chelate Ni2 atom. The Ni–O bond lengths vary from 2.001(8) Å to 2.199(7) Å whereas the Ni–N bond lengths are in the range of 2.052(10)–2.114(10) Å (Table 1). All the copper atoms adopt distorted square pyramidal (4+1) geometry. Cu1 is coordinated to three different $dpkO_2$ ligands (ligated through N5, O5; O2; O3 atoms) and one acetate ligand (O9 atom). For Cu2, the coordination sites are occupied by three different $dpkO_2$ ligands (O7, N7; O1 and O5 atoms) and one acetate ligand (O11 atom). Cu3 is ligated to one $dpkO_2$ ligand (O2, N2), two bridging μ–OH_2 (O13, O13_a) and one coordinated water molecule (O12W atom).The Cu–O/N equatorial bond lengths are in the range of 1.907(7)–2.035(10) Å and the Cu–O apical bond lengths vary from 2.312(7) Å to 2.73(2) Å. Ni1, Ni2, Cu1 and Cu2 form a distorted cubane like structure with a missing one edge (Figure 4, 7).

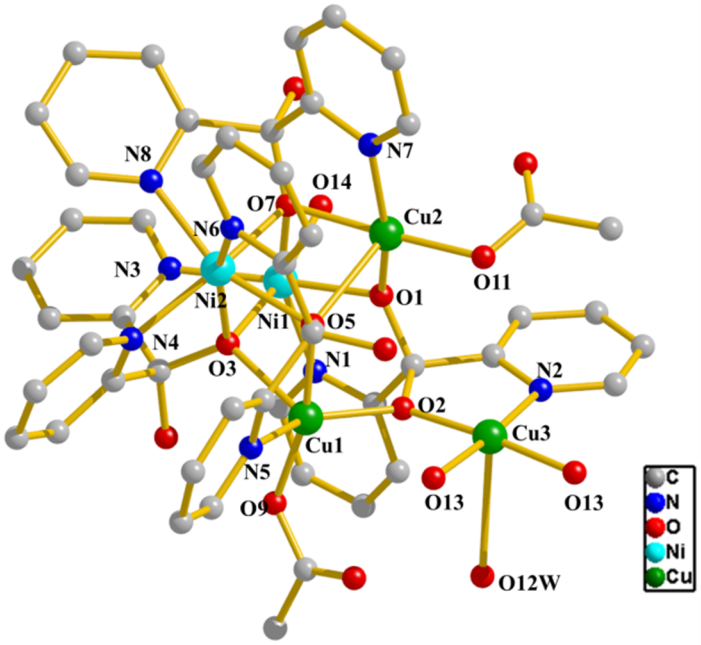

Figure 4. The pentanuclear core of the $[Ni_4Cu_6]$ cluster.

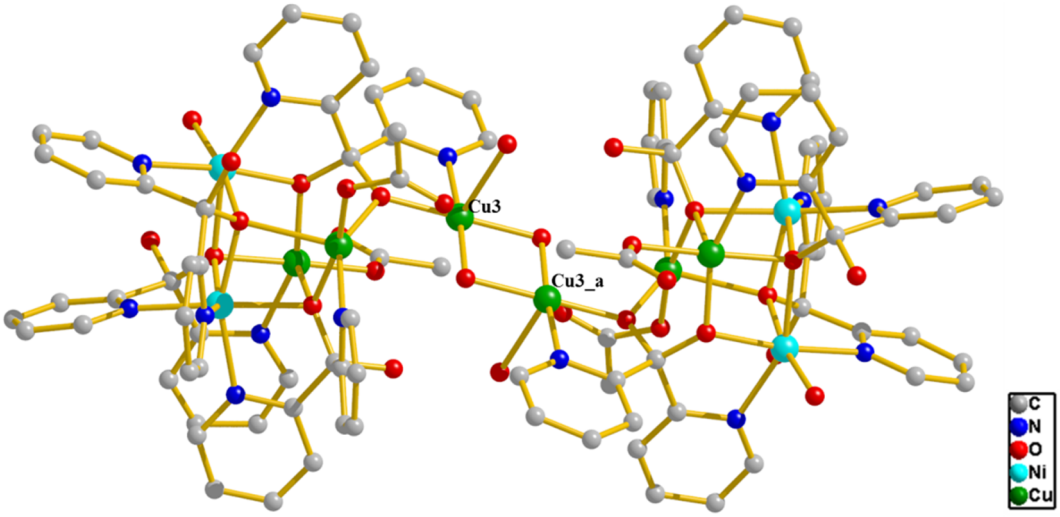

Figure 5. Water bridged decanuclear core of 1 consisting symmetry related pentanulcear cores.

Selected bond distances and bond angles are given in Table 1. In the cubane core, μ_3–O5, μ_3–O3 and μ_3–O7 atoms coming from three different dpkO2 ligands bridge Cu1, Cu2, Ni2; Cu1, Ni1, Ni2 and Ni1, Ni2, Cu2 respectively, while Cu2 and Ni1 atoms are doubly bridged by μ_2–O1 atom. The μ_2–O2 atom bridges Cu1 and Cu3 which result in the extension of this cubane to the pentanuclear core (Figure 4). Two pentanuclear cores are further bridged by two water molecules (μ_2–O13 and μ_2–O13_a) to form the novel decanuclear core (Figure 5).

Table 1. Selected Bond Distances (Å) and Angles (°) for **1**.

Ni1-Ni2	3.195	Ni1-Cu2	3.144
Ni2-Cu2	3.190	Ni1-Cu1	3.666
Ni2-Cu1	3.155	Cu1-Cu2	3.664
Cu1-Cu3	3.357	Cu1-O2	1.979(7)
Cu1-O3	2.312(7)	Cu1-O5	1.935(7)
Cu1-O9	1.923(8)	Cu1-N5	2.035(10)
Cu2-O1	1.926(8)	Cu2-O5	2.487(6)
Cu2-O7	1.972(7)	Cu2-O11	1.918(9)
Cu2-N7	2.006(11)	Cu3-O2	1.907(7)
Cu3-O12W	2.73(2)	Cu3-O13	1.926(7)
Cu3-N2	1.969(9)	Cu3-O13_a	1.956(7)
Ni1-O1	2.001(8)	Ni1-O3	2.055(7)
Ni1-O7	2.199(7)	Ni1-O14	2.080(7)
Ni1-N1	2.062(11)	Ni1-N3	2.085(9)
Ni2-O3	2.073(7)	Ni2-O5	2.099(7)
Ni2-O7	2.130(7)	Ni2-N4	2.052(10)
Ni2-N6	2.114(10)	Ni2-N8	2.088(9)
Cu3-O13-Cu3_a	95.4(3)	Cu2-O1-Ni1	106.4(4)
Cu1-O2-Cu3	119.6(4)	Cu1-O3-Ni1	114.1(3)
Cu1-O3-Ni2	91.9(3)	Ni1-O3-Ni2	101.4(3)
Cu1-O5-Cu2	111.4(3)	Cu1-O5-Ni2	102.8(3)
Cu2-O5-Ni2	87.7(2)	Cu2-O7-Ni1	97.7(3)

Symmetry code: a =2−x, −y, −z

Crystal data for 1:

Mr = 2932.2, monoclinic, space group $P2_1/c$, a = 11.8188(6) Å, b = 23.7544(15) Å, c = 22.5442(14) Å, β =98.730(4), V = 6255.9(6) Å^3, Z = 2, Dc = 1.528 g cm^{-3}, R_{int} = 0.132, R_1 = 0.0669, R_w= 0.2009 (R = $\sum||F_o|-|F_c||/\sum|F_o|$, R_w = $[\sum\{w(F_o^2-F_c^2)^2\}/\sum\{w(F_o^2)^2\}]^{1/2}$) for 3665 reflections with $I\geq 2\sigma(I)$, GOF=1.02, $\Delta\rho$ max/min [e Å^{-3}]= 1.09/−0.56.

3.3.2 Magnetic properties

The temperature dependent magnetic studies have been performed for the polycrystalline powder sample of **1** in the temperature range 300–3 K (Figure 6). At room temperature the $\chi_M T$ value is 7.3 cm^3 mol^{-1} K which is slightly higher for four isolated Ni(II) ions and six isolated Cu(II) ions (corresponding theoretical value is 6.4 assuming the limit of g = 2.00). As can be seen from the structural description, decanuclear complex is constructed by the union of two symmetry related pentanuclear cores via di–aqua bridging. In view of this symmetry and to avoid an absolute overparameterization, we

have taken the option to study the magneto-structural correlation for the pentanuclear core which is given in Figure 7.

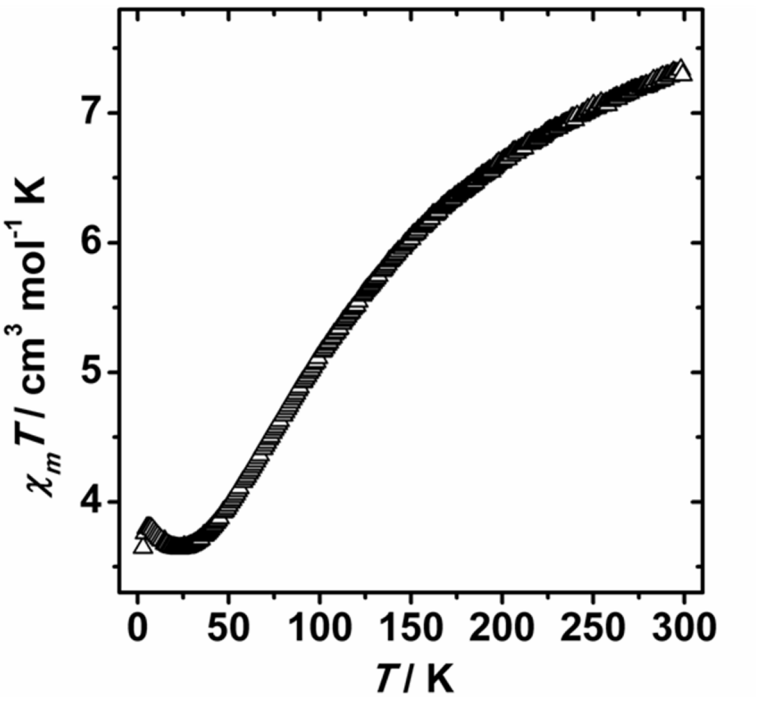

Figure 6. The plot of $\chi_M T$ vs. T for the decanuclear compound (**1**) at 500 Oe.

To avoid an extremely complicated calculation, this hypothesis assumes that the coupling between the two pentanuclear cores is zero, although it is not completely correct. In all the discussion, we have assumed that the important signature of the clear

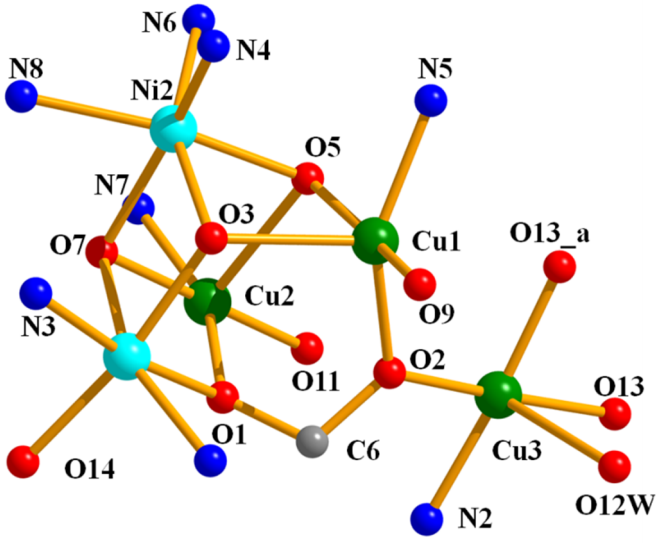

Figure 7. The pentanuclear core showing the metal–ligand bridging. The corresponding magnetic exchange pathways are shown in Table 2.

antiferromagnetism in the $\chi_M T$ *vs. T* plot is due to the antiferromagnetic character of the Ni–O–Ni pathway, which is well documented in the literature for such kind of geometries.[10]

Thus at low temperature contribution of the two Ni(II) ions would be cancelled. As theoretical calculations suggests[11], the magnetic pathway between Cu1–Cu3 would be ferromagnetic where the Cu–O–Cu angle is 119.6(4)°. If the whole system undergoes antiferromagnetic coupling, the final $\chi_M T$ value at 3 K value would be zero and the magnetic interaction between the two pentanuclar cores would be cancelled. Instead, the $\chi_M T$ value at 3 K is 3.5 cm^3 mol^{-1} K, which is rather small for six unpaired copper atoms that are ferromagnetically coupled. On the contrary, the reduced magnetization at 3 K (Figure 8) tends to be 6 $M/N\beta$ (relative to the number of unpaired electrons, i.e. six). This apparently contradictory behaviour indicates that the ferromagnetic couplings are rather weak. Beyond 5 K, there is a small decrease of the $\chi_M T$ product which is probably due to the *D* parameter of Ni(II) ions. The fitting of the magnetic data for the pentanuclear core has been performed using the MAGPACK program[12] with or without the *D* (Zero Field Splitting of the Ni(II) ions). It is worth mentioning that there are differences if we consider *D* or not (which seems to be very logical) in our calculation. The sign of certain coupling constants changes with this variation (see Table 2), but in both cases, the magne-

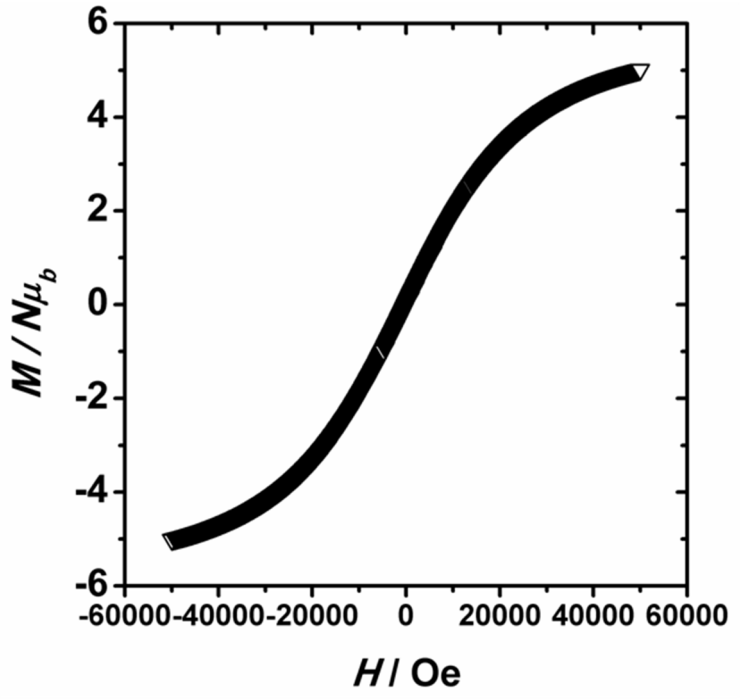

Figure 8. The *M vs. H* curve for **1** at 3 K.

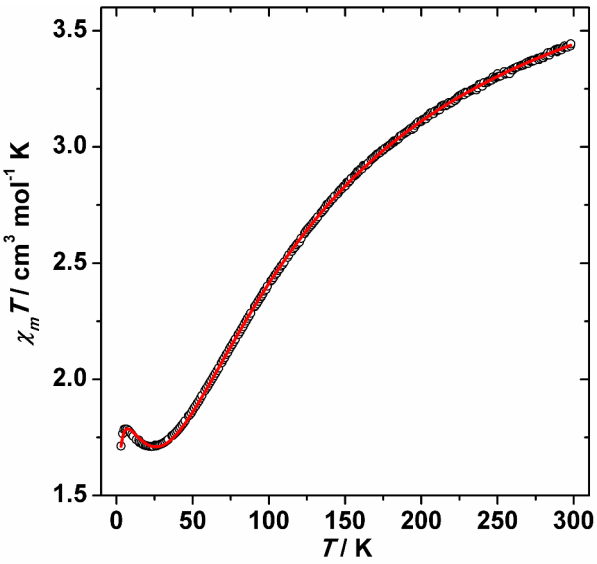

Figure 9. Experimental (black points) and best fit obtained (red line) for the pentanuclear core. (For *J* and *D* values see Table 2).

-tic pathway between Cu1–Cu3 remains ferromagnetic. The best fit calculated by this method can be seen in Figure 9. With or without *D*, the Figure is practically the same, although the R factors are different (with *D* is worse because we have limited the possible *D* value to 20 cm^{-1}, which is high for standard Ni(II) ions[13].

As a conclusion, these fits indicate that the system has multiple analytical solutions and the most reliable values should be assumed as the calculated ones, considering our qualitative predictions. Some of the coupling constants have been assumed as negligible (see Table 2) to minimize the number of variables in the fit process.

Table 2. *J* and *D* values for the pentanuclear core following the labels of Figure 6.

Magnetic pathway	*J*	*D*= 0	*D* variable
Ni1–Ni2	*J*1	–42.9	–41.1
Ni1–Cu2	*J*2	13.5	–6.1
Ni1–Cu1	*J*3	14.7	–5.1
Ni2–Cu2	*J*4	19.0	34.4
Ni2–Cu1	*J*5	–23.8	–3.8
Cu1–Cu3	*J*6	19.3	12.1
	g	2.35	2.35
	D	0	20 (limit imposed)
	R	0.97×10^{-4}	0.88×10^{-3}
Cu1–Cu2		Negligible d(Cu2–O) = 2.5 A	
Ni1–Cu3		Negligible (syn–anti quasi perpendicular)	
Cu2–Cu3		Negligible (syn–anti quasi perpendicular)	

Furthermore, the central magnetic pathway Cu_2O_2 should be ferromagnetic, as anticipated from the Cu3–O–Cu3_a angle of 95.4(3)°. To understand the interaction between the pentanuclear cores, we have performed computational study based on density functional theory (DFT) within the broken symmetry (BS) formalism[14a] using GAUSSIAN 03 package[14b] at the B3LYP level employing the LanL2DZ basis set. Our result shows that the triplet state is more stable than the singlet state by 0.003371 eV suggesting the dominant ferromagnetic exchange interaction between the two pentanuclear cores. The ferromagnetic interactions can be further confirmed by spin density plot (Figure 10).

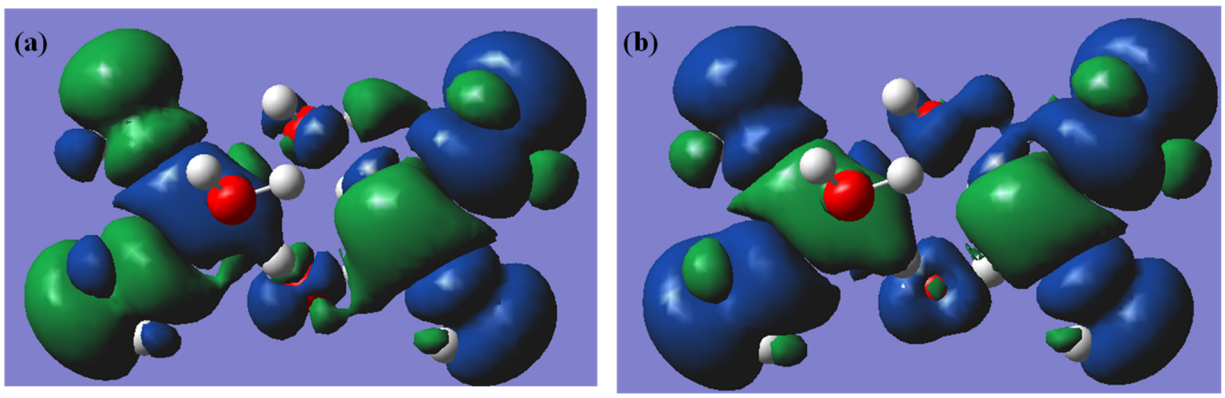

Figure 10. Spin density plot for (a) singlet and (b) triplet state for the water bridged two Cu atoms connecting two pentameric cores.

3.4 CONCLUSION

In summary, through the assembly between two different metal ions, Cu(II) and Ni(II) and the multinucleating ligand dpk a new heterometallic decanuclear cluster $[Ni_4Cu_6(\mu\text{–}OH_2)_2(dpkO_2)_8(OAc)_4(H_2O)_4]$ has been synthesized with the *in situ* formation of the ligand $dpkO_2$ and is structurally and magnetically characterized. This is the first example of decanuclear complex based on Ni(II) and Cu(II). The pentanuclear core shows dominant antiferromagnetic interactions between the metal centres; while ferromagnetic interaction operates between the two pentanuclear cores. Thus judicious choice of the blocking ligand with suitable binding mode and their self-assembly with metal ions with compatible geometry can lead to the formation of desired heterometallic cluster.

3.5 REFERENCES

[1] (*a*) E. Coronado, P. Delhaes, D. Gatteschi and J.S. Miller, *Molecular magnetism: From the molecular assemblies to the Devices*, NATO ASI series no. E321, Dordrecht, 1996; (*b*) S. Mukherjee, B. Gole, Y. Song and P. S. Mukherjee, *Inorg. Chem*., 2011, **50,** 3621; (*c*) A. Biswas, M. G. B. Drew, J. Ribas, C. Diaz and A. Ghosh, *Eur. J. Inorg. Chem*., 2011, 2405.

[2] (*a*) M. Andruh, J. Costes, C. Diaz and S. Gao, *Inorg. Chem*., 2009, **48**, 3359; (*b*) Y. Chen, L. Zheng, S. She, Z. Chen, B. Hu and Y. Li, *Dalton Trans*., 2011, **40**, 4970; (*c*) P. Thuery, *Cryst. Growth Des.*, 2010, **10**, 2061; (*d*) D. Pogozhev, S. A. Baudron and M. W. Hosseini, *Inorg.Chem.*, 2010, **49**, 331; (*e*) A. Deak, T. Tunyogi and G. Palinkas, *J. Am. Chem. Soc.*, 2009, **131**, 2815.

[3] D. E. Fenton and H. Okawa, *Chem. Ber./Recl.*, 1997, **130**, 433.

[4] (*a*) R. Sessoli, H. L. Tsai, A. R. Schake, S. Wang, J. B. Vincent, K. Folting, D. Gatteschi, G. Christou and D. N. Hendrickson, *J. Am. Chem. Soc*., 1993, **115**, 1804; (*b*) R. Sessoli, D. Gatteschi, A. Caneschi and M. A. Novak, *Nature*, 1993, **365**, 141; (*c*) L. Thomas, F. Lionti, R. Ballou, D. Gatteschi, R. Sessoli and B. Barbara, *Nature,* 1996, **383**, 145; (*d*) D. Gatteschi and R. Sessoili, *Angew. Chem. Int. Ed*., 2003, **42**, 268.

[5] (*a*) H. Miyasaka, K. Nakata, L. Lecren, C. Coulon, Y. Nakazawa, T. Fujisaki, K. Sugiura, M. Yamashita and R. Clerac, *J. Am. Chem. Soc*., 2006, **128**, 3770; (*b*) M. Murugesu, W. Wernsdorfer, K. A. Abboud, E. K. Brechin and G. Christou, *Dalton, Trans*., 2006, 2285.

[6] (*a*) H. Miyasaka and M. Yamashita, *Dalton Trans*., 2007, 399; (*b*) G. Christou, D. Gatteschi, D. N. Hendrickson and R. Sessoli, *MRS Bull*., 2000, **25**, 66; (*c*) D. Gatteschi and R. Sessoli, *J. Magn. Magn. Mater*., 2004, **272**, 1030.

[7] (*a*) H. Oshio, M. Nihei, A. Yoshida, H. Nojiri, M. Nakano, A. Yamaguchi, Y. Karaki and H. Ishimoto, *Chem. Eur. J*., 2005, **11**, 843; (*b*) V. Chandrasekhar, B. Pandian, R. Azhakar, J. Vittal and R. Clerac, *Inorg. Chem*., 2007, **46**, 5140; (*c*) L. Zou, L. Zhao, Y. Guo, G. Yu, Y. Gu, J. Tang and Y. Li, *Chem. Commun*., 2011, **47**, 8659.

[8] (*a*) L. -C. Kang, X. Chen, X. -S. Wang, Y. –Z. Li, Y. Song, J. –L Zuo and X. –Z. You, *Dalton Trans*., 2011, **40**, 5200; (*b*) N. Lalioti, C. Raptopoulou, A. Terzis, A.

Aliev, I. P. Gerothanassis, E. Manessi-Zoupa and S. Perlepes, *Angew. Chem. Int. Ed*., 2001, **40**, 3211.

[9] (*a*) SMART (V 5.628), SAINT (V 6.45a), XPREP, SHELXTL; Bruker AXS Inc. Madison, Wisconsin, USA, 2004; (*b*) G. M. Sheldrick, Siemens Area Detector Absorption Correction Program, University of Göttingen, Göttingen, Germany, 1994; (*c*) A. Altomare, G. Cascarano, C. Giacovazzo and A. Gualaradi, *J. Appl. Cryst*., 1993, **26**, 343; (*d*) G. M. Sheldrick, SHELXL-97, Program for Crystal Structure Solution and Refinement; University of Göttingen, Göttingen, Germany, 1997; (*e*) A. L. Spek, *J. Appl. Cryst*., 2003, **36**, 7; (*f*) L. J. Farrugia, WinGX–A Windows Program for Crystal Structure Analysis, *J. Appl. Crystallogr*., 1999, **32**, 837.

[10] M.A. Palacios, A. J. Mota, J. E. Perea-Buceta, F. J. White, E. K. Brechin and E. Colacio, *Inorg. Chem*., 2010, **49**, 10156.

[11] D. Venegas–Yazigi, D. Aravena, E. Spodine, E. Ruiz and S. Alvarez, *Coord. Chem. Rev*., 2010, **254**, 2086 and references therein.

[12] (*a*) J. J Borrás-Almenar, J. Clemente, E. Coronado and B. S. Tsukerblat, *Inorg. Chem*., 1999, **38**, 6081; (*b*) J. J. Borrás-Almenar, J. Clemente, E. Coronado and B. S. Tsukerblat, *J. Comput. Chem*., 2001, **22**, 985.

[13] (*a*) R. Boca, *Coord. Chem. Review*, 2004, **248**, 757; (*b*) R. Boca, *Structure and Bonding*, 2006, **117**, 1.

[14] (*a*) L. Noodleman, *J. Chem. Phys*., 1981, **74**, 5737. (*b*) M. J. Frisch et al. GAUSSIAN 03, Revision C.02, Gaussian Inc., Wallingford, CT, 2004.

Chapter 4

Dimensionality Control in Cu-Azido System Based on Blocking Amine Stoichiometry: Synthesis and Magneto-structural Correlation

Abstract

This chapter describes syntheses, structural characterization and magnetic behaviour of three different Cu(II)-azido compounds, ranging from a discrete dinuclear complex to an extended 2D network. The compounds, $[Cu(\mu_{1,1}\text{–}N_3)(N_3)(Me_2en)]_2$ **(1)**, $[Cu_2(\mu_{1,3}\text{–}N_3)(\mu_{1,1}\text{–}N_3)(N_3)_2(Me_2en)_2]_n$ **(2)** and $[Cu_3(\mu_{1,1,1}\text{–}N_3)_2(\mu_{1,1,3}\text{–}N_3)(\mu_{1,1}\text{–}N_3)_2(\mu_{1,3}\text{–}N_3)(Me_2en)]_n$ **(3)**, have been synthesized by controlling the relative concentration of the blocking ligand, N,N′–dimethylethylenediamine (Me_2en). Compound **1** is a dinuclear compound which is formed by doubly $\mu_{1,1}\text{–}N_3$ bridging ligand, while compound **2** has a 1D chain structure, possessing alternatively $\mu_{1,1}\text{–}N_3$ and $\mu_{1,3}\text{–}N_3$ bridging ligands. Compound **3** is a rare Cu-azido system, where four different types of binding modes of azide ligands are present in a single compound. It contains a hexanuclear core, where the Cu(II) centres are connected to each other by $\mu_{1,1,1}$, $\mu_{1,1}$ and $\mu_{1,1,3}$ bridging azide ligands. The hexanuclear core acts as a secondary building block and further assembles via $\mu_{1,3}$ and $\mu_{1,1,3}$ azide ions, forming a 2D sheet in the crystallographic *ac* plane. Temperature dependent magnetic study suggests that the dinuclear compound **1** exhibits antiferromagnetic interaction through the $\mu_{1,1}\text{–}N_3$ bridging. Compound **2** shows both ferro and antiferromagnetic behaviour, as anticipated from the structure, where both $\mu_{1,1}\text{–}N_3$ and $\mu_{1,3}\text{–}N_3$ bridging ligands are present. In case of compound **3**, an overall dominant ferromagnetic interaction is exhibited at higher temperature, whereas at lower temperature, antiferromagnetic interaction operates between the hexanuclear cores. Intensive DFT calculations have been carried out for all the three compounds, which supports the experimental findings.

4.1 INTRODUCTION

Discrete polynuclear clusters and extended networks of coordination polymers containing paramagnetic metal ions have been a fascinating research topic to the inorganic chemists in the recent past. Their studies are highly motivated due to the structural novelty as well as the potential applications in the field of molecular magnetism.[1] The magnetic exchange in these materials is mediated via suitable bridging ligands and various factors like appropriate bridging modes, strict and accidental orthogonality of magnetic orbitals,[2] spin polarization,[3] delocalization of unpaired electrons[3c] etc. influence the type of magnetic coupling between the paramagnetic centres. Pseudohalogens are found to be versatile and proficient ligands for making such bridge to construct molecular magnets.[4a] Among them, azide ion has been extensively studied and still is in the current focus due to its excellent ability to propagate different kinds of magnetic properties. In particular, a rich diversity of structures is possible with copper coordination compounds as Cu(II) can adopt different kinds of geometries with the different binding modes of azide (Scheme 1).[4-7] The most commonly observed bridging modes of azide ion are end-to-end (EE) and end-on (EO). In general, the former mode propagates antiferromagnetic interaction whereas the latter one can mediate both ferro and antiferromagnetic interactions depending on the Cu–N–Cu bond angle.[3] Calculations based on density functional theory (DFT) predicted that EO mode can exhibit antiferromagnetic behaviour if the Cu–N_{EO}–Cu angle is above the critical angle 104°.[3c] Experimentally there are very few reports on antiferromagnetic Cu(II)-azido system with a Cu–N_{EO}–Cu angle less than 108°[3d] and it is a real challenge to synthesize such systems. Moreover, in an extended Cu-azido system, where metal centres are connected through different types of bridging modes, the prediction of magnetic behaviour becomes even more difficult. Alternate chain system having both EO and EE modes are well documented in the literature[4], but to best of our knowledge, there is no report on alternate system where both $\mu_{1,1}$–N_3 (end on) and $\mu_{1,1}$–N_3 (end to end) mode are present which give rise to antiferromagnetic and ferromagnetic interaction, respectively.

The synthesis of compounds with different structural topologies and dimensionalities using same set of metal-ligand system is highly demanding and challenging, as it can provide better insight into the observed properties, through proper

structure-property relationship. Indeed, using different coligand, bipyridine,[5a] phenanthroline[5b] and different amines[4] etc., discrete molecular entities to higher dimensional compounds in Cu-azido systems is well documented. However, dimensionality control by changing the stoichiometry of the coligand and their systematic magnetic study is extremely rare.[7] We envisioned that changing the concentration of the blocking ligand would be a key approach to synthesise versatile Cu-azido systems, as the decrease of coligand concentration will provide more available coordination sites for azide, which would lead to the formation of higher dimensional structure and novel magnetic properties would be furnished by the subtle balance between azide binding and dimensionality.

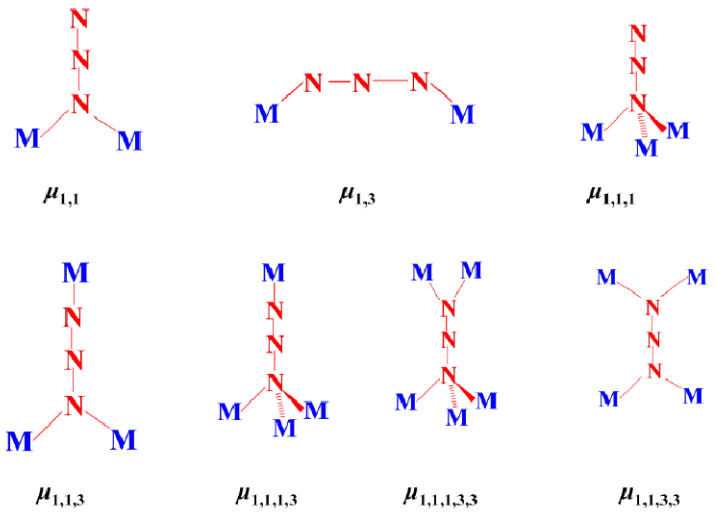

Scheme 1. Various observed binding modes for azido ion with metal.

We have tried to envisage the structural change and variation of dimensionality based on such synthetic strategy. By tuning the relative molar ratios of the reactants, N,N′–dimethylethylenediamine (Me_2en), sodium azide and Cu(II), we were able to synthesize three new compounds, ranging from a discrete dinuclear complex to an extended 2D network. Here in this chapter, we report synthesis, structural characterization and magnetic studies of $[Cu(\mu_{1,1}–N_3)(N_3)(Me_2en)]_2$ **(1)**, $[Cu_2(\mu_{1,3}–N_3)(\mu_{1,1}–N_3)(N_3)_2(Me_2en)_2]_n$ **(2)** and $[Cu_3(\mu_{1,1,1}–N_3)_2(\mu_{1,1,3}–N_3)(\mu_{1,1}–N_3)_2(\mu_{1,3}–N_3)(Me_2en)]_n$ **(3)**. Compound **1** is a unique discrete dinuclear complex which has a Cu–N_{EO}–Cu angle of 101.1(2)° and shows antiferromagnetic interaction, while compound **2** is a 1D copper(II)

chain with alternate single end-on and single end-to-end azido bridging having both ferro and antiferromagnetic domain. Compound **3** is a unique 2D metal-azido system consisting of hexanuclear building blocks, which are linked by four different kind of azide bridging modes ($\mu_{1,3}$, $\mu_{1,1}$, $\mu_{1,1,1}$, $\mu_{1,1,3}$ and $\mu_{1,1,1}$). Temperature dependence magnetic measurements suggest that within the hexanuclear core, the spins are ferromagnetically coupled while weak antiferromagnetic interaction operates between the hexanuclear cores.

4.2 EXPERIMENTAL SECTION

4.2.1 Materials

All the reagents and solvents employed are commercially available and used as supplied without further purification. $Cu(OAc)_2 \cdot H_2O$, $Cu(ClO_4)_2 \cdot 6H_2O$, sodium azide (NaN_3) and N,N′-dimethylethylenediamine (Me_2en) were obtained from the Aldrich chemical Co.

4.2.2 Synthesis

$[Cu(\mu_{1,1}\text{-}N_3)(N_3)(Me_2en)]_2$ (1) $Cu(OAc)_2 \cdot H_2O$ (1 mmol, 0.099 g) was dissolved in 10 mL water and 2 mmol (109.2 μL) of Me_2en was dropwise added to the above metal solution. The resulting blue coloured solution was stirred for ten minutes. Then aqueous solution (10 mL) of NaN_3 (2 mmol, 0.13 g) was dropwise added to the above reaction mixture. The resulting green coloured solution was stirred for one hour and filtered. The filtrate was kept for slow evaporation at room temperature and after one weak green crystals were isolated. Yield, 52%, relative to Cu. Selected IR data (KBr, cm^{-1}) 3316 m, 3256 m, 2054 s, 2032 s, 1385 m, 1053 m, 783 m (Figure 1). Anal. calcd. for $C_8H_{24}Cu_2N_{16}$: C, 20.38; H, 5.13; N,47.53. Found: C, 20.49; H, 5.42; N, 47.98%. The phase purity was checked by comparing the PXRD pattern of the bulk powder sample with the simulated data from single-crystal (Figure 2).

$[Cu_2(\mu_{1,3}\text{-}N_3)(\mu_{1,1}\text{-}N_3)(N_3)_2(Me_2en)_2]_n$ (2) 1 mmol (54.6 μL) of Me_2en was dropwise added to an aqueous solution (10 mL) of $Cu(OAc)_2 \cdot H_2O$ (1 mmol, 0.099 g) and the resulting blue coloured solution was stirred for five minutes. Then aqueous solution (10 mL) of NaN_3 (2 mmol, 0.13 g) was dropwise added to the above reaction mixture and the resulting green coloured solution was stirred for one hour and filtered. The filtrate was

kept for slow evaporation at room temperature and after ten days green crystals were isolated. Yield, 64%, relative to Cu. Selected IR data (KBr, cm^{-1}) 3428 br, 3317 m, 2920 m, 2055 s, 2032 sh, 1583 m, 1052 m, 554 m (Figure 1). Anal. calcd. for $C_8H_{24}Cu_2N_{16}$: C, 20.38; H, 5.13; N,47.53. Found: C, 20.41; H, 5.31; N, 47.55%. The well correspondence of the simulated and bulk phase PXRD patterns indicates high purity of the sample (Figure 3).

$[Cu_3(\mu_{1,1,1}\text{-}N_3)_2(\mu_{1,1,3}\text{-}N_3)(\mu_{1,1}\text{-}N_3)_2(\mu_{1,3}\text{-}N_3)(Me_2en)]_n$ (3) An aqueous solution (20 mL) of NaN_3 (2 mmol, 0.13 g) was mixed with 0.33 mmol (54.6 μL) of Me_2en and the resulting blue solution was stirred for 20 min. to mix well. $Cu(ClO_4)_2{\cdot}6H_2O$ (1 mmol, 0.370 g) was dissolved in 10 mL methanol and 2.5 mL of this metal solution was slowly and carefully layered with the above mixed ligand solution using 1 mL buffer (1:1 of water and MeOH) solution in a crystal tube to give a three-layer system, which was sealed and left undisturbed at room temperature. Slow diffusion yielded green block crystals of **3** after 20 days. Compound purity was verified by PXRD (Figure 4) and elemental analysis result. Yield 51%, relative to Cu(II). Selected IR data (KBr, cm^{-1}) 3314 m, 3268 m, 2096 s, 2062 sh, 1466 m, 1278 m (Figure 1). Anal. calcd. for $C_4H_{12}Cu_3N_{20}$: C, 9.05; H, 2.28; N,52.76. Found: C, 9.08; H, 2.31; N, 52.68%.

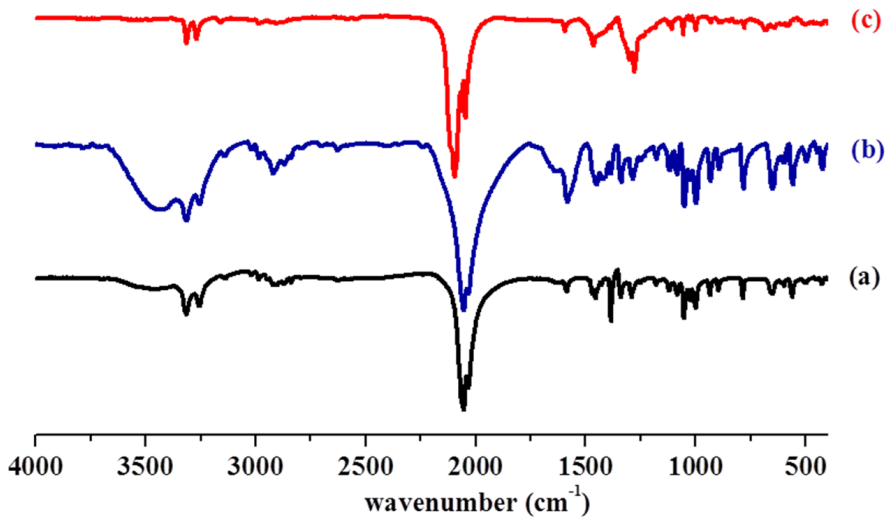

Figure 1. IR spectra of compounds **1**(a), **2** (b) and **3** (c).

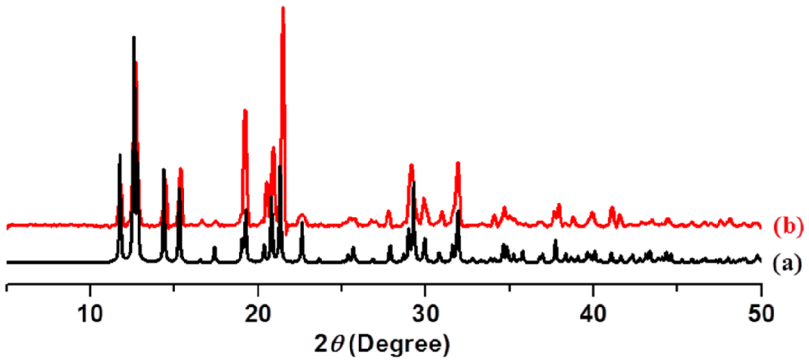

Figure 2. PXRD patterns of compound **1**: (a) simulated; (b) bulk as-synthesized. Similarity in simulated and as-synthesized pattern indicates high purity of the compound.

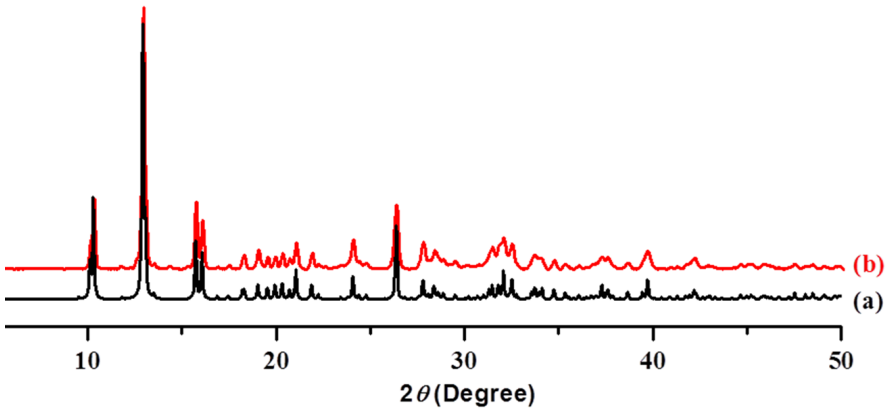

Figure 3. PXRD patterns of compound **2**: (a) simulated; (b) bulk as-synthesized. Similarity in simulated and as-synthesized pattern indicates high purity of the compound.

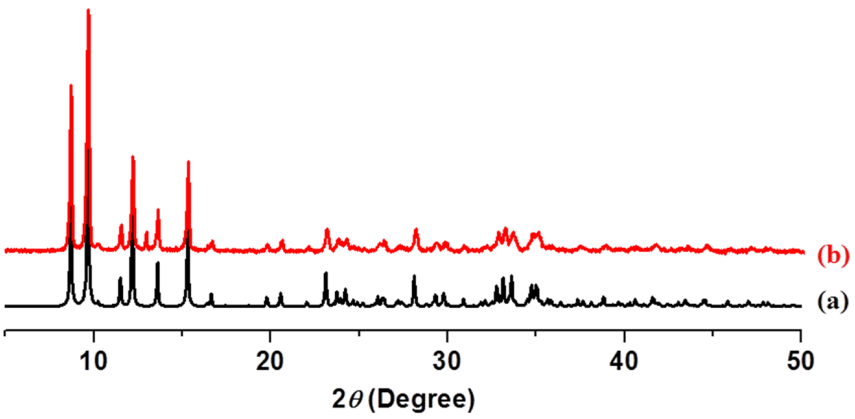

Figure 4. PXRD patterns of compound **3**: (a) simulated; (b) bulk as-synthesized. Similarity in simulated and as-synthesized pattern indicates high purity of the compound.

4.2.3 Single-crystal X-ray Diffraction

X-ray single-crystal structural data of **1**–**3** were collected on a Bruker Smart-CCD diffractometer equipped with a normal focus, 2.4 kW sealed tube X-ray source with graphite monochromated Mo–Kα radiation (λ = 0.71073 Å) operating at 50 kV and 30 mA. The program SAINT[9a] was used for integration of diffraction profiles and absorption correction was made with SADABS[9b] program. All the structures were solved by SIR 92[9c] and refined by full matrix least square method using SHELXL-97.[9d] All the non hydrogen atoms were refined anisotropically and all the hydrogen atoms were fixed by HFIX and placed in ideal positions. All calculations were carried out using SHELXL 97, PLATON[9e] and WinGX system, Ver 1.70.01[9f]. All crystallographic and structure refinement data of **1**–**3** are summarized in Table 1. Selected bond lengths and angles are displayed in Tables 2-4.

4.2.4 Physical Measurements

Elemental analyses were carried out on a Perkin Elmer 2400 CHN analyzer. IR spectra were recorded in KBr pellets on a Bruker IFS 66v/S spectrophotometer in the region of 4000 – 400 cm^{-1}. Powder X-ray diffraction (PXRD) patterns were recorded on a Bruker D8 Discover instrument using Cu–Kα radiation. The magnetic measurements (300–2.5 K) for polycrystalline powder sample of **1**–**3** were carried out using Vibrating Sample Magnetometer (VSM) in physical property measurement system (PPMS, Quantum Design, USA). Susceptibility data were collected under an external applied magnetic field of 500 Oe and obtained data were corrected with respect to the diamagnetic contribution of the constituent atoms (on the basis of Pascal constants).[8]

4.2.5 Computational details:

All the spin-unrestricted DFT calculations were performed using Gaussian03[10] program suits employing hybrid B3LYP[11] exchange and correlation functional and 6-31+g(d,p) basis set for all atoms except for Cu for which we use an effective core potential with LANL2DZ basis set[12]. In previous studies, the usage of B3LYP functional has been proved to give reliable results in predicting the magneto-structural interactions in transition metal complexes[13a,4]. The magnetic exchange coupling constant (*J*) for the azido-bridged binuclear complex was calculated by making use of the simple 1D

Heisenberg Hamiltonian for the interaction of two spins[14] and was estimated as the energy difference (E) between the high spin (HS) and low spin (LS) broken symmetry[15] singlet state using the following expression: $J = 2\Delta E/S(S+1)$ where S corresponds to the z-component of the total spin (S_z^t) for the HS state.

4.3 RESULTS AND DISCUSSION

4.3.1 Crystal Structure Description

4.3.1.1 Structural description of $[Cu(\mu_{1,1}\text{-}N_3)(N_3)(Me_2en)]_2$ (1)

Compound **1** crystallizes in the monoclinic $P2_1/n$ space group. Single-crystal X-ray structure determination revealed that **1** is a dinuclear complex formed by doubly $\mu_{1,1}$–N_3 bridging ligand. Each Cu(II) locates itself in a distorted square pyramidal geometry with CuN_5 chromophore (Figure 5). The four coordination sites of Cu(II) in the equatorial plane are furnished by N1 and N2 nitrogen atoms from a chelated Me_2en ligand, N6 atom of the monodentate azide and N3 atom of the bridging $\mu_{1,1}$-N_3 ligand. The apical position is occupied by another nitrogen atom (N3_a) of the symmetry related bridging $\mu_{1,1}$-N_3 group, resulting in the formation of doubly $\mu_{1,1}$–N_3 bridged dinuclear complex. Cu–N (equatorial) bond distances are in the range of 1.953 (6)–2.048 (5) Å while the apical bond length is 2.356 (6) Å. The Cu1–N3–Cu1_a angle is found to be 101.1(2)° in this complex. The distance between Cu1 and Cu1_a is 3.364 Å. The *cisoid* angles are varying

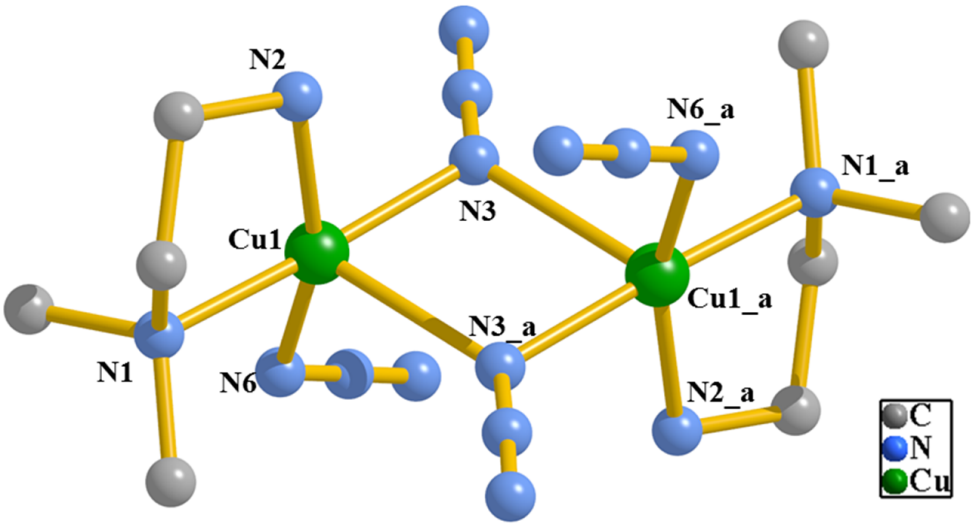

Figure 5. Coordination environment around Cu in the dinuclear complex **1**. Symmetry code: a = 1-x, -y, -z.

from 78.9(2)° to 100.1 (2)° and the *transoid* angles are 173.6 (2)° and 160.1 (3)° (Table 2) indicating the degree of distortion from ideal square pyramidal geometry. The value of addison parameter (τ)[16] for the Cu(II) centre is 0.23. From symmetry point of view, the dimers pack in the lattice with the application of 2_1-screw axis along *b* direction while the two metal centres within the dimer are related by an inversion centre.

4.3.1.2 Structural description of $[Cu_2(\mu_{1,3}\text{-}N_3)(\mu_{1,1}\text{-}N_3)(N_3)_2(Me_2en)_2]_n$ (2)

Compound **2** crystallizes in the orthorhombic chiral $P2_12_12_1$ space group. Single-crystal X-ray structure determination revealed that in the asymmetric unit, two crystallographically independent Cu(II) centres, both present in a distorted square pyramidal coordination environment (Figure 6). For Cu1, the equatorial plane is composed of one chelated Me_2en ligand (N1, N2 atoms), N11 atom of one monodentate azide ligand and N8 atom of bridging $\mu_{1,3}$-N_3 ligand while N5 atom of the bridging $\mu_{1,1}$-N_3 group occupies the axial position. In case of Cu2, equatorial coordination sites are furnished by N3, N4 atoms of Me_2en ligand, N14 atom of one monodentate azide and N5 atom of the bridging $\mu_{1,1}$–N_3 ligand. The nitrogen atom (N10) from bridging $\mu_{1,3}$–N_3 occupies the apical position. The equatorial Cu–N bond lengths are in the range 1.969(3)–2.060(2) Å while apical bond lengths are 2.305(2) Å and 2.561(3) Å, for Cu1 and Cu2, respectively (Table 3). The degree of distortion from the ideal square pyramidal geometry

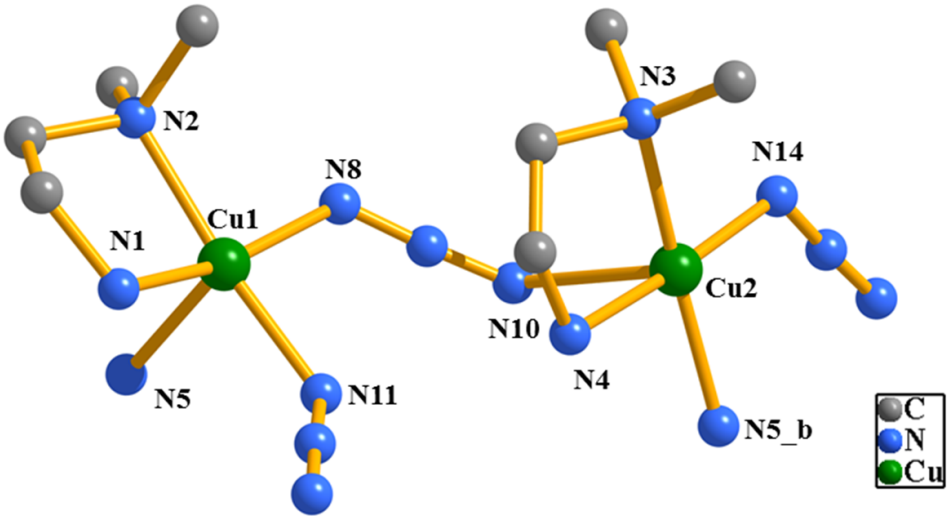

Figure 6. Coordination environment around Cu in **2**.

is reflected in the angles of the equatorial plane of the Cu atoms (Table 3). The addison parameter (τ)[16] have been calculated and the values are 0.12 and 0.13 for Cu1 and Cu2, respectively.

Cu1 and Cu2 atoms are bridged by $\mu_{1,1}$–N_3 (through N5 atom) and $\mu_{1,3}$-N_3 group (N8-N9-N10) resulting in the formation of a 1D helical chain (Figure 7). The Cu1–N5–Cu2 angle between Cu1 and Cu2 through the end–on bridging is 108.30(10)°. Distances between Cu1 and Cu2 through $\mu_{1,1}$–N_3 and $\mu_{1,3}$-N_3 group (N8-N9-N10) are 3.498 Å and 5.406 Å, respectively.

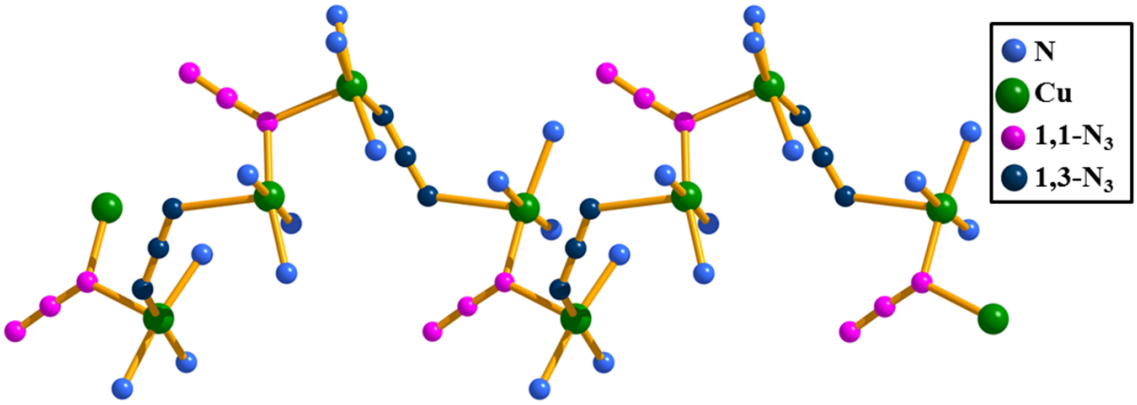

Figure 7. Extended 1D chain of **2**.

4.3.1.3 Structural description of $[Cu_3(\mu_{1,1,1}\text{-}N_3)_2(\mu_{1,1,3}\text{-}N_3)(\mu_{1,1}\text{-}N_3)_2(\mu_{1,3}\text{-}N_3)(Me_2en)]_n$ (3)

Compound **3** crystallizes in the triclinic $P\bar{1}$ space group and the structure determination by single-crystal X-ray diffraction reveals a 2D coordination polymer of Cu(II), construction of which is facilitated by four bridging azide ions. In the asymmetric unit, there are three crystallographically independent Cu(II) centres (Cu1, Cu2 and Cu3) having different coordination environments (Figure 8) and they are connected to each other by $\mu_{1,1,1}$, $\mu_{1,1}$ and $\mu_{1,1,3}$ bridging azide ions (through N7, N10 and N16 nitrogen atoms) forming a trinuclear core. In the trinuclear core, Cu1 is octahedrally coordinated to six different nitrogen atoms (N1, N7, N1_c, N4, N10 and N15_d) from six different azide ions. N1, N4, N10 and N7 are present in the equatorial plane while N1_c and N15_d occupy the axial positions. Cu2 is found in a distorted square pyramidal geometry with coordinations coming from N13, N4, N1, N16 and N7_c atoms of different azide groups

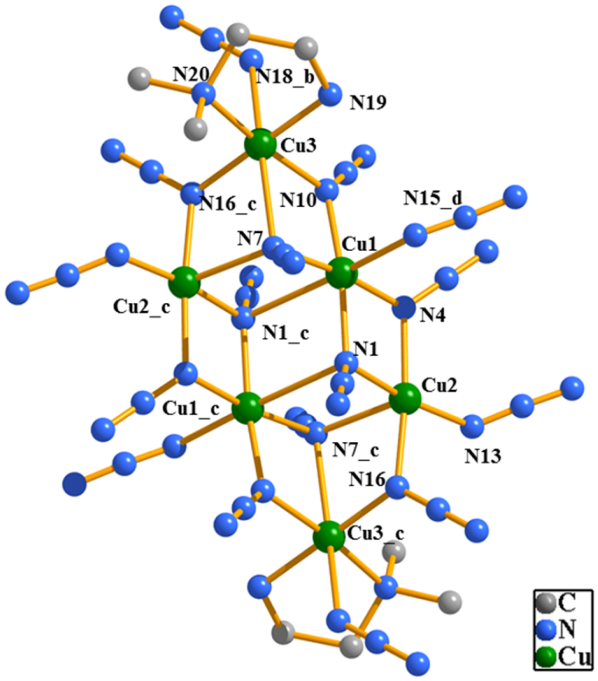

Figure 8. Coordination environment around Cu in the hexameric core of **3**.

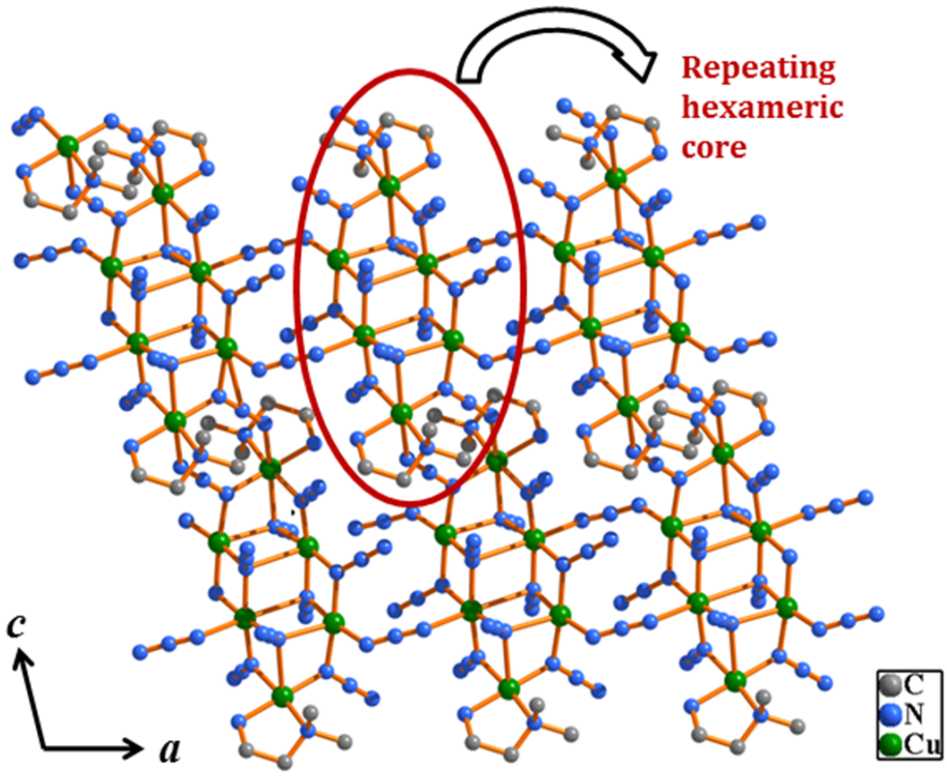

Figure 9. View of the 2D sheet of **3** formed by repeating hexameric core lying in the crystallographic *ac* plane.

($\mu_{1,3}$, $\mu_{1,1}$, $\mu_{1,1,1}$, $\mu_{1,1,3}$ and $\mu_{1,1,1}$).The value of addison parameter (τ)[16] for the Cu2 centre is 0.018. Cu3 adopts a distorted octahedral coordination geometry with coordinations furnished by one chelated Me_2en ligand (through N19, N20 atoms) and three different azide groups having $\mu_{1,1,3}$ and $\mu_{1,1}$ and $\mu_{1,1,1}$ binding modes (N16, N18, N10 and N7). Axial and equatorial coordinations are furnished by N7, N18_b and N19, N20, N10, N16_c nitrogen atoms, respectively. The equatorial and axial Cu–N bond lengths are in the range of 1.937(10)–2.052(9) Å and 2.360(11)–2.670(8) Å, respectively. Selected bond distances and angles for **3** are listed in Table 4. The trinuclear core is linked to its symmetry related counterpart via $\mu_{1,1}$ and $\mu_{1,1,1}$ bridging azide ions (N1 and N4 atoms, respectively) forming a hexanuclear core, which acts as a secondary building block. The hexanuclear building blocks are connected to each other via $\mu_{1,3}$ and $\mu_{1,1,3}$ azide ions resulting in the 2D sheet in the crystallographic *ac* plane (Figure 9).

Table 1. Crystallographic data for compounds **1**, **2** and **3**.

Parameters	**1**	**2**	**3**
empirical formula	$C_8H_{24}Cu_2N_{16}$	$C_8H_{24}Cu_2N_{16}$	$C_4H_{12}Cu_3N_{20}$
M_r	471.48	471.48	530.91
Crystal system	Monoclinic	Orthorhombic	Triclinic
Space group	$P2_1/n$	$P2_12_12_1$	$P\bar{1}$
a (Å)	9.3636(9)	10.1434(2)	8.5602(2)
b (Å)	10.7124(13)	11.0170(3)	10.6248(3)
c (Å)	9.6384(10)	17.1453(4)	11.4803(5)
α (°)	90	90	103.612(2)
β (°)	104.864(7)	90	106.749(2)
γ (°)	90	90	111.431(1)
V (Å ^{3})	934.44(18)	1915.99(8)	860.07(5)
Z	2	4	2
T (K)	298	298	298
λ (Mo K_α)	0.71073	0.71073	0.71073
D_c (g / cm^3)	1.662	1.621	2.043
μ (mm$^{-1)}$	2.307	2.250	3.717
θ_{max} (°)	26.0	32.1	25.7
F(000)	476	952	522
Total data	7765	45995	9919
Data [$I>2\sigma(I)$]	1010	5307	2460
R^a	0.0539	0.0375	0.0632
$R_w{}^b$	0.1314	0.0969	0.2116
GOF	0.97	1.02	1.05

$^a R = \sum||F_o|-|F_c||/\sum|F_o|$. $^b R_w = [\sum\{w(F_o^2-F_c^2)^2\}/\sum\{w(F_o^2)^2\}]^{1/2}$

Table 2. Selected Bond Distances [Å] and Angles [°] for Compound **1**.

Cu1-N1	2.048(5)	Cu1-N2	2.030(5)
Cu1-N3	1.989(6)	Cu1-N6	1.953(6)
Cu1-N3_a	2.356(6)		
N1-Cu1-N2	84.8(2)	N1-Cu1-N3	173.6(2)
N1-Cu1N6	91.1(2)	N1-Cu1-N3_a	99.9(2)
N2-Cu1-N3	89.3(2)	N2-Cu1-N6	160.1(3)
N2-Cu1-N3_a	99.8(2)	N3-Cu1-N6	95.2(3)
N3-Cu1-N3_a	78.9(2)	N3_a-Cu1-N6	100.1(2)
Cu1-N3-Cu1_a	100.1(2)		

Symmetry codes: a = 1−x, −y, −z

Table 3. Selected Bond Distances [Å] and Angles [°] for Compound **2**.

Cu1-N1	2.026(2)	Cu1-N2	2.060(2)
Cu1-N5	2.305(2)	Cu1-N8	1.997(3)
Cu1-N11	1.983(3)	Cu2-N3	2.069(3)
Cu2-N4	2.013(2)	Cu2-N5	2.005(2)
Cu2-N14	1.969(3)	Cu2-N10_b	2.561(3)
N1-Cu1-N2	84.54(9)	N1-Cu1-N5	95.57(12)
N1-Cu1-N8	164.85(12)	N1-Cu1-N11	94.46(10)
N2-Cu1-N5	97.79(9)	N2-Cu1-N8	88.49(10)
N2-Cu1-N11	172.22(11)	N5-Cu1-N8	98.70(12)
N5-Cu1-N11	89.99(11)	N8-Cu1-N11	90.62(10)
N3-Cu2-N4	84.81(11)	N3-Cu2-N5	168.57(11)
Cu1-N5-Cu2	108.30(10)	N3-Cu2-N14	91.74(11)
N3-Cu2-N10_b	100.63(11)	N4-Cu2-N5	88.45(11)
Compound 2 continued			
N4-Cu2-N14	176.52(11)	N4-Cu2-N10_b	86.10(12)
Cu1-N11-Cu2	88.28(11)	N5-Cu2-N11	73.11(8)
N5-Cu2-N14	95.02(12)	N5-Cu2-N10_b	88.09(9)
N10_b-Cu2-N14	94.13(12)		

Symmetry codes: b= 1−x, 1/2+y, 1/2−z

Table 4. Selected Bond Distances [Å] and Angles [°] for Compound **3**.

Cu1-N1	2.000(6)	Cu1-N4	2.030(9)
Cu1-N7	2.002(8)	Cu1-N10	1.998(7)
Cu1-N1_c	2.670(8)	Cu1-N15_d	2.360(11)
Cu2-N1	2.007(8)	Cu2-N4	2.016(7)
Cu2-N13	1.937(10)	Cu2-N16	2.034(6)
Cu2-N7_c	2.394(8)	Cu3-N7	2.466(6)
Cu3-N10	2.041(9)	Cu3-N19	2.002(9)
Cu3-N20	2.052(9)	Cu3-N18_b	2.595(8)
Cu3-N16_c	2.018(8)		
N1-Cu1-N4	79.2(3)	N7-Cu3-N18_b	159.4(3)
N1-Cu1-N7	96.2(3)	N7-Cu3-N16_c	79.4(3)
N1-Cu1-N10	168.0(3)	N10-Cu3-N19	87.9(3)

Table 4 continued…			
N1-Cu1-N1_c	80.7(3)	N10-Cu3-N20	172.4(4)
N1-Cu1-N15_d	96.0(4)	N10-Cu3-N18_b	89.5(3)
N4-Cu1-N7	173.0(3)	N10-Cu3-N16_c	90.0(3)
N4-Cu-N10	97.2(3)	N19-Cu3-N20	84.8(4)
N1_c-Cu1-N4	92.7(3)	N18_b-Cu3-N19	89.4(3)
N4-Cu1-N15_d	97.8(4)	N16_c-Cu3-N19	176.9(3)
N7-Cu1-N10	86.3(3)	N18_b-Cu3-N20	92.2(3)
N1_c-Cu1-N7	81.3(3)	N16_c-Cu3-N20	97.5(3)
N7-Cu1-N15_d	87.9(4)	N16_c-Cu3-N18_b	88.4(3)
N1_c-Cu1-N10	88.0(3)	Cu1-N1-Cu2	101.3(3)
N10-Cu1-N15_d	95.9(4)	Cu1-N1-N2	127.5(6)
N1_c-Cu1-N15_d	168.2(3)	Cu1-N1-Cu1_c	99.3(3)
N1-Cu2-N4	79.4(3)	Cu2-N1-N2	122.8(6)
N1-Cu2-N13	171.0(4)	Cu1_c-N1-Cu2	90.6(3)
N1-Cu2-N16	92.7(3)	Cu1_c-N1-N2	106.6(6)
N1-Cu2-N7_c	88.6(3)	N1-N2-N3	178.2(11)
N4-Cu2-N13	97.9(4)	Cu1-N4-Cu2	100.0(3)
N4-Cu2-N16	172.1(3)	Cu1-N4-N5	124.6(7)
N4-Cu2-N7_c	98.1(3)	Cu2-N4-N5	126.4(7)
N13-Cu2-N16	90.0(4)	N4-N5-N6	177.9(11)
N7_c-Cu2-N13	100.3(3)	Cu1-N7-Cu3	92.6(3)
N7_c-Cu2-N16	80.8(3)	Cu1-N7-N8	117.5(6)
N7-Cu3-N10	74.1(3)	Cu1-N7-Cu2_c	99.2(3)
N7-Cu3-N19	102.1(3)	Cu3-N7-N8	124.1(6)
N7 -Cu3-N20	105.7(3)	Cu2_c-N7-Cu3	87.5(2)

Symmetry codes: b = x, y, 1+z; c =2−x, 1−y, −z; d = 3−x, 1−y, −z

4.3.2 Magnetic properties

4.3.2.1 Magnetic properties of Complex 1

The temperature dependence of χ_M and $\chi_M T$ product for **1** is shown in Figure 10. Upon cooling, χ_M increases, reaching a maximum value of 0.094 cm^3 mol^{-1} around 3.1 K, and then rapidly decreases with temperature. The $\chi_M T$ product at room temperature, 0.87 cm^3 mol^{-1} K, is slightly higher than the spin-only value of 0.75 cm^3 mol^{-1} K expected for two isolated Cu(II) ions (S = ½) assuming g =2.00. As the temperature is lowered, $\chi_M T$ decreases slowly up to 30 K and then sharply to 0.22 cm^3 mol^{-1} K upon cooling to 2.5 K. This characteristic behaviour indicates antiferromagnetic coupling in the dimer. To estimate the magnitude of the antiferromagnetic coupling, the magnetic susceptibility data (300–2.5 K) were fitted to the modified Bleaney-Bowers equation for two Cu(II) ions (S = ½) with the Hamiltonian in the form $\hat{H} = -J\hat{S}_1 \hat{S}_2$. The susceptibility equation for such a dimeric system can be written as follows:

$$\chi_M = (2N\beta^2 g^2/kT)\,[3 + \exp(-J/kT)]^{-1}(1-\rho) + N\beta^2 g^2 \rho/2kT \quad \ldots\ldots\ldots\ldots (1)$$

Where N, g,β, k and ρ parameters bear their usual meaning. The best fit parameter shows $J = -5.05$ cm^{-1} with g = 2.01, $\rho = 0.09$ and $R = 1.6\times10^{-6}$ $\{R = \sum[(\chi_M)^{obs} - (\chi_M)^{calc}]^2/[(\chi_M)^{obs}]^2\}$ (Figure 10).

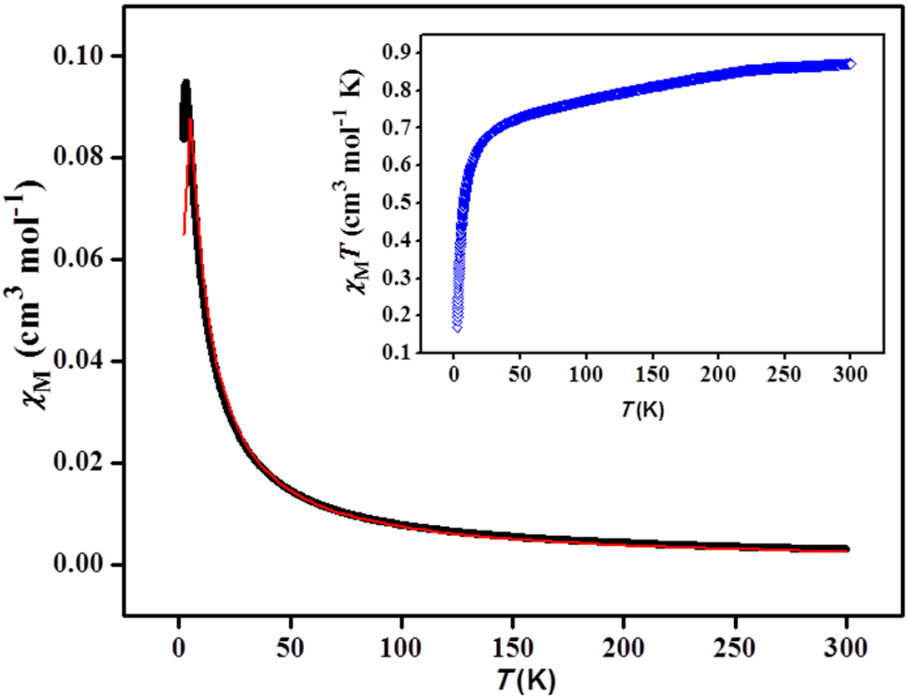

Figure 10. The plots of χ_M *vs*. T and $\chi_M T$ *vs*. T (inset) for **1**. The solid red line indicates the best fit obtained.

To understand the energetics of magneto-structural interactions, we have carried out extensive theoretical calculation using first-principles DFT method as implemented in Gaussian03 package. All the calculation details are presented in computational details section. We have considered a dinuclear core for the compound **1** and the initial structure modelled from X-ray crystallography was subjected to partial geometry optimization considering only hydrogen position minimization, as X-ray analysis cannot predict the position of hydrogen atoms correctly. Model **1** represents the DFT optimized geometry for the compound **1** (Figure 11). In order to find out the minimum energy magnetic ground state, spin unrestricted DFT calculations were performed considering all possible spin states corresponding to different z–component of total spin (S_z^t). Our results show that for the dinuclear model **1**, the LS antiferromagnetic state is more stable than the HS ferromagnetic state with a marginal energy difference and the calculated J value is ~3.7

cm^{-1} (Table 5), which corroborates well with the experimental findings. An analysis of Mulliken spin density shows that the two Cu(II) ions bear 0.48 e which is coupled antiferromagnetically while a significant part of the spin density is distributed over the N_3^- bridging ligand, as also can be seen from Figure 12(a). Moreover, calculated spin density at the N_3^- bridging ligand shows that the end nitrogen atoms of the two N_3^- groups contribute a significant amount to the overall spin density of the complex. Our analysis predicts that the binuclear complex would show weak antiferromagnetic interaction, which supports the experimental result.

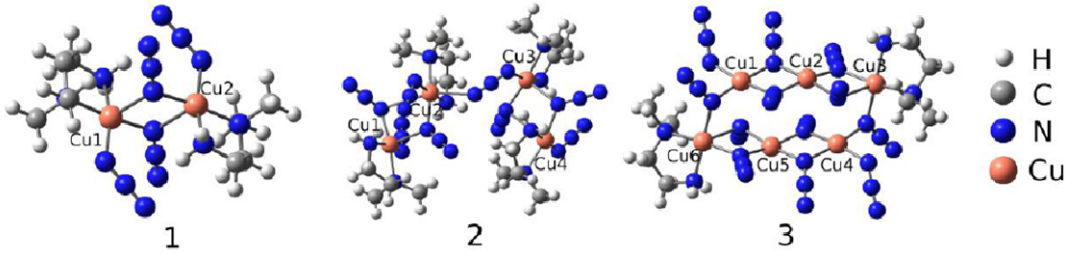

Figure 11. The optimized structures of binuclear (**1**), tetranuclear (**2**), and hexanuclear (**3**) models used for computational studies. All the magnetic centers are labelled as Cu1, Cu2 etc.

Accidental orthogonality can be realized in dinuclear Cu(II) compounds which gives rise to ferromagnetic interaction and this situation is favoured when the bridging angle is close to 90°. If the angle is quite deviated from 90°, antiferromagnetic interaction is anticipated. Thompson *et al.*[17] predicted the possibility of antiferromagnetic behaviour for this kind of compounds when the Cu-N_{EO}-Cu angle is above than the critical angle 108°, while Ruiz *et al.*[3c] calculated this critical angle to be 104° based on DFT calculations. For **1**, this angle is 101.1(2)˚ and to the best of our knowledge there is only one report[3d] of a dimer $[Cu_2L_2(N_3)_2]$ (L = 1-(*N*-salicylideneamino)-2-aminoethane), showing antiferromagnetic interaction and having a Cu-N_{EO}-Cu angle of 89.1°. An insight into the structure of **1** reveals that N3 atom of the azido ligand connecting two Cu(II) centres through an end-on bridge belongs to the basal plane of Cu1 but occupies apical position of square pyramidal coordination geometry of Cu1_a. In the dimeric structure, N3_a also binds Cu1 and Cu1_a in a similar fashion. Thus the interaction between the magnetic orbitals is expected to be very weak resulting in a small *J* value. Again the Cu-N3_a distance (2.356 (6) Å) is quite higher than the critical Cu–N distance

(2.05 Å) for the interaction being ferromagnetic[3a]. Probably these factors cumulatively results in the observed antiferromagnetic behaviour of **1**.

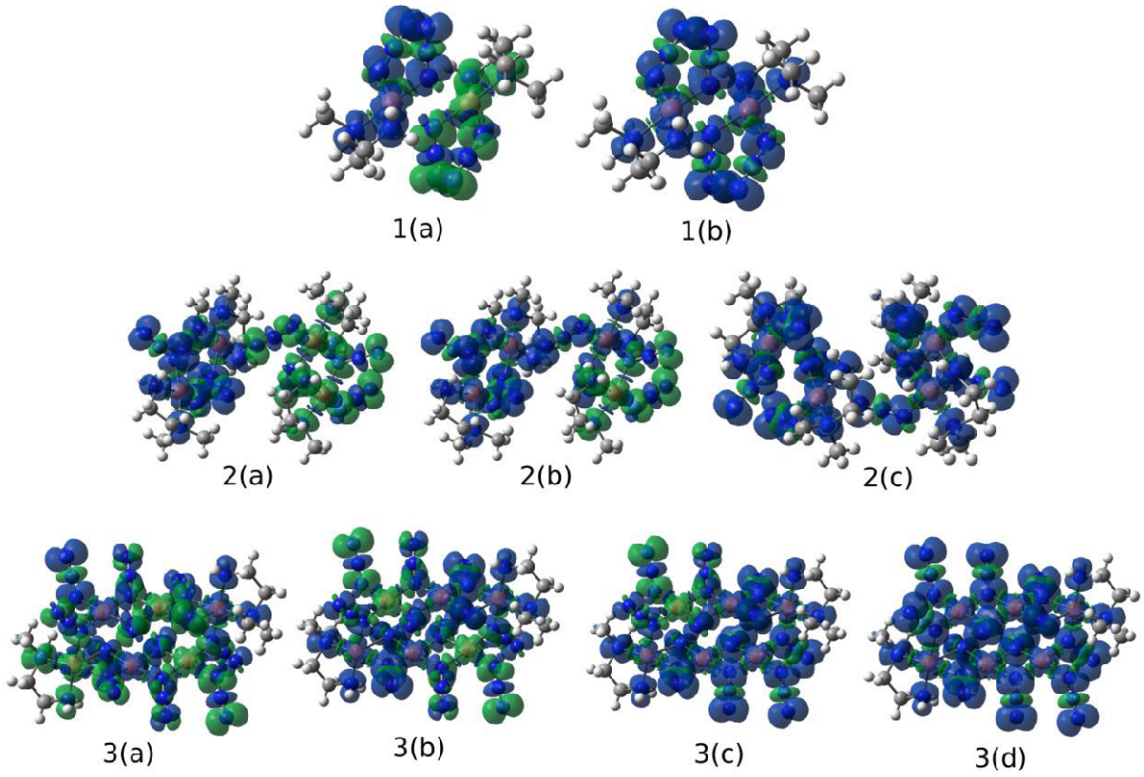

Figure 12. Spin density plots for the models **1**, **2**, and **3** consisting of two, four, and six Cu (II) centres, respectively. 1(a) and 1(b) represent spin densities for the two different spin states of complex **1** corresponding to the S_z^t = 0 and 1, respectively. Spin density in 2(a), 2(b), 2(c) represent three different spin states of model **2** corresponding to S_z^t = 0, 1, 2, respectively, while 3(a), 3(b), 3(c) and 3(d) indicate the spin density distribution of model **3** with S_z^t = 0, 1, 2, 3, respectively.

4.3.2.2 Magnetic properties of Compound 2

The temperature dependence of χ_M and $\chi_M T$ product for **2** is displayed in Figure 13. With decrease in temperature, χ_M increases and reaches a maximum value at 3.4 K, and then decreases with temperature. The $\chi_M T$ product (room temperature value 0.82 cm^3 mol^{-1} K) increases up to 200 K and then slowly increases till 80 K followed by a final decrease. The nature of $\chi_M T$ versus T plot is unusual; however, $\chi_M T$ versus T plot suggests the presence of both ferromagnetic as well as antiferromagnetic interaction, which can be attributed to the different kind of azide bridging modes. Compound **2** can be considered as an alternate chain structure with two interaction parameters (via the two

different azido bridge) and its magnetic data can be analyzed with the following Heisenberg spin Hamiltonian:

$$H = -J\sum_{i=1}^{n/2}[S_{A_{2i}} \cdot S_{A_{2i-1}} + \alpha S_{A_{2i}} \cdot S_{A_{2i+1}}]$$

An analytical expression of the magnetic susceptibility for this spin Hamiltonian has been given by Kahn[1j]:

$\chi_M = (N\beta^2g^2/kT)\,[(A + Bx+Cx^2)/(1+Dx+Ex^2+Fx^3)]$ …….(2)

Where $x=|J|/kT$, A=0.25, B= -0.062935+ 0.11376α, C=0.0047778-0.033268α+0.12742α^2-0.32918α^3 + 0.25203α^4, D = 0.053860 + 0.70960α, E = – 0.00071302 – 0.10587α + 0.54883α2 – 0.20603α^3, and F = 0.047193 – 0.008377α + 0.87256α^2 – 2.7098α^3 + 1.97980α^4.

A fit using this equation shows that the two coupling values are −4.85 cm^{-1} and 1.81 cm^{-1} with g = 2.3 and $R = 4.8\times10^{-6}$. Unfortunately, the best fit obtained is not very satisfactory though the different sign of the two J values suggests the presence of both ferromagnetic and antiferromagnetic interactions. Though there are reports on alternating chains of Cu(II)–azido compound[4c], the $\chi_M T$ versus T plot of **2** is uncommon and the exact exchange mechanism operating here is difficult to interpret without knowing the spin electronic structure. However, the DFT results provide an insight into the magnetic behaviour. Based on the structural unit, we have considered a tetranuclear fragment (model **2**) for the compound **2** and the initial structure was modelled from X-ray crystallography considering only hydrogen position minimization (Figure 11). We have looked at the magnetic exchange pathways in model **2** with three possible spin configurations corresponding to S_z^t = 0, 1, and 2, and the results obtained are tabulated in Table 5. We find that the HS (S_z^t = 2) state is stable compared to the other two spin states by a very small energy scale. Based on the calculated results, we speculate that both the S_z^t = 1 and 2 spin configurations are possible to exist, which accounts for the ferromagnetic behaviour in the$\chi_M T$ versus T plot. We also looked at the spin density distribution for all possible spin configurations which are shown in Figure 12(a), 12(b), and 12(c) for S_z^t = 0, 1 and 2, respectively. The distribution of computed spin density reveals that a major contribution of the spin density is distributed over the bridging ligands, in particular over the bridging N_3^- groups. Moreover, we find that all the Cu(II) centres possesses ~0.5 e which eventually take part in magnetic interactions.

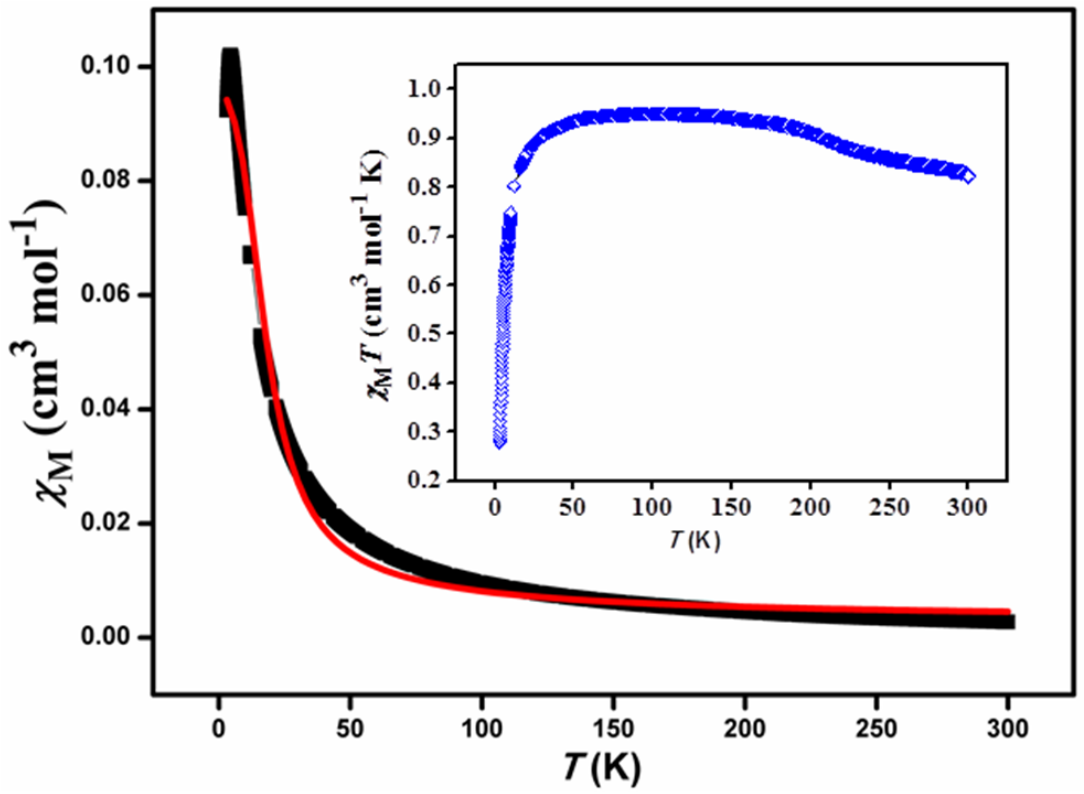

Figure 13. The plots of χ_M *vs.* T and $\chi_M T$ *vs.* T (inset) for **2**. The solid red line indicates the best fit obtained.

Note that, the model **2** contains two different N_3^- bridging ligands ($\mu_{1,1}$ and $\mu_{1,3}$) and consequently, has two distinctive magnetic exchange interactions pathways. In order to understand the exchange interactions via these two different pathways, we have analysed two different dinuclear Cu(II) fragments, modelled from the tetranuclear fragment **2**; one of which consists of $\mu_{1,1}$–N_3 bridging and another one contains $\mu_{1,3}$ bridging mode of the azide ion (Figure 14). The geometries of these two fragments are fully optimized within the same level of calculations as mentioned above. We find that $\mu_{1,1}$ bridging of N_3^- ligand results in weak antiferromagnetic interactions and the $S_z^t = 0$ state is more stable than the ferromagnetic $S_z^t = 1$ by 1.5 cm^{-1} whereas the $\mu_{1,3}$–N_3 bridging mode favours the moderate ferromagnetic coupling between the two Cu(II) centres and the $S_z^t = 1$ state has lower energy by 35.3 cm^{-1} than $S_z^t = 0$ state, resulting in overall weak ferromagnetic state. The spin density distribution corresponding to each spin state is shown in Figure 14 for the two fragments. We find that each Cu(II) centre

possesses ~0.5 e as the net spin moment and a significant part of the spin density is distributed over the bridging groups as was found for the parent fragment **2**.

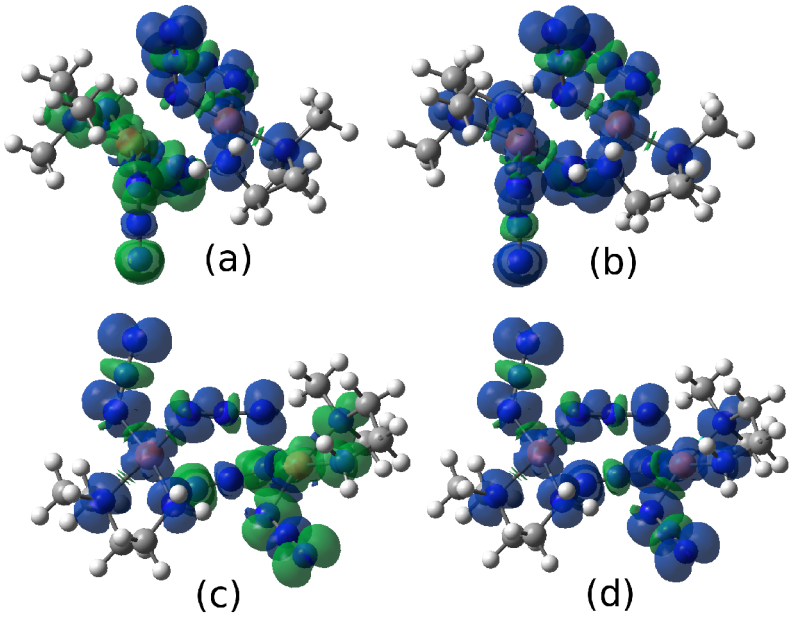

Figure 14. Spin density plots for the model fragments of compound **2** consisting of two Cu (II) centres. (a), (b) and (c), (d) represent spin densities for the two different spin states corresponding to the $S_z^t = 0$ (a, c) and 1 (b, d), respectively, of two fragments with $\mu_{1,1}$– (a, b) and $\mu_{1,3}$–(c, d) N_3 bridging.

As we have mentioned before, a Cu–N distance which is larger than the critical Cu–N distance (2.05 Å), can assist antiferromagnetic behaviour. Thus antiferromagnetic interaction through the $\mu_{1,1}$–N_3 bridging can be facilitated because of the Cu1–N5 distance (2.305(2) Å). Moreover, the antiferromagnetic interaction can also be a consequence of the Cu1–N5–Cu2 angle (108.30(10)°), which is close to the critical angle 108°. The ferromagnetic interaction through $\mu_{1,3}$–N_3 mode can be explained by the quasi–orthogonality of magnetic orbitals[4c], as observed in the Cu1–N8–N9–N10–Cu2 pathway.

4.3.2.2 Magnetic properties of Compound 3

The plot of χ_M and $\chi_M T$ versus T for **3** is displayed in Figure 15. Upon cooling, χ_M increases and reaches a maximum value of 0.24 cm^3 mol^{-1} at around 6.8 K, and then decreases with temperature. The room temperature $\chi_M T$ value (1.47 cm^3 mol^{-1} K) gradually increases giving a maximum value of 2.04 cm^3 mol^{-1} K at 14 K and then decreases to 0.51 cm^3 mol^{-1} K upon cooling to 2.5 K. The nature of $\chi_M T$ versus T plot

indicates a dominant ferromagnetic interaction at higher temperature and antiferromagnetic interaction at low temperature.

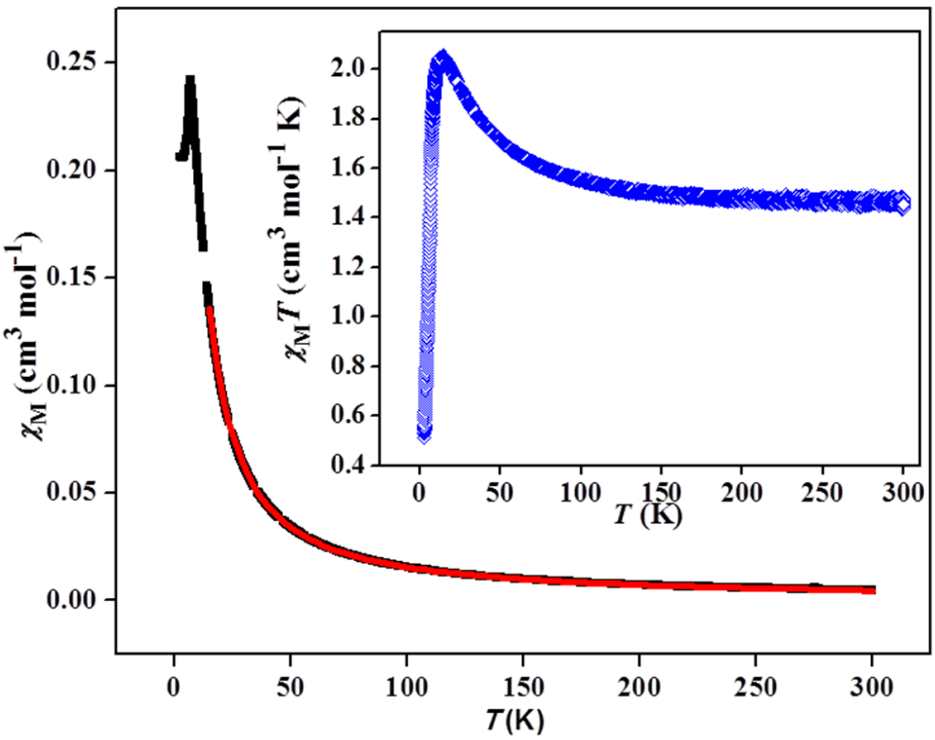

Figure 15. The plots of χ_M *vs*. T and $\chi_M T$ *vs*. T (inset) for **3**. The solid red line indicates the best fit obtained.

To get insight into the magnetic exchange mechanism, we attempted to have a closer look into the structure. The geometry around the Cu(II) ions is either square pyramidal or octahedral with axially elongated bond suggesting that the unpaired electron on each Cu(II) resides in the basal $d_{x^2-y^2}$ orbital, while the d_{z^2} orbital contains the paired electrons. Now the magnetic exchange between the Cu(II) ions is mediated via the different azido bridging ligands as mentioned earlier. It is an obvious case of over parameterization and we have looked at into the repeating hexanuclear cluster by considering only the significant interactions where azido groups links the equatorial sites of the Cu(II). In the hexanuclear core, there are six significant exchange pathways (Cu1-N10-Cu3, Cu1-N1-Cu2, two involving Cu1-N4-Cu2 and two involving Cu2-N16-Cu3 pathways, through the $\mu_{1,1}$, $\mu_{1,1,1}$, $\mu_{1,1}$ and $\mu_{1,1,3}$ azido bridging, respectively), which we have taken to be equivalent for further simplification as the bond angles and bond

distances involved are similar. Thus for the interactions in the hexanuclear core, the following Heisenberg Hamiltonian (eq 3) is used:

$H = -6J.\hat{S}_1\,\hat{S}_2$…….(3)

As we have mentioned earlier that the hexanuclear cores are further connected by $\mu_{1,1,3}$-N_3 and $\mu_{1,3}$-N_3 groups forming a 2D network, therefore an interhexamer zj' term was introduced which results the final expression of susceptibility as:

$\chi_M = (\chi_M)_{hexa}/[1 - (2zj'/N\beta^2g^2)(\chi_M)_{hexa}]$

$(\chi_M)_{hexa} = (N\beta^2g^2/kT)[A/B]$

Where A= 14 + 9 exp(-5J/kT) + 25 exp(-3J/kT) and B= 7 + 27 exp(-5J/kT) + 5 exp(-6J/kT)+ 25 exp(-3J/kT).

The values giving best fit (300-15 K) are J = 7.06 cm^{-1} with g = 2.26, zj' = -1.58 cm^{-1} and $R = 9.8\times10^{-9}$ $\{R = \sum[(\chi_M)^{obs} - (\chi_M)^{calc}]^2/[(\chi_M)^{obs}]^2\}$ (Figure 15). Fitting below 15 K was not satisfactory, which could be due to complex intermolecular interactions.

For the theoretical study, we have considered a hexanuclear core (model **3**) with all possible spin states for compound **3** (the DFT optimized geometry is shown in Figure 11). As can be seen from the Table 5, the minimum energy structure is the magnetic state with $S_z^t = 1$, and other two spin states ($S_z^t = 0$ and 1) are degenerate with 129.40 cm^{-1} in higher energy compared to the $S_z^t = 1$ state while the HS state with $S_z^t = 2$ is destabilized by 258.82 cm^{-1}. From an analysis of the spin density on each magnetic Cu(II) centre, we find that the minimum energy state is the frustrated spin configuration state with triangular lattice arrangements (see 3(b) in Figure 12). In the hexanuclear core, there are different end-on azido groups having different Cu–N_{EO}–Cu angles which are expected to give rise to both ferromagnetic and antiferromagnetic domain and the calculations also supports that a spin frustrated $S_z^t = 1$ state to be the ground state. These can give rise to an overall dominant ferromagnetic interaction as obtained experimentally. We also find that each Cu(II) bears ~0.5 e spin density and a significant part of the overall spin density is spread over the associated ligands.

In the hexanuclear core, there are different end-on azido groups with different Cu–N_{EO}–Cu angles (see Table 4) which probably give rise to both ferromagnetic and antiferr-

Table 5. Results for the all possible spin states of the model systems **1**, **2**, and **3**. S_z^t represents the z-component of the total spin. The energy (E) is scaled with respect to the lowest energy magnetic state and the spin density values for all Cu(II) centers are given only for the low energy spin state.

Compound	S_z^t	E (cm^{-1})	Spin density (e)
1	0	0.00	Cu1 (0.48)
	1	3.66	Cu2 (-0.48)
2	0	3.25	Cu1 (0.46)
	1	0.32	Cu2 (0.46)
	2	0.000	Cu3 (0.48)
			Cu4 (0.44)
3	0	129.40	Cu1 (-0.47)
	1	0.00	Cu2 (0.45)
	2	129.40	Cu3 (0.47)
	3	258.82	Cu4 (-0.47)
			Cu5 (0.45)
			Cu6 (0.47)

-omagnetic domain in 3. Experiment shows that overall dominant interaction in the hexanuclear core is ferromagnetic and the exchange interaction between the clusters is weakly antiferromagnetic which is mediated via end-to-end azide groups.

4.4 CONCLUSION

By controlling the relative concentration of the blocking ligand and using simple self-assembly approach, we were able to control the dimensionalities in Cu(II)-azido system. Synthesis, structural characterization and magnetic studies of three novel magnetic systems, ranging from a discrete dinuclear complex to an extended 2D network, are presented. The origin of the different magnetic exchange behaviour in these compounds have been correlated to their structure and DFT calculations. Our results suggest that by changing the stoichiometry of the coligand, azide and metal system, it is possible to synthesize different compounds with different dimensionalities. To get insight into the complex magnetic structures of such systems, it is highly desirable to fabricate these systems in a rational way, where magnetic properties can be modulated based on the structures.

4.5 REFERENCES

[1] (*a*) E. Coronado, P. Delhaes, D. Gatteschi and J. S. Miller, Dordrecht, *Molecular magnetism: From the molecular assemblies to the Devices*, NATO ASI series no. E321, Dordrecht, 1996; (*b*) T. C. Stamatatos, A. G. Christou, C. M. Jones, B. J. O'Callaghan, K. A. Abboud, T. A. O'Brien, and G. Christou, *J. Am. Chem. Soc.*, 2007,**129**, 9840; (*c*) R. Bagai, K. A. Abboud and G. Christou, *Inorg. Chem*., 2007, **46**, 5567; (*d*) J. J. Vittal, *Coord. Chem. Rev*., 2007, **251**, 1781; (*e*) J. Yoon and E. I. Solomon, *Coord. Chem. Rev*., 2007, **251**, 379; (*f*) C. F. Lee, D. A. Leigh, R. G. Pritcharg, D. Schults, S. J. Teat, G. A. Timco and R. E. P. Winpenny, *Nature*, 2009, **458**, 314; (*g*) R. E. P. Winpenny, *Angew Chem. Int. Ed*., 2008, **47**, 7992. (*f*) R. E. P. Winpenny, *Dalton Trans*., 2002, 1; (*h*) V. Chandrasekhar and B. Murugesapandian, *Acc. Chem. Res*., 2009, **42**, 1047; (*i*) V. Chandrasekhar, B. Murugesapandian and J. J. Vittal, *Inorg. Chem*., 2009, **48**, 1148; (*j*) O. Kahn, *Molecular Magnetism*. VCH, New York, 1993.

[2] (*a*) O. Kahn, M. F. Charlot, *Nouu. J. Chim.*, 1980, **4***,* 567; *(b)* P. J. Hay, J. C. Thibeault and R. J. Hoffmann, *J. Am. Chem. Soc.*, 1975, **97***,* 4884; (*c*) V. M. Crawford, H. W. Richardson, J. R. Wasson, D. J. Hcdgson and W. E. Hatfield, *Inorg. Chem.*, 1976, **15***,* 2107; (*d*) D. J. Hodgson, *Inorg. Chem.*, 1976, **15***,* 3174.

[3] (*a*) L. K. Thompson and S. K. Tandon, *Comments Inorg. Chem*., 1996, **18**, 125; (*b*) R. D. Willett, D. Gatteschi and O. Kahn, *Magneto-Structural Correlations in Exchange Coupled Systems*, Dordrecht, The Netherlands, 1985; (*c***)** E. Ruiz, J. Cano, S. Alvarez and P. Alemany, *J. Am. Chem. Soc*., 1998, **120**, 11122; (*d*) S. Koner, S. Saha, T. Mallah and K. -I. Okamoto, *Inorg. Chem.*, 2004, **43**, 840.

[4] (*a*) Y. Song, S. Ohkoshi, Y. Arimoto, H. Seino, Y. Mizobe and K. Hashimoto, *Inorg*. *Chem.*, 2003, **42**, 1848; (*b*) M. A. M. Abu-Youssef, A. Escuer, M. A. S. Goher, F. A. Mautner and G. J. Reib and R. Vicente, *Angew. Chem., Int. Ed.*, 2000, **39**, 1624; (*c*) P. S. Mukherjee, T. K. Maji, G. Mostafa, T. Mallah and N. Ray Chaudhuri, *Inorg. Chem.*, 2000, **39**, 5147; (*d*) T. K. Maji, P. S. Mukherjee, G. Mostafa, T. Mallah, J. Cano-Boquera and N. Ray Chaudhuri, *Chem. Commun.*, 2001, 1012.

[5] (*a*) H. Wen, J. Zuo, W. Liu, Y. Song and X. You, *Inorg. Chim. Acta,* 2005, 2565; (*b*) M. Liang, W. Wang, Z. Liu, D. Liao, Z. Jiang, S. Yan and P. Cheng, *J. Coord.*

Chem., 2003. **56**, 1473; (*c*) M. Monfort, L. Resino, J. Ribas and H. Stoeckli-Evans, *Angew. Chem. Int. Ed.*, 2000, **39**, 191; (*d*) E.-Q. Gao, Y.-F. Yue, S.-Q. Bai, Z. He and C.-H. Yan, *J. Am. Chem. Soc.*, 2004, **126**, 14.

[6] (*a*) A. M. Abu-Youssef, A. Escuer, F. A. Mautner and Lars Öhrström, *Dalton Trans.*, 2008, 3553; (*b*) F.-C. Liu, Y.-F. Zeng, J. R. Li, X.-H. Bu, H. J. Zhang and J. Ribas, *Inorg. Chem.*, 2005, **44**, 7298; (*c*) F.-C. Liu, Y.-F. Zeng, J. Jiao, J. R. Li, X.-H. Bu, J. Ribas and S. R. Batten, *Inorg. Chem.*, 2006, **45**, 6129; (*d*) F.-C. Liu, Y.-F. Zeng, J. Jiao, J. R. Li, X.-H. Bu, J. Ribas and S. R. Batten, *Inorg. Chem.*, 2006, **45**, 2776; (*e*) S. Naiya, C. Biswas, M. G. B. Drew, C. J. Gomez-Garcıa, J. M. Clemente-Juan, and A. Ghosh, *Inorg. Chem*., 2010, **49**, 6616.

[7] (*a*) K. C. Mondal and P. S. Mukherjee, *Inorg. Chem.*, 2008, **47**, 4215; (*b*) S. Mukherjee, B. Gole, R. Chakrabarty and P. S. Mukherjee, *Inorg. Chem.*, 2009, **48**, 11325; (*c*) S. Mukherjee, B. Gole, Y. Song, and P. S. Mukherjee, *Inorg. Chem.*, 2011, **50**, 3621.

[8] E. König, *Landolt-Börnstein, Neue Serie*; Springer: Berlin, 1966; Vol. II/2, 1.

[9] (*a*) SMART (V 5.628), SAINT (V 6.45a), XPREP, SHELXTL; Bruker AXS Inc. Madison, Wisconsin, USA, 2004; (*b*) G. M. Sheldrick, Siemens Area Detector Absorption Correction Program, University of Göttingen, Göttingen, Germany, 1994; (*c*) A. Altomare, G. Cascarano, C. Giacovazzo, A. Gualaradi, *J. Appl. Cryst.*, 1993, **26**, 343; (*d*) G. M. Sheldrick, SHELXL-97, Program for Crystal Structure Solution and Refinement; University of Göttingen, Göttingen, Germany, 1997; (*e*) A. L. Spek, *J. Appl. Cryst.*, 2003, **36**, 7; (*f*) L. J. Farrugia, WinGX - A Windows Program for Crystal Structure Analysis. *J. Appl. Crystallogr.*, 1999, **32**, 837.

[10] Gaussian 03, Revision C.02, M. J. Frisch, G. W. Trucks, H. B. Schlegel, G. E. Scuseria, M. A. Robb, J. R. Cheeseman, J. A. Montgomery, Jr. , T. Vreven, K. N. Kudin, J. C. Burant, J. M. Millam, S. S. Iyengar, J. Tomasi, V. Barone, B. Mennucci, M. Cossi, G. Scalmani, N. Rega, G. A. Petersson, H. Nakatsuji, M. Hada, M. Ehara, K. Toyota, R. Fukuda, J. Hasegawa, M. Ishida, T. Nakajima, Y. Honda, O. Kitao, H. Nakai, M. Klene, X. Li, J. E. Knox, H. P. Hratchian, J. B. Cross, V. Bakken, C. Adamo, J. Jaramillo, R. Gomperts, R. E. Stratmann, O. Yazyev, A. J. Austin, R. Cammi, C. Pomelli, J. W. Ochterski, P. Y. Ayala, K. Morokuma, G. A. Voth, P. Salvador, J. J. Dannenberg, V. G. Zakrzewski, S.

Dapprich, A. D. Daniels, M. C. Strain, O. Farkas, D. K. Malick, A. D. Rabuck, K. Raghavachari, J. B. Foresman, J. V. Ortiz, Q. Cui, A. G. Baboul, S. Clifford, J. Cioslowski, B. B. Stefanov, G. Liu, A. Liashenko, P. Piskorz, I. Komaromi, R. L. Martin, D. J. Fox, T. Keith, M. A. Al-Laham, C. Y. Peng, A. Nanayakkara, M. Challacombe, P. M. W. Gill, B. Johnson, W. Chen, M. W. Wong, C. Gonzalez, J. A. Pople, Gaussian, Inc. , Wallingford CT, 2004.

[11] (*a*) C. Lee, W. Yang and R. G. Parr, *Phys. Rev. B*, 1988, **37**, 785; (b) B. Miehlich, A. Savin, H. Stoll and H. Preuss, *Chem. Phys. Lett*., 1989, 157, 200; (*c*) A. D. Becke, *J. Chem. Phys.*, 1993, **98**, 5648.

[12] (*a*) P. J. Hay and W. R. Wadt, *J. Chem. Phys*., 1985, **82**, 270; (*b*) W. R. Wadt and P. J. Hay, *J. Chem. Phys.* 1985, **82**, 284; (*c*) P. J. Hay and W. R. Wadt, *J. Chem. Phys.*, 1985, **82**, 299.

[13] (*a*) D. Maity, A. K. Manna, D. Karthigeyan, T. K. Kundu, Swapan K. Pati, and T. Govindaraju, *Chem. Eur. J.*, 2011, **17**, 11152; (*b*) K. L. Gurunatha, S. Dutta, G. Mostafa, S. K. Pati, and T. K. Maji, *Inorg. Chim. Acta*, 362, **3745**, 2009.

[14] (*a*) W. J. Caspers, Spin Systems, World Scientific, Singapore, 1989; (*b*) J. M. Ricart, R. Dovesi, C. Roetti and V. R. Saunders, *Phys. Rev. B.*, 1995, **52**, 2381. [Erratum: J. M. Ricart, R. Dovesi, C. Roetti and V. R. Saunders, *Phys. Rev. B*., 1997, **55**, 15942.

[15] (*a*) L. Noodleman, *J. Chem. Phys*., 1981, **74**, 5737; (*b*) L. Noodleman, E. R. Davidson, *Chem. Phys*., 1986, **109**, 131; (*c*) L. Noodleman, C. Y. Peng, D. A. Case and J. M. Mouesda, *Coord. Chem. Rev*., 1995, **144**, 199.

[16] A. W. Addison, T. N. Rao, J. Reedijk, J. van Rijn and G. C. Verschoor, ***J.*** *Chem. Soc., Dalton Trans*., 1984, 1349.

[17] S. S. Tandon, L. K. Thompson, M. E. Manuel and J. N. Bridson, *Inorg. Chem.*, 1994, **33**, 5555.

Chapter 5

3D Porous Bimetallic Co(II)-Ag(I) and Ni(II)-Ag(I) Frameworks: Coexistence of Canted Antiferromagnetism and CO_2 Selectivity

Abstract

This chapter articulates synthesis, characterization, adsorption and magnetic properties of two isomorphous bimetallic Co(II)/Ni(II)-Ag(I) 3D porous frameworks synthesized based on a mixed-ligand system. The cyanide-bridged M(II)-Ag(I) bimetallic compounds, $[M^{II}(pip)\{Ag(CN)_2\}_2 \cdot 5H_2O]$ (M = Co, **1**; Ni, **2**; pip = piperazine) have been synthesized by liquid phase diffusion method at room temperature. Structure determination revealed that both the structures have α-polonium type topology, formed by the connection of 2D M(II)-$Ag(CN)_2$ layers by the piperazine linker. The 3D frameworks are 2-fold interpenetrated and this renders structural rigidity and high thermal stability, which is evidenced by the powder X-ray diffraction analysis. Temperature dependent magnetic study reveals that at low temperature, magnetized states exist for both the compounds and spin canting behaviour is observed below 5 K and 14 K, for **1** and **2**, respectively. Design of the 3D porous structure where anisotropic Co(II) and Ni(II) ions have been employed, results into the spin canting behaviour. The 3D frameworks provide two different channels occupied by guest molecules. The pore surfaces are decorated with polar –CN groups, making the compounds CO_2 selective. Selective adsorption of CO_2 over other gases, such as N_2, H_2, O_2 and Ar at 195 K is exhibited by the dehydrated frameworks **1′** and **2′**.

5.1 INTRODUCTION

The field of crystal engineering has achieved an extraordinary advancement over the past several years and a large number of structures have been reported by synthetic chemists.[1] With the potential to synthesize such versatile structures, the main focus is now to develop smart multifunctional materials that combine a set of well-defined properties e.g. porosity and magnetism. In the context of magnetic materials, physicists have already provided an array of target lattices.[2] The versatility of coordination chemistry affords immense opportunities to discover such materials and to appreciate elemental magnetic phenomenon, such as long range ordering and spin canting.[3] Invoking porosity into such magnetic materials is an attractive and challenging goal. Because of the incompatibility in the properties, combining magnetism and porosity in a single material is not trivial. The strength of magnetic coupling decreases with long distances and hence a significant magnetic exchange generally requires short bridges between the spin carriers. On the other hand, porosity is usually enhanced with long distance and relies on the use of long connecting ligands. Thus synthesis of a microporous solid that behaves as a magnet at ambient temperature remains an open challenge. There are only few reports on compounds showing both long-range magnetic ordering and porous framework structure[4] and most of these compounds are antiferromagnetic possessing no net magnetic moment in the ordered state. Magnetic hysteresis and spin canting have been rarely achieved for truly microporous solids.[4g] Use of 2D magnetic layers and connecting them with organic linkers in a mixed-ligand system would be a key approach to construct such materials, as already demonstrated by Maji *et al.*[4f] Moreover, the presence of such mixed-ligand system in metal-organic frameworks (MOFs) evokes structural flexibility, which brings up many interesting properties like selective adsorption, gated and stepwise adsorption etc.[5]

In the context of magnetism, nearest-neighbour interactions have been into the main focus and there have been very limited interests on the next-neighbour interactions. Eventually, there are very few reports on the use of $[Ag(CN)_2]^-$ metallo-ligand, the chemistry of which is yet to be properly explored. However, a recent report shows that long range magnetic ordering can efficiently be established through the NC–Ag–CN bridge.[6] In our work, the goal was to exploit this $[Ag(CN)_2]^-$ metallo-ligand to generate 2D magnetic sheets and to study their magnetic behaviour. Incorporation of organic linkers in this 2D magnetic layers helps to construct the 3D porous structures which can

be exploited for gas adsorption. In this regard, there are special interests in efficient storage and separation of the green-house CO_2 gas.[7] In recent years, selective CO_2 adsorption has gained considerable importance in the context of natural gas purification and in environmental issues such as the increasing CO_2 concentration in the atmosphere, and MOFs are one of the promising materials to solve such problems. Introduction of polar groups into the pore surfaces of the frameworks can efficiently render CO_2 selectivity, due to the fact that CO_2 has a large quadrupole moment.[7d]

While the use of the long organic linkers in MOF chemistry generally helps to design the 3D structure, it can also lead to interpenetration in the structure[8] and regulation of this interpenetration is important to remove any obstacles to porous functionalities. However, recently it has been established that the possibility of obtaining open porous frameworks is not inhibited by interpenetration.[9] Furthermore, interpenetrated frameworks are promising candidates for studying adsorption properties as these compounds are very rigid and they retain porosity even after the loss of guest molecules.

We, herein have perceived a rational synthetic strategy to design 3D frameworks where different features and properties have been combined into a single material, such as long range magnetic ordering, permanent porosity and guest selectivity. We have employed a mixed-ligand system (dicyanoargentate(I), $[Ag(CN)_2]^-$ and piperazine) with anisotropic Co(II) and Ni(II) ions and have synthesized two isomorphous 3D porous frameworks with the general formula $[M^{II}(pip)\{Ag(CN)_2\}_2.5H_2O]$, (M = Co, **1**; Ni, **2**; pip=piperazine). The frameworks are 2-fold interpenetrated which renders structural rigidity. With strong anisotropy resulted from single ions arranged in the 3D structure and a low symmetry M–NC–Ag–CN–M exchange pathway provided by the dicyanoargentate bridging, these compounds show spin canting. **1** and **2** exhibit spin canting behaviour below 5 K and 14 K, respectively. Piperazine acts as a pillar which helps to construct the 3D porous structure invoking porosity as well as providing interaction sites. Presence of the polar –CN groups in the pore surfaces makes these compounds CO_2 selective. The 2-fold interpenetration in these compounds render structural rigidity and there is no significant structural change in the dehydrated frameworks of **1** (**1′**) and **2** (**2′**), respectively, as reflected by their PXRD patterns. **1′** and **2′** show selective adsorption of CO_2 over other gases, such as N_2, H_2, O_2 and Ar at 195 K.

5.2 EXPERIMENTAL SECTION

5.2.1 Materials

All the reagents and solvents employed were commercially available and used as supplied without further purification. $Co(OAc)_2 \cdot 4H_2O$, $Ni(OAc)_2 \cdot 4H_2O$, piperazine and $K[Ag(CN)_2]_2$ were obtained from the Aldrich Chemical Co.

5.2.2 Synthesis

$[Co(pip)\{Ag(CN)_2\}_2 \cdot 5H_2O]$ (1) An aqueous solution (10 mL) of $K[Ag(CN)_2]_2$ (1 mmol, 0.199 g) was mixed with an aqueous solution (10 mL) of piperazine (0.5 mmol, 0.043 g) and the resulting solution was stirred for 20 min. to mix well. $Co(OAc)_2 \cdot 4H_2O$ (0.5 mmol, 0.124 g) was dissolved in 10 mL methanol and 2.5 mL of this metal solution was slowly and carefully layered with the above mixed ligand solution using 1 mL buffer (1:1 of water and MeOH) solution in a crystal tube to give a three-layer system, which was sealed and left undisturbed at room temperature. Slow diffusion yielded transparent and orange block crystals of **1** after 15 days. Bulk amount of the compound was synthesized by the direct mixing of the corresponding ligand solution with methanolic solution of Co(II). Yield 82%, relative to Co(II). Selected IR data (KBr, cm^{-1}); 3495 br, 3260 m, 2979 m, 2936 m, 2167 s, 1448 m, 1417 m, 1068 m, 1007 m, 877 s, (Figure 1). Compound purity was verified by PXRD and elemental analysis result. Anal. calcd. for $C_8H_{20}CoAg_2N_6O_5$: C, 17.31; H, 3.63; N,15.14. Found: C, 17.67; H, 3.31; N, 14.96.

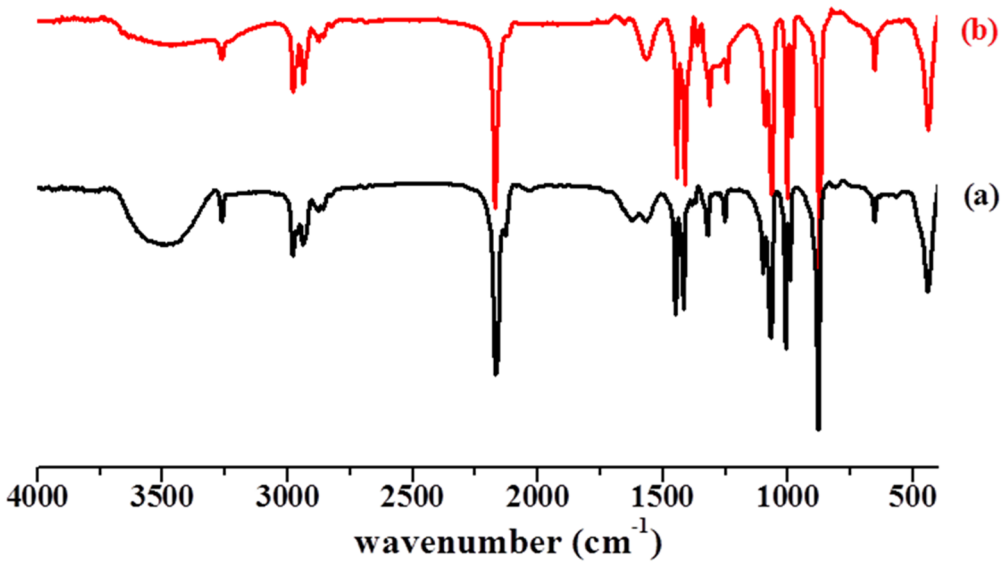

Figure 1. FT-IR spectra for (a) **1** and (b) **2**.

[Ni(pip){Ag(CN)$_2$}$_2$·5H$_2$O] (2) Similar methodology was adopted to synthesize compound **2** except that Co(OAc)$_2$·4H$_2$O was replaced by Ni(OAc)$_2$·4H$_2$O (0.1 mmol, 0.124 g). Blue colour block shaped crystals of **2** were isolated after 15 days. Yield 79%, relative to Ni(II). Selected IR data (KBr, cm^{-1}); 3510 br, 3270 m, 2981 m, 2938 m, 2176 s, 1462 m, 1407 m, 1075 m, 1007 m, 883 s, (Figure 1). Compound purity was verified by PXRD and elemental analysis result. Anal. calcd. for $C_8H_{20}NiAg_2N_6O_5$: C, 17.32; H, 3.63; N,15.15. Found: C, 17.71; H, 3.42; N, 15.65.

5.2.3 Single-crystal X-ray Diffraction

X-ray single-crystal structural data of **1** and **2** were collected on a Bruker Smart–CCD diffractometer equipped with a normal focus, 2.4 kW sealed tube X-ray source with graphite monochromated Mo–Kα radiation (λ = 0.71073 Å) operating at 50 kV and 30 mA. The SAINT program[10a] was used for integration of diffraction profiles and absorption correction was made with SADABS[10b] program. Both the structures were solved by SIR 92[10c] and refined by full matrix least square method using SHELXL 97.[10d] All the non hydrogen atoms were refined anisotropically and all the hydrogen atoms were fixed by HFIX and placed in ideal positions. All calculations were carried out using SHELXL 97, PLATON[10e] and WinGX system, Ver 1.70.01.[10f] All crystallographic and structure refinement data of **1** and **2** are summarized in Table 1. Selected bond lengths and angles are displayed in Table 2.

5.2.4 Physical Measurements

The elemental analyses were carried out using a Perkin Elmer 2400 CHN analyzer. IR spectra were recorded on a Bruker IFS 66v/S spectrophotometer using KBr pellets in the region 4000–400 cm^{-1}. Thermogravimetric analyses (TGA) were carried out on METTLER TOLEDO TGA850 instrument in the temperature range of 25–500 °C under nitrogen atmosphere (flow rate of 50 mL min^{-1}) at a heating rate of 5 °C min^{-1}. Powder X-ray diffraction (PXRD) patterns were recorded on a Bruker D8 Discover instrument using Cu–Kα radiation. DC magnetic susceptibility data of powdered crystalline samples of **1** and **2** were collected on a Vibrating Sample Magnetometer, PPMS (Physical Property Measurement System, Quantum Design, USA) in the temperature range of 2 K to 300 K with different applied field (50, 100 and 500 Oe). Field variation (−5 kOe to 5 kOe) magnetization measurement was carried out at 2 K. The

ac magnetic susceptibility measurements were carried out at H_{ac} = 5 Oe and at different frequencies.

5.2.5 Adsorption Measurements

Adsorption isotherms of CO_2, Ar, O_2 at 195 K and N_2, H_2 at 77 K were recorded with the dehydrated samples **1′** and **2′** using QUANTACHROME QUADRASORB-SI analyser. To prepare the dehydrated samples, approximately 100 mg of sample was taken in a sample holder and degassed at 160 ºC under 10^{-1} pa vacuum for about 12 hours prior to the measurements. Dead volume of the sample cell was measured using helium gas of 99.999% purity. The amount of gas adsorbed was calculated from the pressure difference ($P_{cal} - P_e$), where P_{cal} is the calculated pressure with no gas adsorption and P_e is the observed equilibrium pressure. All the operations were computer-controlled and automatic.

5.3 RESULTS AND DISCUSSION

5.3.1 Crystal Structure Description

Single–crystal X–ray structure determination reveals compounds **1** and **2** are isostructural and crystalizes in the orthorhombic *Cmcm* space group. The asymmetric unit of compound **1** contains one Co(II) centre, two $Ag(CN)_2$ ligands, one pip linker and five guest water molecules. Co(II) centre is present in a distorted octahedral geometry and coordinated to four nitrogen atoms (N1, N1_a, N2 and N2_a) from –CN groups. The other two coordination sites are furnished by N3 and N3_a atoms from pip pillar (Figure 2). Deviation from ideal octahedral geometry can be realized from the *cisoid* and *transoid*

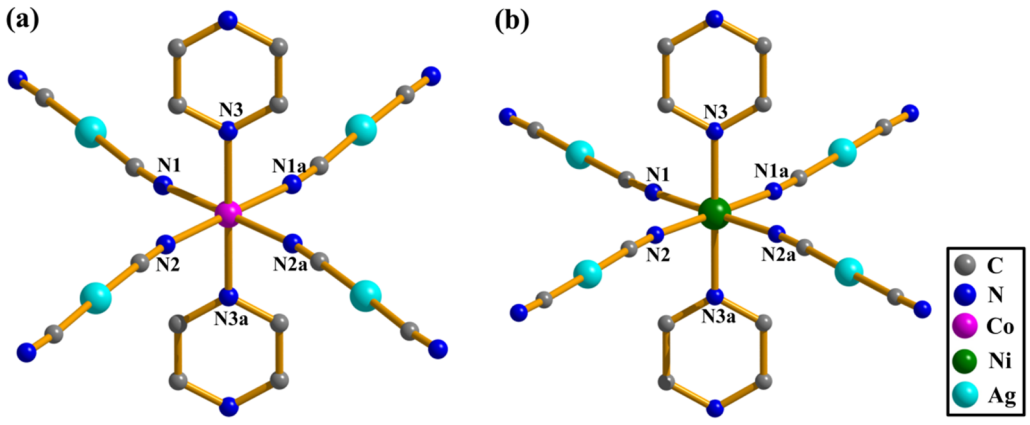

Figure 2. View of the coordination environment around Co(II)/ Ni(II): (a) for compound **1** and (b) for compound **2**. Symmetry code: a = 1−x, y, ½−z.

angles (Table 2). The Co–N bond lengths are in the range of 2.116(12)–2.154(12) Å (Table 2). The Co(II) centres are connected by $Ag(CN)_2^-$ linkers along the *ab* plane to form a 2D corrugated sheet like structure (Figure 3). These 2D sheets are further pillared by pip pillars forming 3D structure with α-polonium topology (Figure 3). Topological analysis of these 3D frameworks using TOPOS 40[11] suggests a 6-connected uninodal net (Figure 4) with Schläfli symbol $\{4^{12}; 6^3\}$. The Co(II)-Co(II) separation along the *ab* plane and along the *c* axis are 10.546 Å and 7.177 Å, respectively. The 3D framework shows a 2-fold interpenetration which finally renders two different types of pore along the *c* direction; a hexagon shaped large pore containing four water molecules per formula and the other smaller diamond shaped pore is occupied by one water molecule per formula (Figure 5). The void space, 337 $Å^3$ (22% total of cell volume), has been calculated using PLATON after removal of all the guest water molecules.

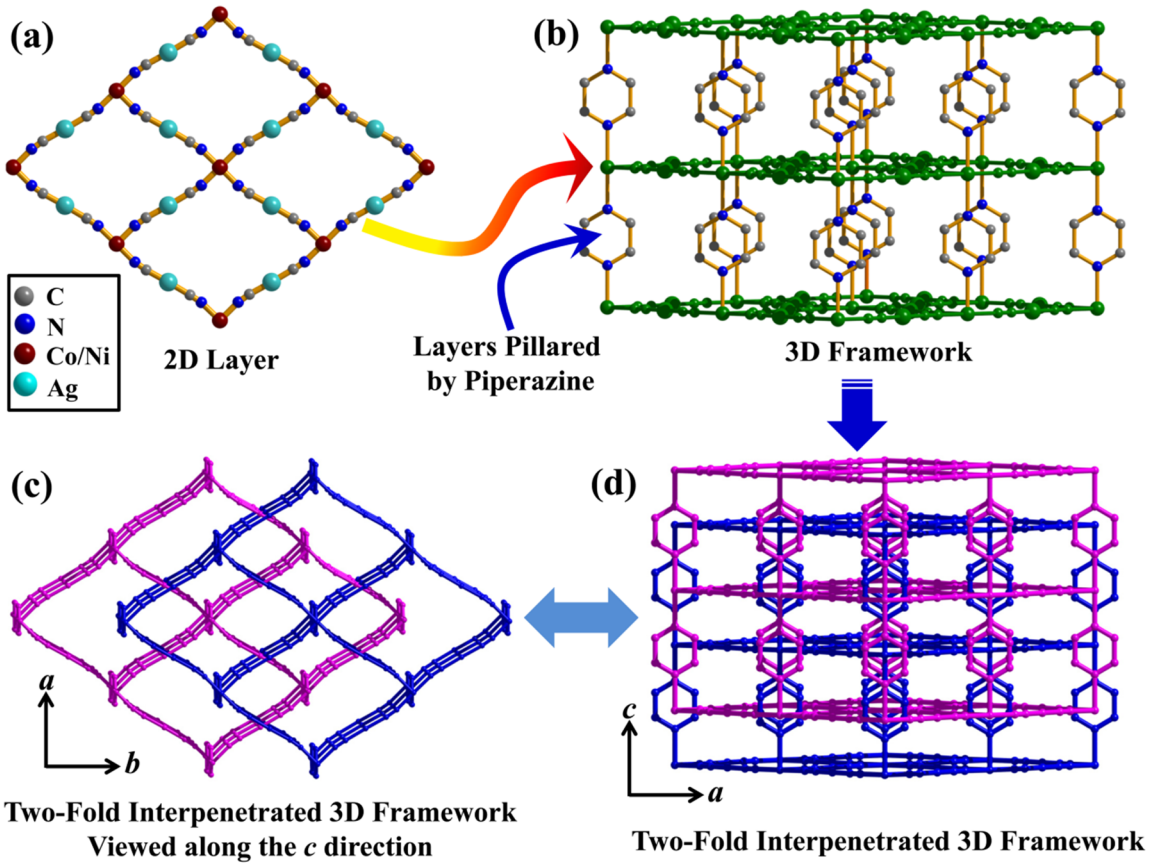

Figure 3. (a) View of the 2D sheet of M-argentocyante in the crystallographic *ab* plane. (b) View of the pillared-layer 3D structure along the crystallographic *a*-axis. (c) View of the 2-fold interpenetrated structure along the crystallographic *c*-axis. (d) View of the 2-fold interpenetrated 3D framework along the crystallographic *b*-axis (hydrogen and non-coordinated water molecules have been omitted for clarity).

Compound **2** bears similar metal (here Ni^{II}) coordination topology (Figure 2) with subtle differences in bond distances and angles. The Ni–N bond lengths vary in the range of 2.088(14)–2.119(14) Å (Table 2). The Ni(II)-Ni(II) separation along the *ab* plane and along the *c* axis are 10.485 Å and 7.116 Å, respectively. Details of the bond angles and distances of both the compounds are mentioned in Table 2. Calculated void space using PLATON for compound **2** was found to be 331 $Å^3$ (22% total of cell volume), which is close to that of compound **1**.

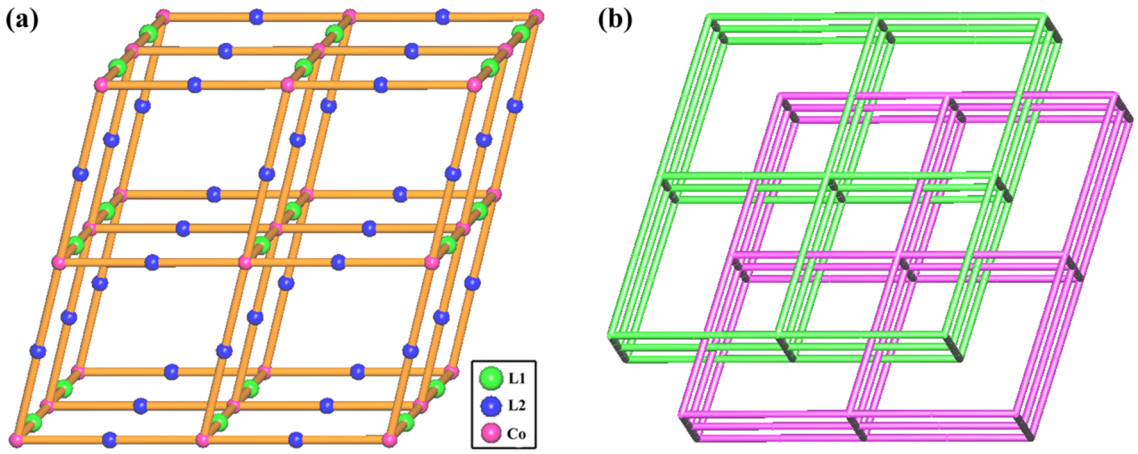

Figure 4. (a) View of the 6-connected uninodal node. In the legend L1 = piperazine; L2 = $Ag(CN)_2$. (b) The 2-fold interpenetrated nets in compound **1**.

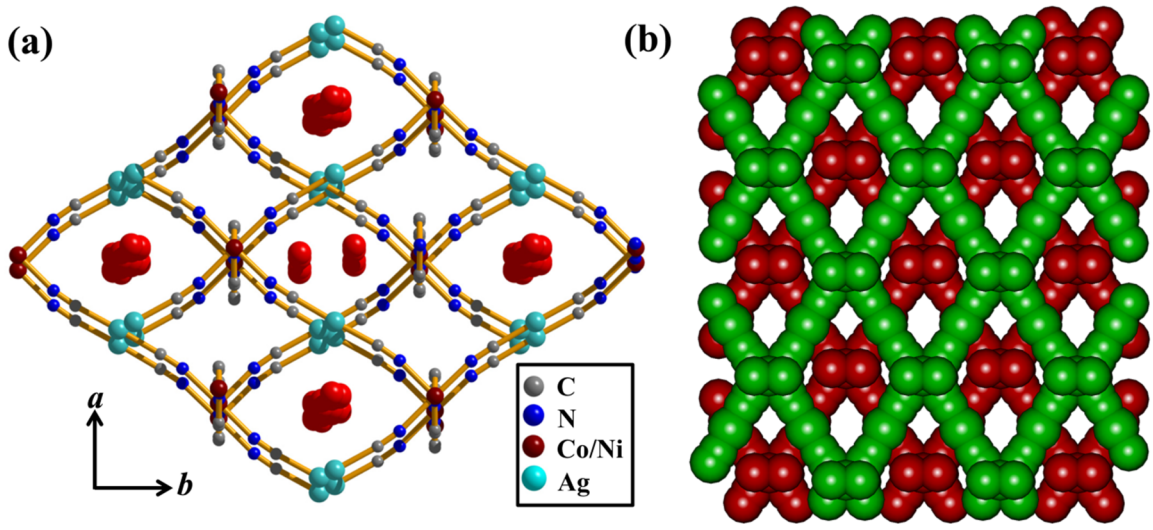

Figure 5. (a) Pore view along the crystallographic *c*-axis showing two different types of channels; one hexagonal and the other diamond shaped occupied by guest water molecules. (b) Space filling diagram of the two-fold interpenetrated 3D framework with the 1-dimensional hexagonal and diamond shaped channels along the crystallographic *c*-axis (hydrogen and non-coordinated water molecules have been omitted for clarity).

Table 1. Crystal data and structure refinement parameters for **1** and **2**.

Parameters	**1**	**2**
Empirical Formula	$C_8H_{20}N_6O_5Ag_2Co$	$C_8H_{20}N_6O_5Ag_2Ni$
Formula Weight	554.95	554.71
Crystal System	Orthorhombic	Orthorhombic
Space Group	*Cmcm* (No. 63)	*Cmcm* (No. 63)
a (Å)	12.5528(2)	12.6541(14)
b (Å)	16.9488(3)	16.7209(17)
c (Å)	7.1769(1)	7.1163(7)
α (°)	90	90
β (°)	90	90
γ (°)	90	90
V (Å^3)	1526.92(4)	1505.7(3)
Z	4	4
T (K)	298	298
μ (mm^{-1})	3.644	3.844
D_{calcd} (g cm^{-3})	2.370	2.403
F (000)	1044	1048
Measured reflections	11319	8582
Unique reflections	763	660
Reflections [$I>2\sigma(I)$]	602	500
R_{int}	0.036	0.092
GOF on F^2	1.17	1.08
$R_1[I>2\sigma(I)]$[a]	0.0642	0.0773
$R_w[I>2\sigma(I)]$[b]	0.2385	0.2233
$\Delta\rho$ max/min [e Å^{-3}]	2.19, -0.74	1.92, -0.98

[a] $R = \sum||F_o|-|F_c||/\sum|F_o|$. [b] $R_w = [\sum\{w(F_o^2-F_c^2)^2\}/\sum\{w(F_o^2)^2\}]^{1/2}$

Table 2. Selected Bond lengths (Å) and angles (°) for compounds **1** and **2**.

Compound 1			
Co1-N1	2.116(12)	Co1-N2	2.124(12)
Co1-N3	2.154(12)		
N1-Co1-N3	89.6(3)	N1-Co1-N1_a	90.0(5)
N1-Co1-N2_a	179.0(5)	N1-Co1-N2	91.0(5)
N3-Co1-N3_a	178.9(6)	N2 -Co1-N3_a	90.4(3)
N2 -Co1-N2_a	88.0(5)		
Compound 2			
Ni1-N1	2.088(14)	Ni1-N2	2.100(14)
Ni1-N3	2.119(14)		
N1-Ni1-N2_a	178.9(5)	N1-Ni1-N3	89.4(3)
N1-Ni1-N1_a	89.8(5)	N1-Ni1-N2_a	91.3(5)
N2-Ni1-N3	90.6(3)	N2-Ni1-N2_a	87.6(5)
N3-Ni1-N3_a	178.3(7)		

Symmetry Codes: a = 1−x, y, 1/2−z.

5.3.2 Framework Stability: TGA, IR and PXRD Analysis

TGA, temperature dependent IR and PXRD analyses of **1** and **2** were carried out to study the thermal stability of the frameworks (Figures 6, 7, 8 and 9). Compound **1** is stable up to 205 °C after initial weight loss of 3.1% which correspond to the loss of one only non-coordinated water molecule. The loss of other four guest water molecules is not reflected in the TGA curve and this may be due to removal of these guest molecules from the sample, even at room temperature. Beyond 205 °C, subsequent ligand loss results into decomposition of the structure. Compound **2** shows similar behaviour and is stable up to 190 °C after initial weight loss of 2.9%.

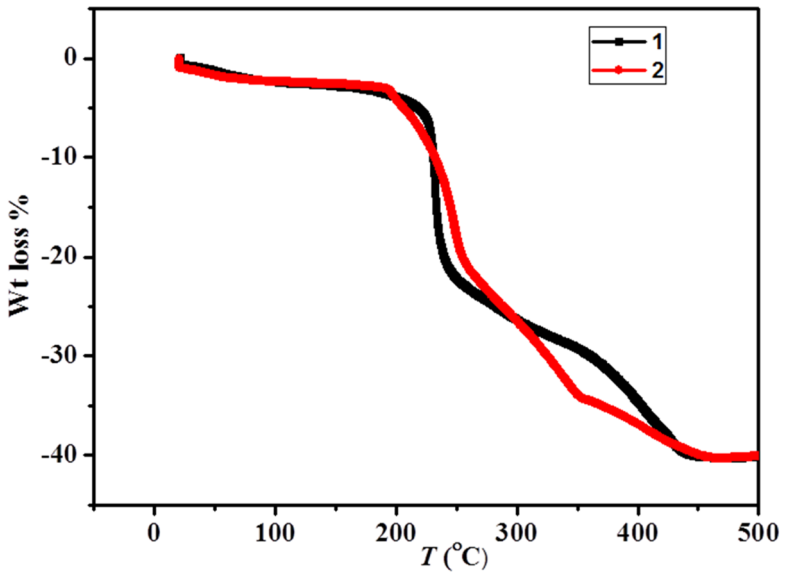

Figure 6. TGA curve for compounds **1** (black) and **2** (red) in the temperature range 25−500 ºC (heating rate 5 °C min^{-1} under nitrogen).

Temperature dependent IR (30 ºC–200 ºC) spectra have been recorded for **1**, which shows no significant change in the stretching frequencies with increase in temperature, except that for the ν(O–H) frequency (Figure 7). The ν(O–H) frequency arises from the coordinated guest water molecules and its intensity decreases with the gradual increase in temperature. At 150 ºC, the peak corresponding to this ν(O–H) frequency disappear with the removal of the guest molecules. Room temperature PXRD patterns of the as-synthesized sample of **1** and **2** correlate well with the simulated patterns, indicating the high purity of the samples (Figure 8 and 9). PXRD pattern of the dehydrated solids of **1′** and **2′** do not show any change in the peak positions compared to as-synthesized pattern, suggesting the rigidity of the frameworks (Figure 8 and 9).

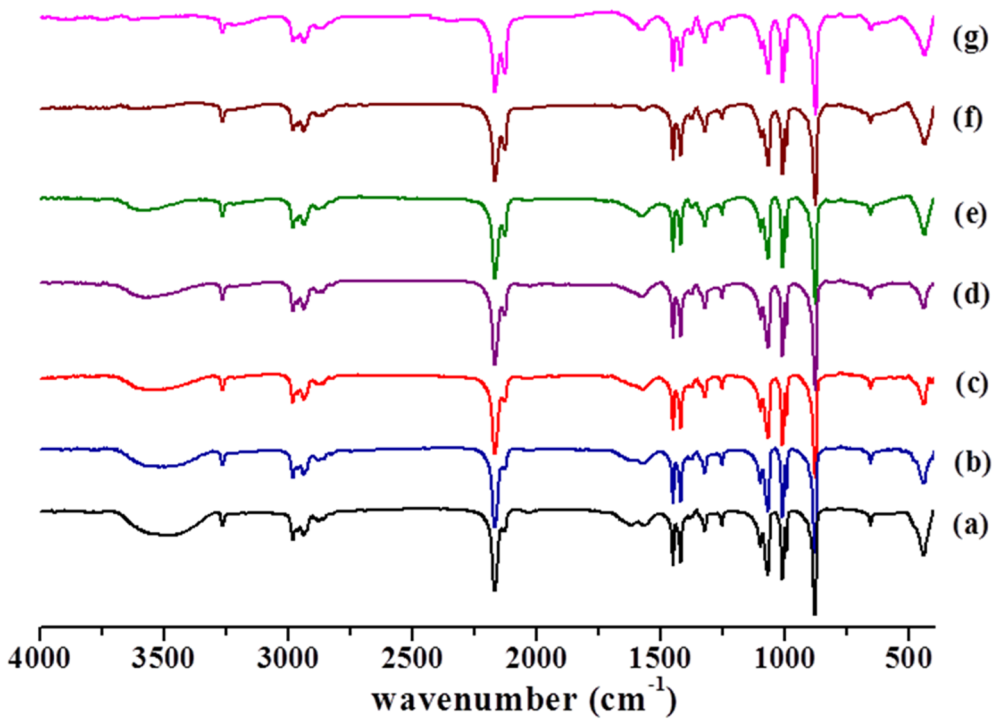

Figure 7. IR spectra for **1** at different temperature; (a) 30 ºC, (b) 60 ºC, (c) 80 ºC, (d) 100 ºC, (e) 120 ºC, (f) 150 ºC, and (g) 200 ºC.

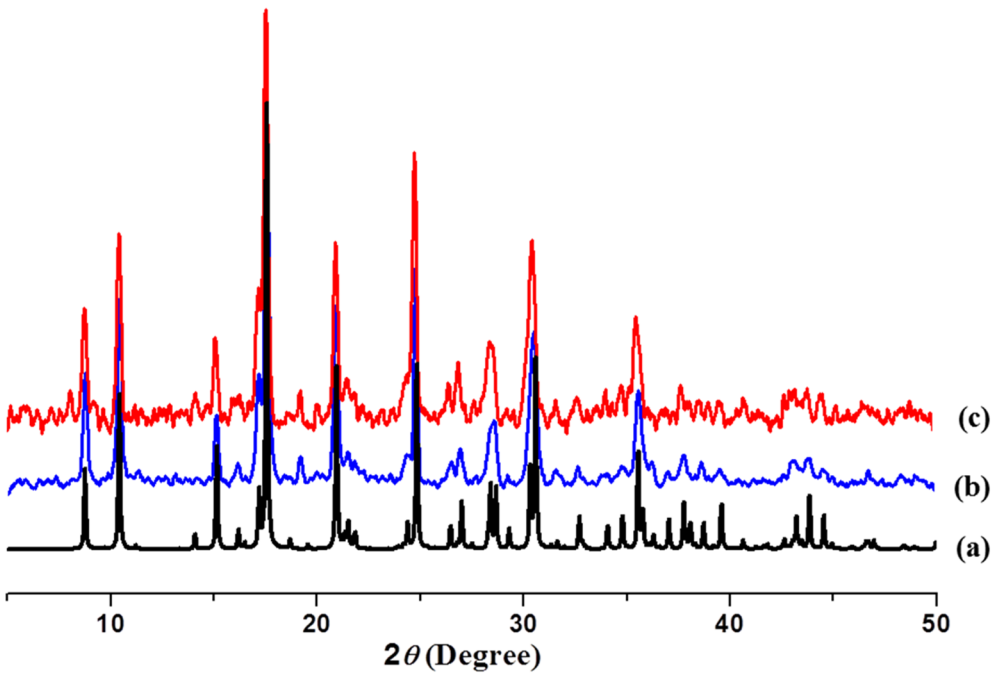

Figure 8. PXRD patterns of **1** in different state: (a) simulated; (b) as-synthesized; (c) desolvated at 160 ºC for 12 h.

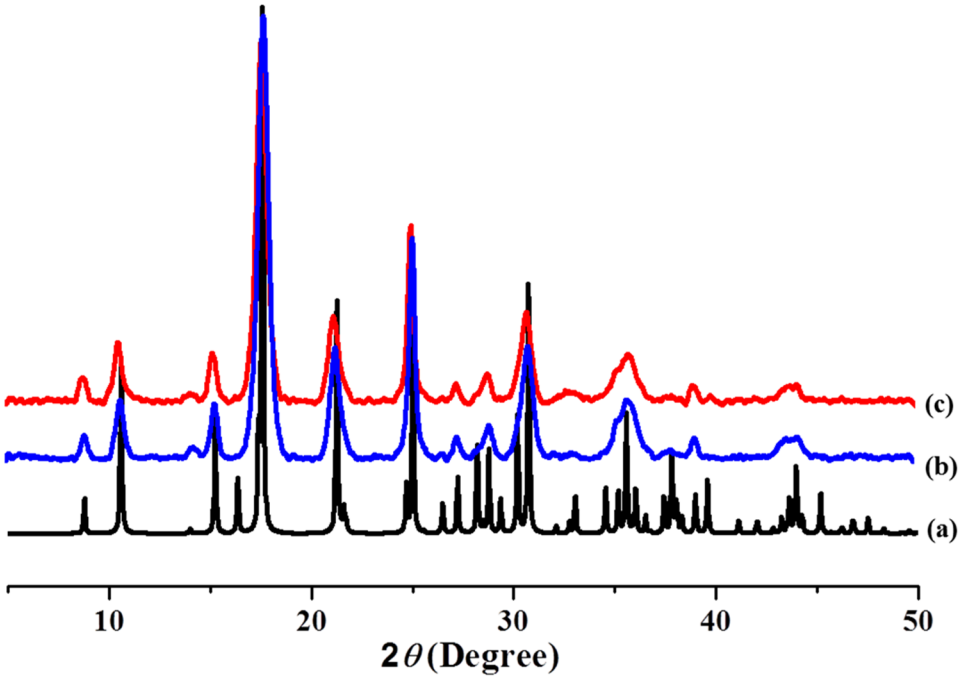

Figure 9. PXRD patterns of **2** in different state: (a) simulated; (b) as-synthesized; (c) desolvated at 160 ºC for 12 h.

5.3.3 Magnetic properties

Figure 10 shows the variable-temperature magnetic susceptibility of **1** measured at 500 Oe using a polycrystalline powder sample. At 300 K, the $\chi_M T$ value is 3.4 cm^3 mol^{-1} K and thus higher than the spin-only value of 1.87 cm^3 mol^{-1} K expected for one high spin Co(II) ions, which is due to the orbital contribution of the octahedral Co(II) centres. The temperature dependence of the reciprocal susceptibility above 70 K (Figure 11) follows the Curie–Weiss law with a Weiss constant θ of −10.8 K, thus indicating an overall antiferromagnetic interaction. The product $\chi_M T$ first decreases smoothly to a minimum of 2.79 cm^3 mol^{-1} K at 31 K and then increases rapidly to a maximum of 8.67 cm^3 mol^{-1} K at 6.3 K and finally decreases on further cooling. The field-cooled (FC) and zero field-cooled (ZFC) magnetization measured at 500 Oe show a bifurcation at 5 K, suggesting a phase transition (Figure 10 inset). Figure 12 shows the temperature dependence of the ac susceptibility measured in a field of 5 Oe. The maximum of χ' observed at Tc = 6 K, in agreement with the above results, confirms the occurrence of a phase transition and magnetic long range ordering. The imaginary χ'' component shows a peak at 5 K, which is the signature of a magnetized state, which indicates a spin canted structure exists below this temperature. No frequency dependence of these transitions is observed, thus excluding the possibility of relaxation behaviour. A plot of field-cooled susceptibility *vs.*

T at different dc field strengths of 50, 100 and 500 Oe shows a field-dependent behaviour below 6 K (Figure 13) and the spontaneous increase of $\chi_M T$ product is more pronounced at lower field strength, confirming spin-canting in this system.

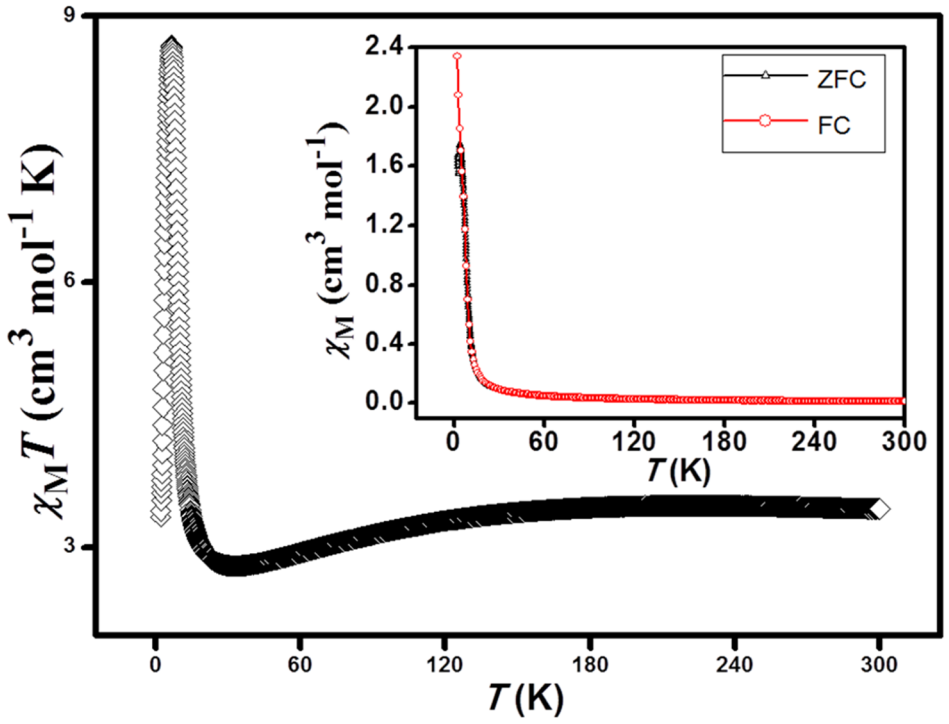

Figure 10. The plots of $\chi_M T$ *vs.* *T* for **1**. The inset shows temperature dependence of the magnetic susceptibility of **1** at 500 Oe under field-cooled (FC) and zero-field-cooled (ZFC) conditions.

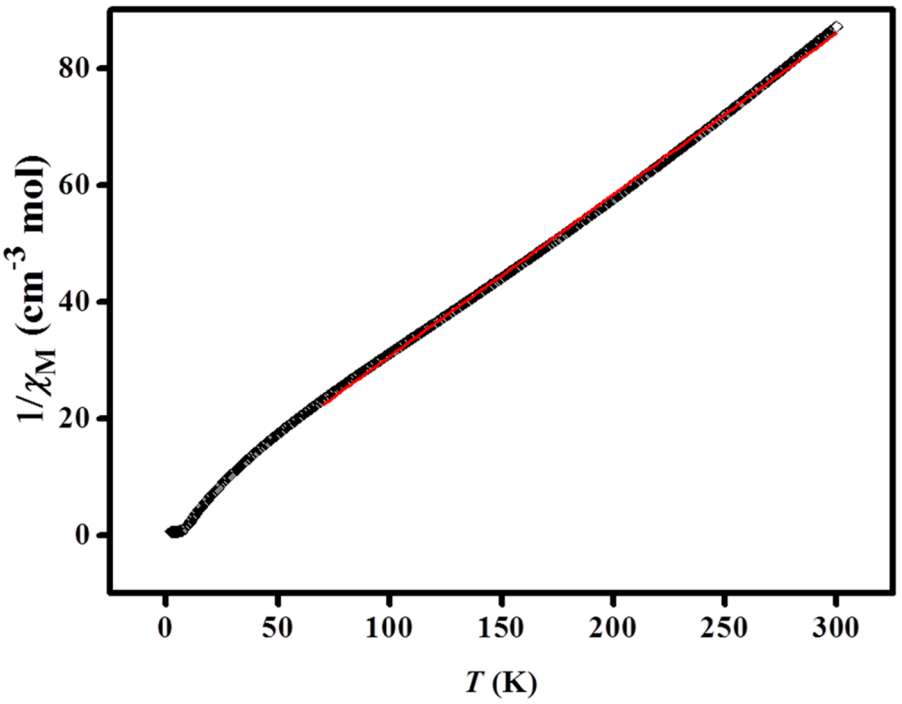

Figure 11. Curie–Weiss fitting of **1** above 70 K. The red line indicates the best fit obtained.

Further information comes from the isothermal magnetization measurements (Figure 14). The plot of the reduced magnetization *vs.* H at 2 K is clearly indicative of a hysteresis plot corresponding to a very soft ferromagnet (small coercive field) and confirms the occurrence of weak ferromagnetic ordering. Figure 14 inset shows zoomed hysteresis loop with a remnant magnetization (M_r) of 0.086 Nβ and a coercive field (H_c) of 309 Oe. Assuming the saturation magnetization value of 3 Nβ (expected value for a spin only Co(II) ion), the estimated canting angle for **1** [$\sin^{-1}(0.086/3)$] is 1.64°.

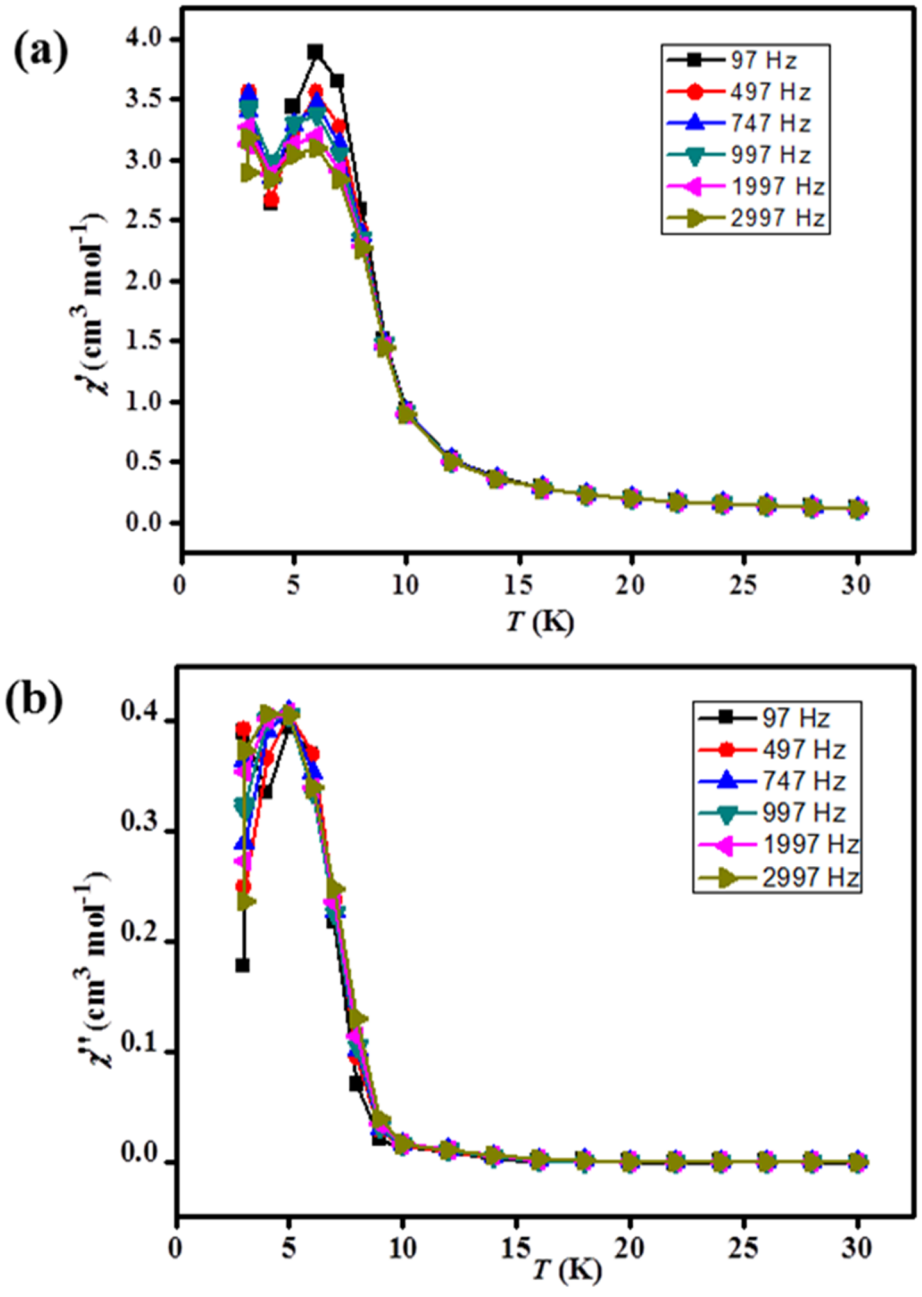

Figure 12. The ac susceptibility in-phase, χ' (a) and out-of-phase, χ'' (b) of **1** at applied field of 5 Oe.

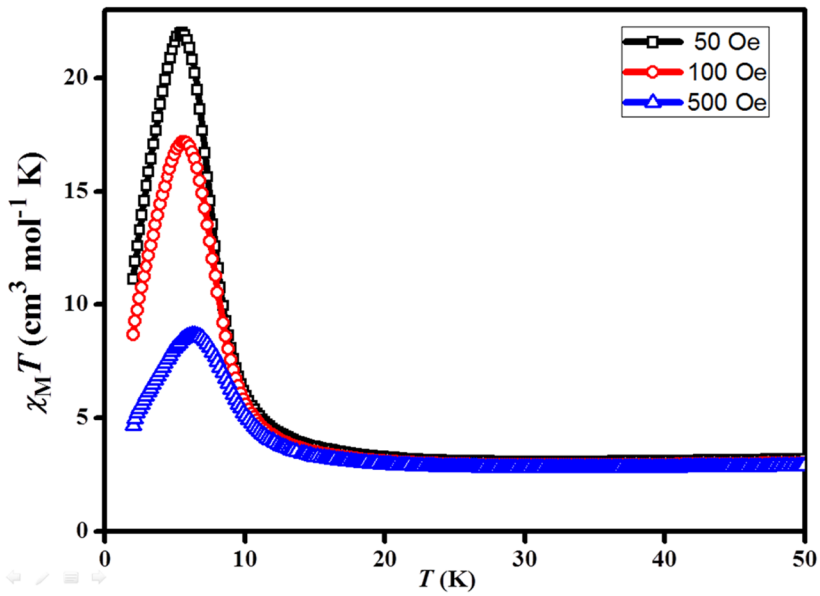

Figure 13. Temperature dependence of the magnetic susceptibility of **1** at 50, 100, and 500 Oe under field-cooled (FC) condition.

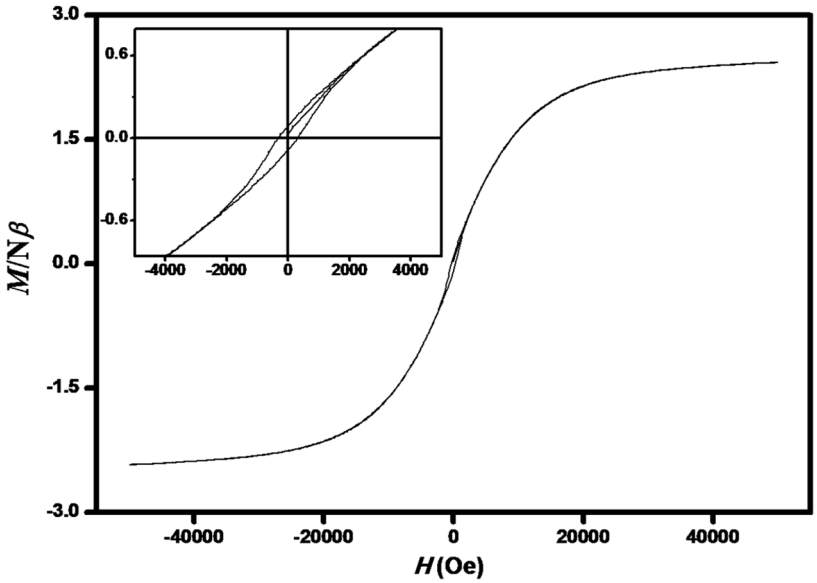

Figure 14. Isothermal magnetization of **1** measured by cycling the field between 50 and -50 KOe at 2 K. The inset shows the hysteresis loop.

Compound **2** exhibits similar magnetic behaviour as **1**, owing to the structural similarity. Figure 15 shows $\chi_M T$ *vs.* T plot where an abrupt increase is observed at a temperature 14 K. The Curie–Weiss fitting of the reciprocal susceptibility above 70 K gives a Weiss constant θ of −5.7 K (Figure 16). The maxima of χ' and χ'' are observed at 16 and 14 K, respectively (Figure 17) and hence a canted antiferromagnetic structure exists below 14 K. The field dependence of $\chi_M T$ product is shown in Figure 18. However, the hysteresis loop (Figure 19) reveals that **2** has a smaller coercive field (235 Oe) than **1**

with a remnant magnetization (M_r) of 0.025 Nβ. Using the same approach as for **1** and the expected 2.1 Nβ per Ni(II), we have estimated the canting [$\sin^{-1}(0.0247/2.1)$] for **2**, which is 0.67°.

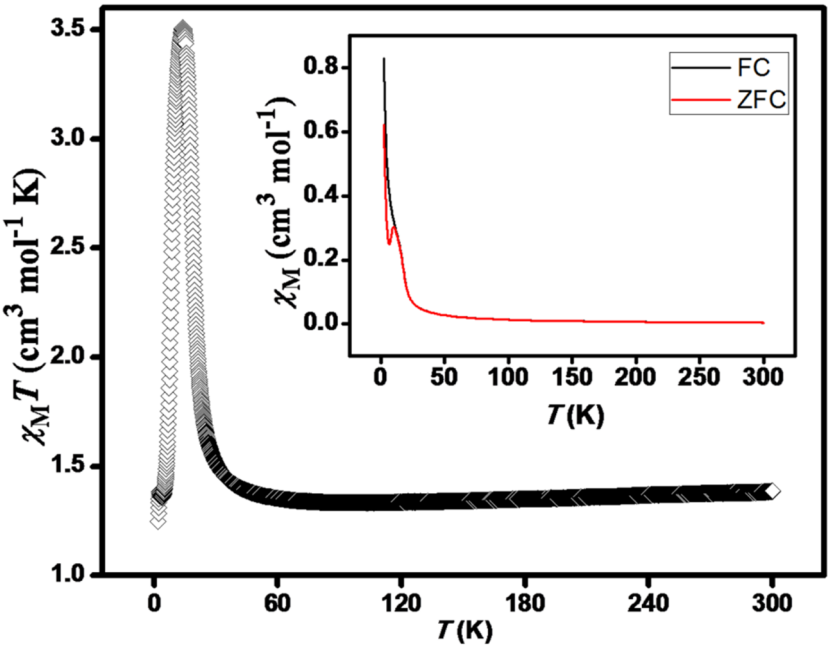

Figure 15. The plots of $\chi_M T$ *vs.* T for **2**. The inset shows temperature dependence of the magnetic susceptibility of **2** at 500 Oe under field-cooled (FC) and zero-field-cooled (ZFC) conditions.

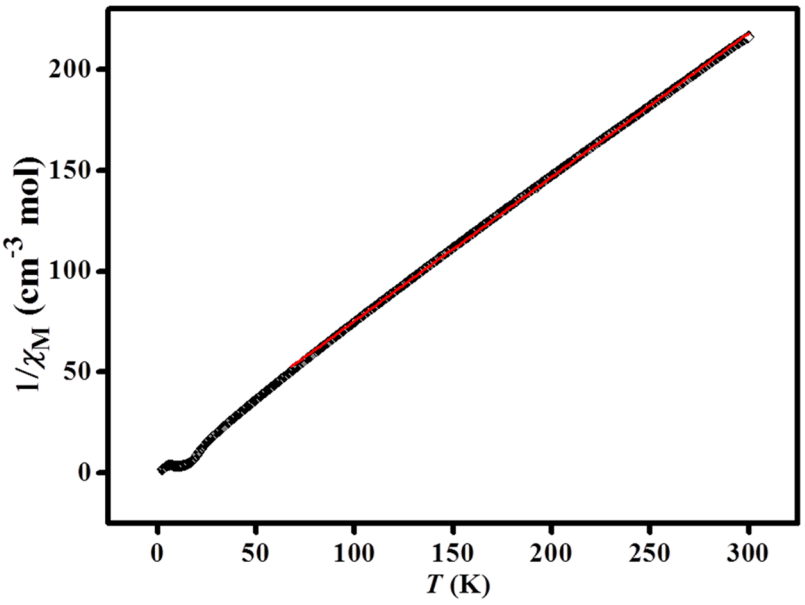

Figure 16. Curie–Weiss fitting of **2** above 70 K. The red line indicates the best fit obtained.

It should be noted the magnetic ions in the unit cell of **1** and **2** are not related by a center of symmetry and as well established, two factors can then result into spin canting[12] (i) single-ion anisotropy, which originates if the anisotropy axes on neighbouring

interacting sites are different and (ii) the antisymmetric Dzyaloshinsky–Moriya (DM)[12] interaction, which cants the spins because the coupling energy is minimized when the two spins are perpendicular to each other. Now both mechanisms favour the spin canting in these compounds as both Co(II) and Ni(II) have magnetic anisotropy and the dicyanoargentate bridging in the 2D corrugated sheet afford a low symmetry exchange pathway.

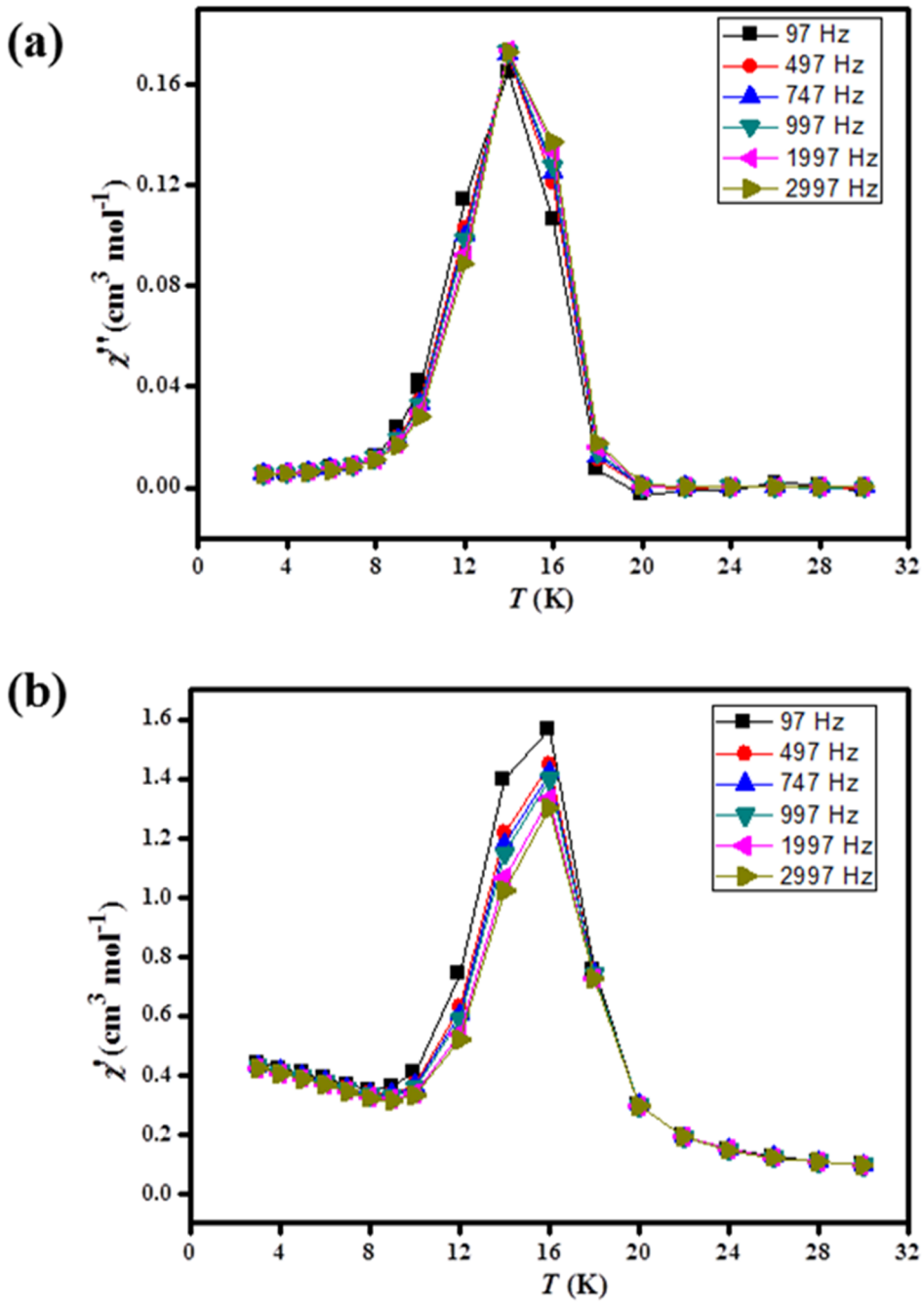

Figure 17. The ac susceptibility in-phase, χ' (a) and out-of-phase, χ'' (b) of **2** at applied field of 5 Oe.

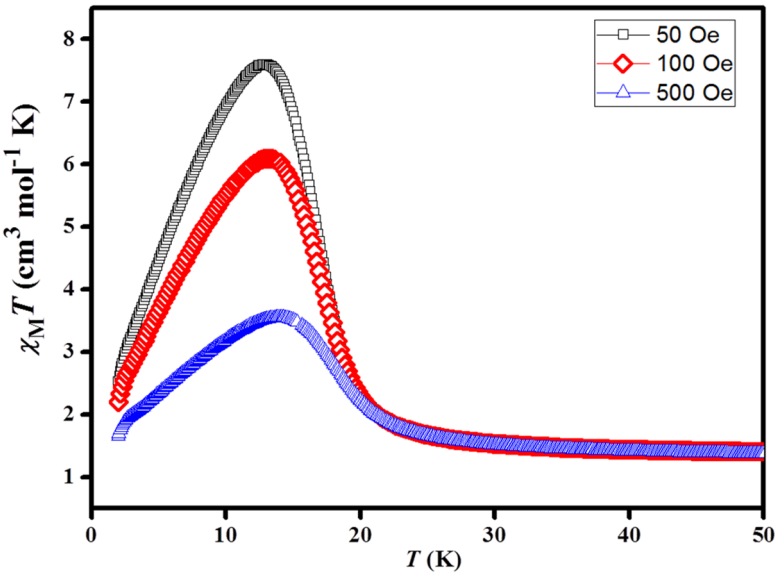

Figure 18. Temperature dependence of the magnetic susceptibility of **2** at 50, 100, and 500 Oe under field-cooled (FC) condition.

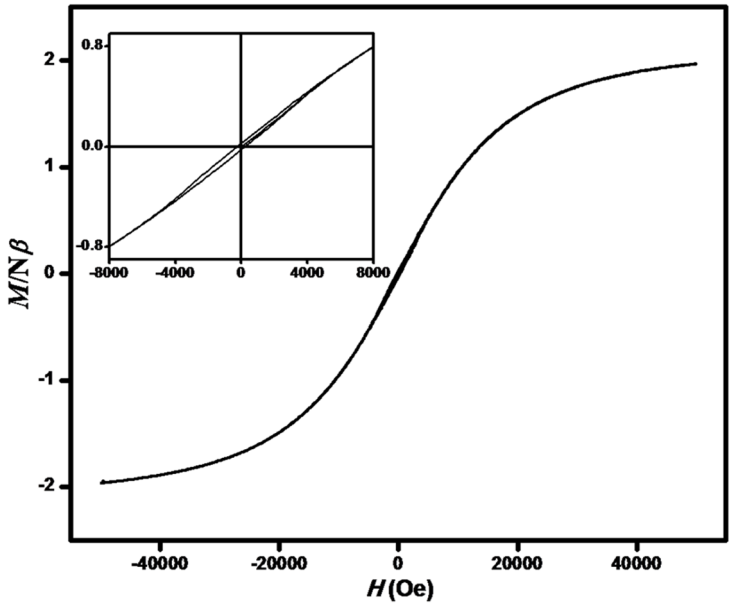

Figure 19. Isothermal magnetization of **2** measured by cycling the field between 50 and -50 KOe at 2 K. The inset shows the hysteresis loop.

Interestingly, **1** has a higher coercive field than **2** despite their structural similarity. However, local anisotropy of the Co(II) ions resulting from unquenched orbital momentum and first-order spin–orbit coupling is greater than that for Ni(II), which is due only to the second order spin–orbit coupling; while for the two isomorphous systems, the antisymmetric exchange should be of the same order. Probably this enhanced anisotropy for **1** gives rise to a greater coercivity than in **2**.

5.3.4 Adsorption study

To investigate the porous properties of the compounds, **1′** and **2′** were subjected to N_2 adsorption measurements at 77 K. Both of the compounds show type II adsorption profile indicating only surface adsorption (Figure 20, 21).

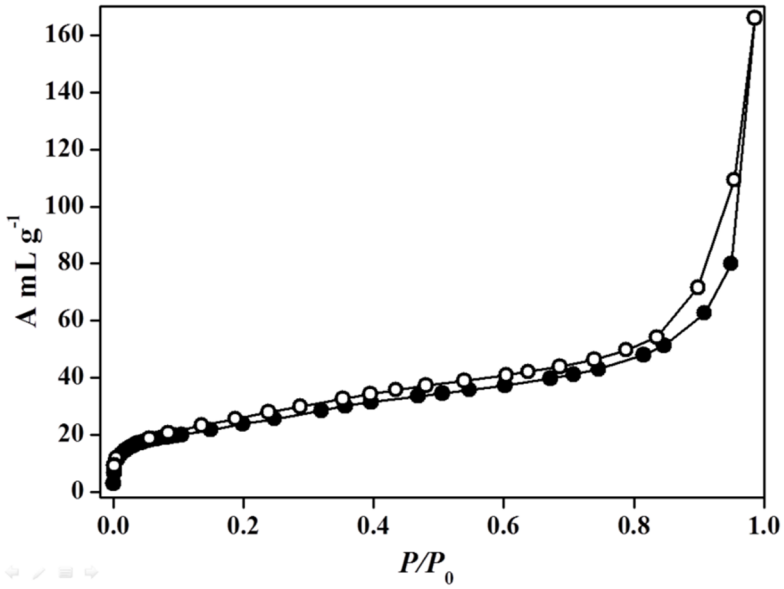

Figure 20. N_2 gas adsorption isotherms for **1′** at 77 K showing only surface adsorption. (Closed symbols indicate adsorption and open symbols indicate desorption, P_0 is the saturated vapour pressure of the adsorbates at measurement temperatures).

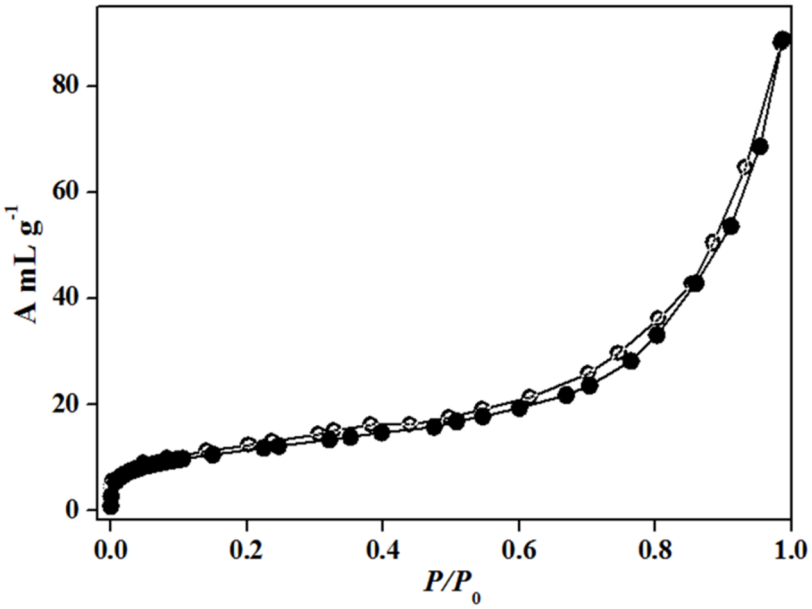

Figure 21. N_2 gas adsorption isotherms for **2′** at 77 K showing only surface adsorption. (Closed symbols indicate adsorption and open symbols indicate desorption, P_0 is the saturated vapour pressure of the adsorbates at measurement temperatures).

The pore sizes of the two different channels of **1** are 4.9 Å × 3.1 Å and 2.4 Å × 2.4 Å, while that for **2** are 4.8 Å × 3.1 Å and 2.1 Å × 2.4 Å, respectively. Probably the high diffusion barrier to accommodate the N_2 (Kinetic diameter 3.64 Å) molecule results in only surface adsorption.

Surprisingly, the frameworks, **1′** and **2′** showed a type I profile for CO_2 (3.4 Å) gas uptake carried out at 195 K and the final uptake volumes are ~ 40 and ~ 45 mL g^{-1}, respectively (Figure 22, 23). Surface area calculated using Langmuir equation from the CO_2 profiles turns out to be ~ 195 and ~ 205 m^2 g^{-1} for **1′** and **2′**, respectively. The profiles were further analyzed by the Dubinin-Radushkevich (DR) equation to realize the adsorbate-adsorbent interaction and the $q_{st,\phi}$ value for **1′** and **2′** are found to be ~ 29 and ~ 30 kJ mol^{-1}, respectively suggesting stronger interaction of CO_2 with the frameworks. The strong and preferential interaction of CO_2 with framework could be attributed to the presence aromatic electron clouds and the –CN groups at the pore surfaces. We further studied the N_2, Ar, H_2 and O_2 gas adsorption at 195 K for both the frameworks and in all cases we observed negligible uptake suggesting compounds **1′** and **2′** as potential selective CO_2 adsorbent.

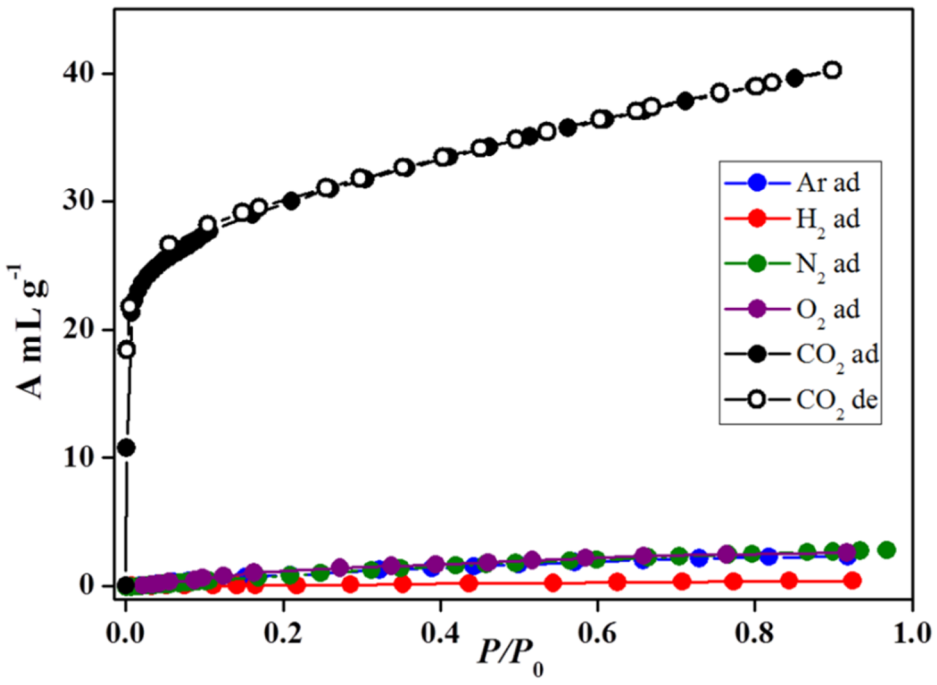

Figure 22. Gas adsorption isotherms for **1′** showing a high selectivity for CO_2: CO_2 (black), Ar (blue), H_2 (red), N_2 (green) and O_2 (red) at 195 K. (closed symbols indicate adsorption and open symbols indicate desorption, P_0 is the saturated vapour pressure of the adsorbates at measurement temperatures).

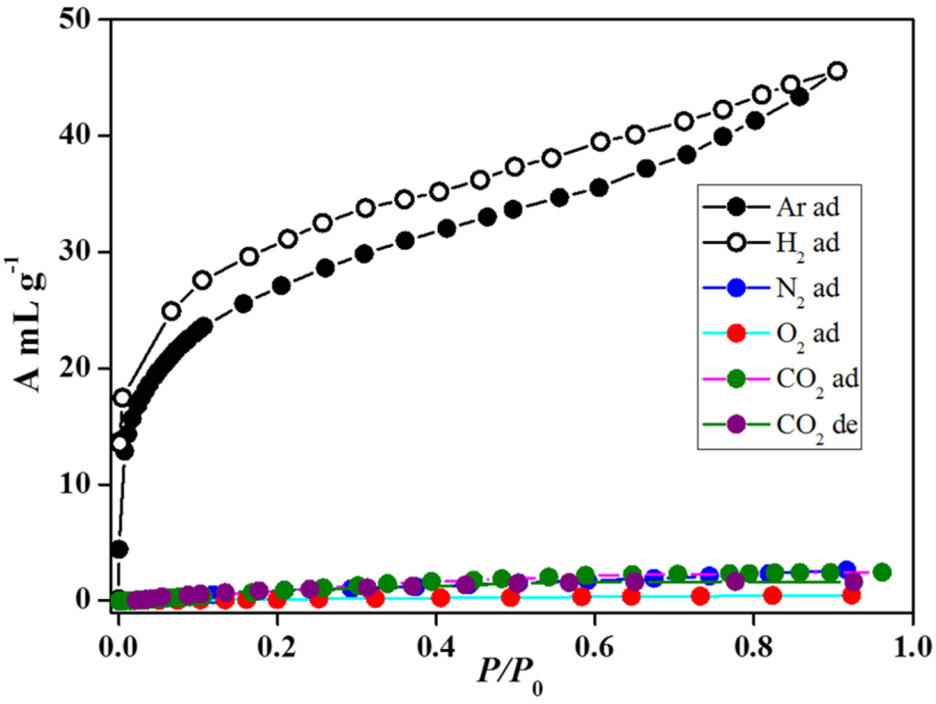

Figure 23. Gas adsorption isotherms for **2′** showing a high selectivity for CO_2: CO_2 (black), Ar (blue), H_2 (red), N_2 (green) and O_2 (red) at 195 K. (closed symbols indicate adsorption and open symbols indicate desorption, P_0 is the saturated vapour pressure of the adsorbates at measurement temperatures).

5.4 CONCLUSION

In summary, two isomorphous 3D porous frameworks $[M^{II}(pip)\{Ag(CN)_2\}_2 \cdot 5H_2O]$ (M = Co, **1**; Ni, **2**; pip = piperazine) have been synthesized by employing mixed-ligand system (dicyanoargentate(I), $[Ag(CN)_2]^-$ and piperazine) and their characterization, adsorption and magnetic properties are presented. The 3D frameworks are 2-fold interpenetrated which render structural rigidity and the frameworks are stable upto ~ 200 °C. **1** and **2** exhibit spin canting behaviour below 5 K and 14 K, respectively, which is attributed to the single-ion anisotropy of Co(II) and Ni(II) ions and the low symmetry M–NC–Ag–CN–M exchange pathway provided by the $[Ag(CN)_2]^-$ bridging. In the pillared-layer structure of **1** and **2**, the pore surfaces are decorated with polar –CN groups, which results selective adsorption of CO_2 over other gases, such as N_2, H_2, O_2 and Ar at 195 K by the dehydrated frameworks.

5.5 REFERENCES

[1] B. Moulton and M. J. Zaworotko, *Chem. Rev*., 2001, **101**, 1629.

[2] E. Manousakis, *Rev. Mod. Phys*., 1991, **63**, 1.

[3] R. L. Carlin, Magnetochemistry, Springer, Berlin-Heidelberg, 1986.

[4] (*a*) K. Barthelet, J. Marrot, D. Riou and G. Fe´rey, *Angew. Chem., Int. Ed.*, 2002, **41**, 281; (*b*) N. Guillou, Q. Gao, P. M. Forster, J.-S. Chang, M. Nogue`s, S.-E. Park, G. Fe´rey and A. K. Cheetham, *Angew. Chem. Int. Ed.*, 2001, **40**, 2831; (*c*) M. Cavellec, D. Riou, C. Ninlaus, J.-M. Grene`che and G. Fe´rey, *Zeolites*, 1996, **17**, 250; (*d*) M. Cavellec, D. Riou, Grene`che, J.-M.; Fe´rey, G. *J. Magn. Magn. Mater.*, 1996, **163**, 173; (*e*) C. M. Nagaraja, R. Haldar, T. K. Maji, and C. N. R. Rao, *Cryst. Growth Des.*, 2012, **12**, 975; (*f*) A. Hazra, P. Kanoo and T. K. Maji, *Chem. Commun*., 2011, **47**, 538; (*g*) L. G. Beauvais and J. R. Long, *J. Am. Chem. Soc*., 2002, **124**, 12097.

[5] (*a*) D. Tanaka, K. Nakagawa, M. Higuchi, S. Horike, Y. Kubota, T. C. Kobayashi, M. Takata and S. Kitagawa, *Angew. Chem. Int. Ed.*, 2008, **47**, 3914; (*b*) M. Higuchi, D. Tanaka, S. Horike, H. Sakamoto, K. Nakamura, Y. Takashima, Y. Hijikata, N. Yanai, J. Kim, K. Kato, Y. Kubota, M. Takata and S. Kitagawa, *J. Am. Chem. Soc.*, 2009, **131**, 10336; (*c*) T. Fukushima, S. Horike, Y. Inubushi, K. Nakagawa, Y. Kubota, M. Takata and S. Kitagawa, *Angew. Chem. Int. Ed.*, 2010, **49**, 4820; (*d*) T. K. Maji, R. Matsuda and S. Kitagawa, *Nat. Mater*., 2007, **6**, 142.

[6] J.-P. Costes, C. Duhayon, L. Vendier, E. Colacio, A. J. Mota Ávila, and J. S. Varela, *Inorg. Chem.*, 2012, **51**, 1011.

[7] (*a*) W. S. Broecker, *Science*, 2007, **315**, 1371; (*b*) E. Marris, *Nature*, 2006, **442**, 624; (*c*) C. Song, *Catal. Today*, 2006, **115**, 2; (*d*) R. Vaidhyanathan, S. S. Iremonger, G. K. H. Shimizu, P. G. Boyd, S. Alavi and T. K. Woo, *Science*, 2010, **330**, 650; (*e*) R. Vaidhyanathan, S. S. Iremonger, K. W. Dawson and G. K. H. Shimizu, *Chem. Commun*., 2009, 5230.

[8] (*a*) R. G. Xiong, J. L. Zuo, X. Z. You, B. F. Abrahams, Z. P. Bai, C. M. Che and H. K. Fun, *Chem. Commun*., 2000, 2061; (*b*) C. J. Kepert and M. J. Rosseinsky, *Chem. Commun*., 1998, 31; (*c*) S. Q. Ma, D. F. Sun, M. Ambrogio, J. A. Fillinger, S. Parkin and H. -C. Zhou, *J. Am. Chem. Soc*., 2007, **129**, 1858; (*d*) H. -Y. Wang, S. Gao, L. -H. Huo, S. W. Ng and J. -G. Zhao, *Cryst. Growth Des*., 2008, **8**, 665; (*e*) M. R. Montney, R. M. Supkowski and R. L. LaDuca, *CrystEngComm*., 2008, **10**,

111; (*f*) L. Zhang, Y. -L. Yao, Y. -X. Che and J. -M. Zheng, *Cryst. Growth Des*., 2010, **10**, 528; (g) S. Y. Vyasamudri and T. K. Maji, *Chem. Phys. Lett.*, 2009, **473**, 312.

[9] (*a*) T. M. Reineke, M. Eddaoudi, D. M. Moler, M. O'Keeffe and O. M. Yaghi, *J. Am. Chem. Soc*., 2000, **122**, 4843; (*b*) M. Kondo, M. Shimamura, S. -i. Noro, S. Minakoshi, A. Asami, K. Seki and S. Kitagawa, *Chem. Mater*., 2000, **12**, 1288; (*c*) L. Carlucci, G. Ciani, P. Macchi, D. M. Proserpio and S. Rizzato, *Chem. Eur. J*., 1999, **5**, 237; (*d*) L. Carlucci, G. Ciani, D. M. Proserpio and S. Rizzato, *Chem. Eur. J*., 2002, **8**, 1519.

[10] (*a*) SMART (V 5.628), SAINT (V 6.45a), XPREP, SHELXTL; Bruker AXS Inc. Madison, Wisconsin, USA, 2004; (*b*) G. M. Sheldrick, Siemens Area Detector Absorption Correction Program, University of Göttingen, Göttingen, Germany, 1994; (*c*) A. Altomare, G. Cascarano, C. Giacovazzo, A. Gualaradi, *J. Appl. Cryst*., 1993, **26**, 343; (*d*) G. M. Sheldrick, SHELXL-97, Program for Crystal Structure Solution and Refinement; University of Göttingen, Göttingen, Germany, 1997; (*e*) A. L. Spek, *J. Appl. Cryst*., 2003, **36**, 7; (*f*) L. J. Farrugia, WinGX–A Windows Program for Crystal Structure Analysis, *J. Appl. Crystallogr*., 1999, **32**, 837.

[11] Spek, A. L. *J. Appl. Crystallogr.*, 2003, **36**, 7.

[12] (*a*) I. Dzyaloshinsky, *J. Phys. Chem. Solids*, 1958, **4**, 241; (*b*) T. Moriya, *Phys. Rev*., 1960, **120**, 91; (*c*) T. Moriya, *Phys. Rev.,* 1960,**117**, 635.

Lists of Publications

[1] Assembly of trinuclear and tetranuclear building units of Cu^{2+} towards two 1D magnetic systems: Synthesis and magneto-structural correlations, A. Chakraborty, K. L. Gurunatha, A. Muthulakshmi, S. Dutta, S. K. Pati and T. K. Maji, *Dalton Trans.*, (2012), DOI: 10.1039/C2DT12511K.

[2] A heterometallic Cu(II)-Ni(II) Decameric cluster containing two distorted cubane-like pentanuclear core: synthesis, structure and magnetic properties, A. Chakraborty *et al*., submitted.